A reliability-based approach to determine the probability of Loss of Containment of Dangerous Goods in a rear-end collision in the automated marshalling process, using a multi-body dynamic model.

Tim Sluiter
Master Thesis, Hydraulic engineering
Hydraulic structures and Flood Risk
Delft University of Technology

TU Delft Delft University of Technology Horvat & Partners ProRail

Cover photo: Marshalling yard Kijfhoek, Zwijndrecht, The Netherlands (Prorail.nl).

A reliability-based approach to determine the probability of Loss of Containment of Dangerous Goods in a rear-end collision in the automated marshalling process, using a multi-body dynamic model.

By

Tim Sluiter

In partial fulfilment of the requirements for the degree of

Master of Science
in Civil Engineering

at the Delft University of Technology.

This thesis is performed in cooperation with:

Student number:	4540883	
Project duration:	November 9, 2020 – July 21, 2021	
Chairman:	Prof. dr. ir. P.H.A.J.M. van Gelder,	*TU Delft*
Thesis committee:	Dr. ir. R.C. Lanzafame,	*TU Delft*
	Ir. A.B. Fărăgău,	*TU Delft*
Supervisors:	Ir. drs. D.A. de Loor,	*Horvat & Partners*
	Ir. I.F. de Graaf ,	*ProRail*

Abstract

The Dutch government provides a calculation method to determine the risks to society outside the boundaries of institutions handling Dangerous Goods (the risk affecting External Safety). The current method to calculate the risk affecting External Safety for train marshalling yards is deterministic, outdated, and not transparent. This thesis aims to improve the calculation method regarding rear-end collisions in automated marshalling. It provides a reliability-based approach to the study case Kijfhoek and uses a multi-body dynamic model to simulate the collisions. A Monte Carlo simulation is performed implementing over twenty-five parameters to determine the probability of damage in case of a rear-end collision. From the results, a simplified method is designed to assess the probability of damage to the wagon's structure. This method uses a newly found relation to determine the absorbed energy at the impact interface in case of a collision. Furthermore, the simplified method reduced the calculation to five parameters and an analytically solvable Limit State function. A first-order reliability method shows that the impact velocity is the single most important parameter in determining the probability of damage.
The simplified method also allows for site-specific values and gives insight into the system and the most important parameters. It is recommended that this method, to determine damage to especially tank wagons in rear-end collisions, is used to improve the existing calculation method for determining the risk affecting External Safety.

Keywords: External Safety, dangerous goods, emplacement yard, multi-body dynamic model, reliability analysis, train collision, energy absorption.

Preface

In this chapter, I would like to express my gratitude to everyone who made it possible for me to graduate and for the support throughout my years at TU Delft. First, I thank my wife and my parents in the support of my decision to go back to university at the age of 27. I really enjoyed my time at TU Delft, and it felt good to acquire intellectual knowledge. Unfortunately, due to the COVID-19 pandemic, the last year was not as enjoyable as the years before, but my family kept my spirits up. Nevertheless, at the same time the highlight of my life was the birth of our daughter in January, which gave me a lot of energy and dedication to do the work and finish on a high. And to that regard, I want to thank my mother, who was so kind to babysit our daughter on Fridays for the last few months so I could finish this thesis in time. The last family member I need to thank is my father-in-law Ton; thank you for helping me rephrase and correct the language used in this thesis.

Next, I would like to thank my whole committee: Pieter van Gelder, Robert Lanzafame, Andrei Fărăgău, Ivo de Graaf and David de Loor for your time, your support, and your energy in these difficult times. All of you were always available for help and your comments throughout the year were always supportive and valuable. Although some of you I will meet in person for the first time at the defence of this thesis, it feels like we have actually met and thank you for the warm welcome. First, Pieter, thank you for your enthusiasm as the chair of this committee. Your interest in the subject of this thesis was evident from the start, and when I needed your expertise, you always made time for me. Second, I would like to thank Robert as my daily supervisor. Before we even decided on a subject, you were already on board, which was flattering and very helpful. Your 'Zoom' office was always open, and we have had many digital conversations, which were always enjoyable and constructive. Third, Andrei, thank you for joining the team for your expertise in dynamics. During my Bachelor thesis, we had worked closely and enjoyably. Although the meetings during this Master thesis were not in person, they were just as pleasant. Fourth, thank you, Ivo, for all your time and dedication in helping me gather the necessary information as well as the unrestricted access to the required documents. In addition, your help, knowledge, and comments regarding the system at Kijfhoek were very helpful and productive. Lastly, David, thank you very much for the meetings every two weeks and whenever I needed more of your time. You were always available, and our discussions always pointed me in the right direction.

To conclude, I thank Horvat & Partners for the possibility to graduate, and their flexibility during the Corona pandemic. Furthermore, my gratitude goes to the Civil Engineering department at TU Delft and its open mindset towards its students and making study and graduating possible, without any delays.

The Hague, July 2021,

Tim Sluiter

Contents

List of Figures

List of Tables

List of Symbols and Abbreviations

Roman Symbol		
A	Area facing direction of motion	
a_1	Length of the buffer's elastic region	m
a_2	Length of the buffer's plastic region	m
c	Damping coefficient	Ns/m
c_{cw}	Damping coefficient of a crashworthy buffer	kg/s
c_D	Drag coefficient	
c_{rr}	Rolling resistance coefficient	
$c_{standard}$	Damping coefficient of a regular buffer	kg/s
D	Diameter	m
D	Damage	
E	Energy	J
$\boldsymbol{e}$	Eigenvector	
E_c	Collision Energy	J
E_{cap}	Energy absorption capacity of the buffers	J
E_d	Design value for the absorbed energy at the impact interface	J
E_k	kinetic energy	J
$e_{sloshing}$	The imposed error due to sloshing	m/s
F	Cumulative distribution function.	
F	Force	N
f	Probability density function.	
f_d	Dynamic factor (Lu, 2002)	
F_1	Force at the end of the combined buffers' plastic region	N
F_2	Mean force of the plastic region of combined buffers	N
F_{basic}	Basic failure frequency	
F_D	Drag force	N
$F_{humping}$	Failure frequency due to the humping process	
f_i	Force function at the interface i	N
F_{max}	The force that engages the plastic region of the buffer	N
F_{rr}	Rolling resistance force	N
$F_{wagon,pl}$	Force to engage the plastic region a wagon's structure	N
g	gravitational acceleration	m/s^2
i	Integer describing the number of the interface in the EOM	
i	integer representing the category of Dangerous Goods	
k	Spring stiffness	N/m
k_{eq}	Equivalent spring stiffness of combined springs	N/m
$k_{tension}$	Spring stiffness of the coupling device	N
l	Length between the final brakes and the stationary wagons	m
m	Mass of a single wagon	kg
m_1	The mass of the run-off's front wagon	kg
M_1, M_2	Mass of two objects colliding. The indices represent the number of The mass of an object. In this thesis mass of a train set.	kg
m_{1s}	The mass of the impacted wagon of the stationary train	kg
n	Integer describing the number of the wagon	

N	Normal force	N
N	Total number of simulations	
n_{axles}	Number of axles on a wagon	
n_f	Number of failures	
$n_{run-off}$	Number of wagons in a run off	
$n_{stationary}$	Number of stationary wagons on the allocation track	
$P(\dots)$	Probability of the term between brackets	
$P(D)$	Probability of damage	
P_f	probability of failure	
$P_i(cat.)$	Probability of a DG being one of the categories affecting External Safety	
R	Resistance force	N
R_1	Ratio factor (Lu, 2002)	
R_E	Normalized energy factor	
t	Time	s
T	Period	s
u	A threshold value	
U-space	Standard normal space	
v	Velocity	m/s
V	coeficicent of variation	
v_{exit}	The velocity at which a run-off exists the final brakes	m/s
v_{impact}	The impact velocity in a collision	m/s
v_{wind}	wind velcoity	m/s
x	Displacement of a wagon	m
X	A stochastic variable	
X_L	Factor to go from $P(D\|TNT)$ to $P(LOC_{ES})$	
$\dot{x}$	Velocity of a wagon	m/s
$\ddot{x}$	Acceleration of a wagon	m/s^2
x_e	The maximum relative displacement of the elastic region of the combined buffers	m
X-space	Physical space	
Z	The limit state function	
Z	Tank wagon class according to UIC	
Z_{type1}	Limit state function for Type 1 damage	
Z_{type2}	Limit state function for Type 2 damage	

Greek symbol

α	sensitivty factor	
β	Reliability index	
β_{HL}	Hasofer-Lind Reliability index	
μ	Friction coefficient	
ρ	Density	kg/m^3
ω	Eigenfrequency	rad/s

Abbreviations

Bevi	Besluit externe veiligheid inrichtingen

CDF	Cumulative distribution function
CI	Confidence interval
COV	Coefficient of variation
DG	Dangerous good
EOM	Equation of motion
ES	External Safety
FEM	Finite element model
FORM	First-order reliability method
'full'	Inside quotation marks, it means partly filled or full. It contains a DG
GPD	Generalized Pareto Distribution
KijfDIS	Planning system of the wagons at Kijfhoek
KNMI	Koninklijk Nederlands Meteorologish Instituut
KS	Kolmogorov-Smirnov
LOC	Loss of Containment
LOC_{ES}	Loss of Containment of DG affecting External Safety
LSF	Limit state function
MBD	Multi-body dynamic (model)
MC	Monte Carlo
MLE	Maximum Likelihood Estimator
MSR32	Software system for automated marshalling at Kijfhoek
NTNT	No tan-no tank collision. Collision between two regular wagons
OTIF	An intergovernmental organization dedicated to international rail transport
PDF	probability density function
PP-plot	Probability -Probability plot
QQ-plot	Quantile-Quantile plot
QRA	Quantitative Risk Assessment
TNT	Tank-no tank collision. Collision between a regular wagon and a tank wagon.
TT	Tank-tank collision. Collision between two tank wagons.
UIC	the International Union of Railways
UN	United Nations

Distributions

Bernoulli	$Bern$(probability (p))
Discreet Uniform	U_d(start value, end value)
GPD	GPD(location (μ), scale (σ), shape (ζ))
Gumbel	G(location (μ), scale (β))
Lognormal	L(shape (σ), location (θ), scale (m))
Normal	N(mean (μ), standard deviation (σ))
t-distribution	t(location (μ), scale (σ), shape (ν))
Weibull	W(shape (k),location (u), scale (α))

1. Introduction

Kijfhoek is the largest train marshalling yard in the Netherlands. The yard is located in the community of Zwijndrecht, which is just south of Rotterdam. Kijfhoek is one of the most important connections for the transport of goods between the Port of Rotterdam and the rest of Europe, mainly Germany. The marshalling yard at Kijfhoek covers an area of about 50 hectares and counts a total of 43 allocation tracks (ProRail, n.d.-a). The marshalling is performed entirely automatically and is called the 'Humping process' because the wagons roll down a hump by utilizing gravity. Specially designed rail brakes and switches guide the wagons with the desired velocity to their dedicated allocation track.

ProRail, the operator at Kijfhoek, handles over 160.000 thousand freight wagons per year, of which about 64% are tank wagons. Tank wagons possible contain Dangerous Goods (DG), which in case of an accident can lead, in the worst-case scenario, to a catastrophic event with many casualties. Therefore, the safety regulations concerning the handling of Dangerous Goods are rather strict and governed internationally[1] by an intergovernmental organization dedicated to international rail transport (OTIF). Originally, this organization has been active since 1893 but is elaborated by the convention of 1980 and obtained its official legal instruments in 1999. Since 1999, the organization has been very active, and the regulations regarding Dangerous Goods are still being updated frequently, with the latest version of regulations dating to the 1st of January this year (OTIF, 2021).

Since 1995, Dutch legislation requires risks assessments for the transport of Dangerous Goods via land. However, the current law for the required safety assessment for institutions handling Dangerous Goods and transport via rail dates back to 2004 (Ministerie van Justitie en Veiligheid). Since then, an extensive calculation method ("Bevi"[2]) considering "External Safety" (ES) is provided by the government for performing a Quantitative Risk Assessment (QRA), which has a separate section specified to rail emplacement yards (SAVE, 2006).

In this specific section for rail emplacements (SAVE, 2006), there are eight different scenarios to be considered, of which one is referring to the humping process. The deterministic failure frequency allocated to this section is relatively high. It includes shunting that used to be a process at which a specially designed locomotive (Shunter) drives against a freight wagon generating an impulse to allocate the wagon to the desired track. However, this shunting process is since 2005 no longer permitted due to the higher probability of incidents. According to the regulations, it is allowed to deviate from the failure frequencies, provided approval is obtained from the 'Human Environment and Transport Inspectorate (ILT)'. Specifically for the humping process, ProRail deviated (with the inspection's approval) from the provided calculation method in their QRA assessment (SAVE, 2009).

Furthermore, ProRail assumed that a rear-end collision in the humping process could not lead to Loss of Containment (LOC)[3] of a DG because the velocities were too low. However, in January 2011, a rear-end collision on the allocation track during the humping process caused a large ethanol fire, fortunately not leading to any casualties. An independent investigation

[1] Most European countries have their own regulations and calculation methods regarding Dangerous Goods, but they are all closely related to the international regulation provided by OTIF, as well as the European Standards.

[2] Bevi – Besluit externe veiligheid Inrichtingen, means Decree External Safety for institutions

[3] Loss of Containment is defined as a leakage of a gas or fluid

(Vrijling et al., 2012) resulted in a change of operations at Kijfhoek, and after that, the probability of another similar accident was deemed negligible. However, since then, several other incidents have led to multiple investigations into the safety of the emplacement. More specifically, four incidents in 2018 initiated an investigation performed by Crisislab (Helsloot et al., 2019), and the emplacement was put under the supervision of the ILT (Lamé, 2018). For the ILT to withdraw its supervision, Kijfhoek has to fulfil specific requirements; amongst others, a further inquiry into the safety of the automated humping process.

Considering the incidents mentioned above, the investigations and the ILT's requirements, this thesis focuses on the rear-end collisions in the automated humping process, using a reliability-based approach. The knowledge of reliability-based analyses was already available in 2005. However, it was not implemented in the calculation method regarding External Safety. Although the current method is risk-based, the origin of failure frequencies is unclear and deterministic. Moreover, these frequencies are based on incidents dating back to pre-1995. Kok-Palma and Timmers already suggested in their study (2014) that a new design method is necessary for a more up to date assessment in the transport of dangerous goods. Unfortunately, their study provided little data specific to rail emplacements, and only a few suggestions are offered in this area.

In his investigation into train collisions, Scholes (1987) stated that energy absorption is of "primary importance" in designing crashworthy structures. With the uprising of computers at the time, it became possible to follow an energy-based approach. Since then, many investigations into train collisions have been based on energy management. A rather extended overview of these studies is published by Zhu et al. (2020). Most of the literature is focused on passenger trains, with collisions into a fixed barrier (Sun et al., 2011, 2012; Xu et al., 2019) or into similar trains (Li et al., 2016; Lu, 1999, 2002; Xu et al., 2019). The results from Lu (2002) showed a simple relation, correlated to the front wagon's initial kinetic energy, to find the amount of energy absorbed at different interfaces in a collision. Xu et al. (2019) discussed that the number of carriages, the mass, and the plastic deformation force influences energy absorption. He used linear regression to improve Lu's simple relation and included the number of carriages and the plastic region's mean force. However, none of these studies proved a relation for the rather specific situation at Kijfhoek, where it concerns freight and tank wagons, and collisions could happen in many different configurations of different wagon types with different energy absorption capacities and different masses.

1.1 Aims and research questions

This study aims to find the probability of loss of containment of Dangerous Goods affecting External Safety (LOC_{ES}) in rear-end collisions in the automated marshalling process at Kijfhoek. The maximum forces and energy absorption at each interface are determined with a multi-body dynamic (MBD) model combined with a probabilistic approach. Next, the damage levels resulting from the dynamic model are assessed. Finally, with the results of the probability assessment at Kijfhoek, a simplified calculation method is created to determine the probability of failure. This simplified method is recommended for use at other automated marshalling yards.

Main research question

How can the present Dutch design guidelines for 'External Safety', to calculate the loss of containment in automated marshalling, be improved through a reliability-based analysis, focusing on rear-end collisions based on the study case at Kijfhoek?

Sub-questions

1. What is the probability that Loss of Containment of Dangerous Goods affecting External Safety occurs due to rear-end collisions on the allocation track during the automated marshalling process at Kijfhoek?
2. What is the impact velocity that leads to Loss of Containment?
3. Is there a simplified relation in which the energy absorption at an interface can be determined?
4. How can the study case at Kijfhoek be transferred to a standard for other automated marshalling yards?
5. To what extent does the automated humping process affect the overall External Safety, considering the other processes at the yard?

1.2 The outline of this thesis

This thesis consists of six Chapters. In the second chapter, a case description is presented, explaining the situation, the systems, and the processes at Kijfhoek. Furthermore, it elaborates on the current calculation method to determine External Safety. The third chapter contains the theoretical framework, explaining the relevant theories necessary for the analyses in this thesis. The reliability-based assessment is performed in the fourth chapter using a Monte Carlo simulation, with all the relevant parameters explained. In the fifth chapter, the sensitivity of the parameters and the dependencies between the parameters of a simplified model is investigated. Finally, the last chapter concludes the main findings and answers the research questions, followed by recommendations for further study.

Disclaimer: This thesis focussed predominantly on determining the probability of damage to tank wagons, and to get to the probability of LOC affecting External Safety, assumptions were necessary. Although the results in this thesis were determined with utmost care and dedication, no rights may be derived from it.

2. Case description

Kijfhoek, located just south of Rotterdam in the town of Zwijndrecht, is the largest freight train assembling yard in the Netherlands (see Figure 2.1). It stretches over about 2.5 kilometres with a total area of around 50 hectares. Kijfhoek forms the most critical connection between the Port of Rotterdam and the rest of Europe to transport goods via rail (ProRail, n.d.-a); its strategic location next to the 'Betuwe Route' ensures quick handling of the goods. The yard is operated and maintained by ProRail. ProRail manages the railway tracks in the Netherlands and is responsible for the safety, maintenance and renewal of 7,000 km of tracks; furthermore, it builds and oversees the regular Dutch railway stations (ProRail, n.d.-b). Operating a marshalling yard is, therefore, not strictly part of ProRail's regular procedures.

Figure 2.1: The location and an aerial view of Kijfhoek (Google, n.d.; photo: Via078, n.d.)

ProRail marshals over 600 wagons per day at Kijfhoek. The wagons are pushed onto a hill, after which the wagons roll off the other side through gravity to one of the 43 allocation tracks. This process is called humping due to the hump in the middle of the yard.

About 65% of the marshalled wagons are tank wagons, possibly containing dangerous goods. By Dutch law (Ministerie van Justitie en Veiligheid, 2004), institutions handling dangerous goods are required to comply with the regulations regarding 'External Safety', which considers the safety of the public outside the boundaries of these institutions. The government also provides the calculation method to determine these risks, expressed in Site-Specific Risk and Group Risk, further elaborated in section 2.3.

The following sections in this chapter first describe the different types of wagons handled at Kijfhoek, followed by a detailed explanation of the system and the processes at Kijfhoek. Furthermore, it elaborates on the current calculation method for assessing the External Safety of marshalling yards in the Netherlands and is finalized by a brief statement of the main problem, regarding External Safety, at Kijfhoek.

2.1 Wagons

Prorail moves many different types of wagons at Kijfhoek. All these wagons have other demands and, therefore, have various specifications. Appendix A lists different types of wagons, their European classifications, and the International Union of Railways (UIC) number coding. More information is found in the product guide of DB-cargo (2011).

Dangerous Goods are carried in tank wagons, and different categories of DG require different requirements and levels of safety. Therefore, there are many different types of tank wagons, but they all look similar from the outside. A typical tank wagon and its dimensions are shown in Figure 2.2. This thesis' probabilistic model distinguishes between a tank wagon and other 'regular' wagons. Side buffers protect the wagons on the longitudinal ends. Buffers are elements capable of absorbing energy.

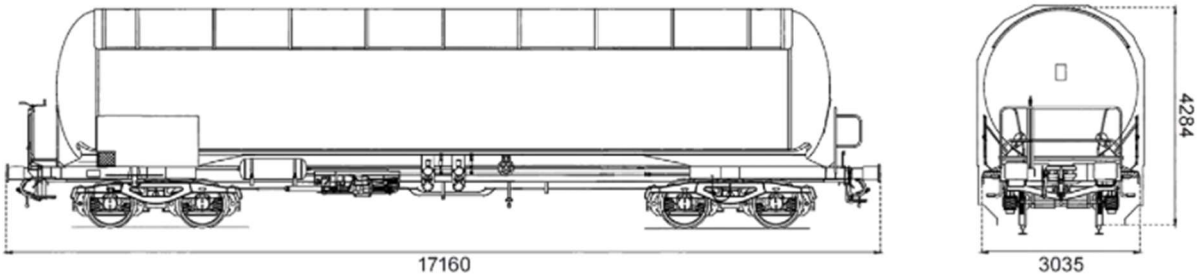

Figure 2.2: Typical tank wagon for the carriage of LPG or Ammonia (4-Axle Tank Wagon for Ammonia | Greenbrier, n.d.).

2.2 Systems and process description at Kijfhoek

The following paragraphs use the Horvat reports (De Loor et al., 2019; Vrijling et al., 2012) and a report provided by ProRail (Lenssen, 2018) to describe the systems and processes.

2.2.1 The systems description

This Paragraph describes the critical systems that ensure smooth and safe handling of the wagons during their stay at Kijfhoek. An aerial view in the figure below shows the long-stretched emplacement divided into four different sections: The 14 arrival tracks, the hump, the allocation tracks, and the departure tracks.

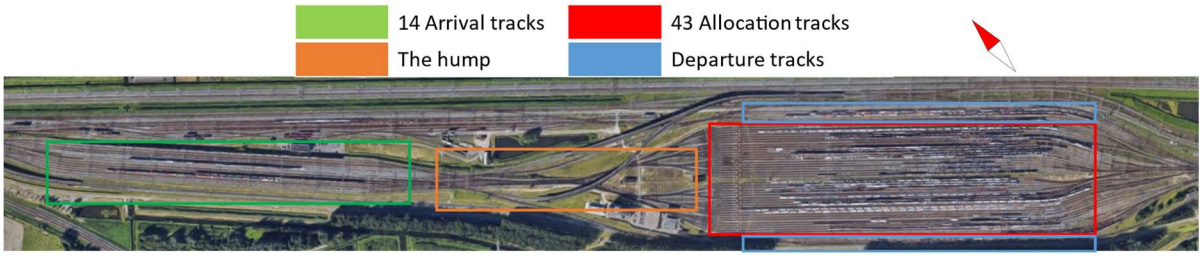

Figure 2.3: Aerial view of Kijfhoek (Google, n.d.).

The arrival tracks are accessible from the North and the South end of the emplacement; Figure 2.8 shows a traffic flow diagram. Tracks leading to the arrival tracks contain a weighing system to measure each wagon's weight. The planning system 'KijfDIS' needs this information. KijfDIS is the planning software to allocate the wagons to the desired Allocation track; it contains all the necessary information on the wagons and their destinations. It shares and provides these data to the control system named MSR32. The software MSR32 runs the automated humping process. It controls the brakes, the switches and also the clearance- and joining system on the allocation track.

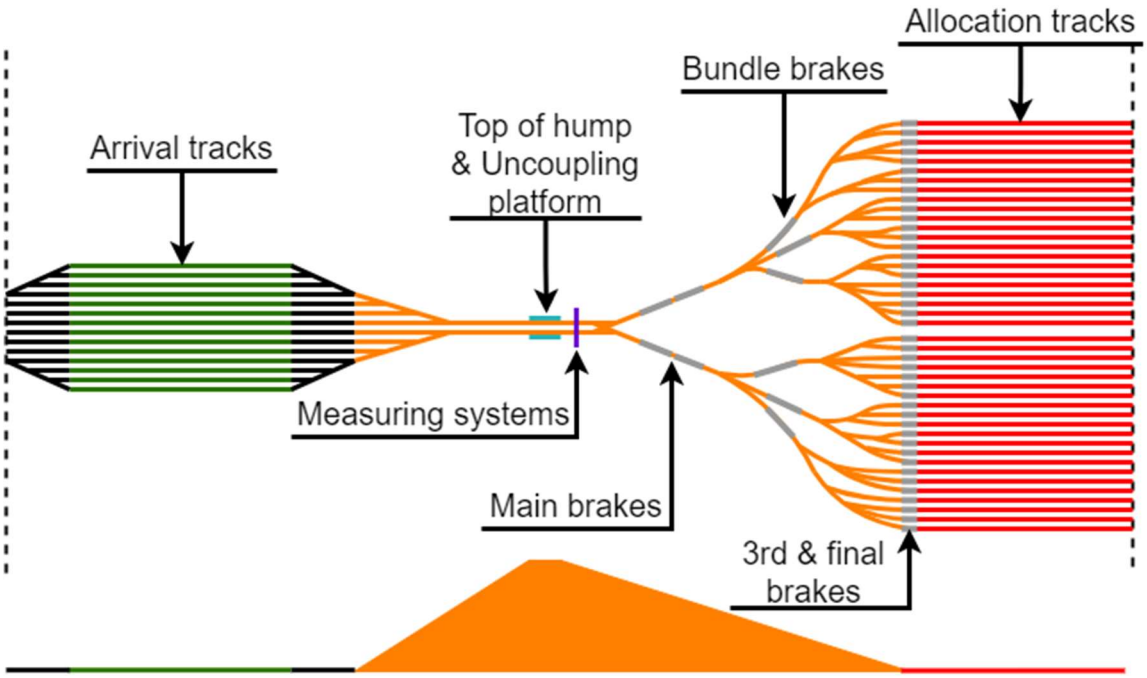

Figure 2.4: Schematization of the essential systems regarding the humping process.

Besides the information from the planning system, MSR32 needs information from the measuring systems to predict the run-offs' velocities and to determine the braking force. A run-off is defined by a wagon, or a set of coupled wagons, running down the hump to the desired allocation track.

Measuring systems

The measuring systems on top of the hump, as Figure 2.4 shows, contain four different elements:

1. The weight sensors determine the weight of each run-off.
2. A laser checks if wagons are coupled or uncoupled and verifies the number of wagons in a run-off provided by the planning system.
3. A measurement device determines the shape of the wagon and the susceptibility to the wind.
4. A weather station measures the wind direction, the wind speed, and the temperature.

All together, MSR32 provides a better estimation of the run-off's velocity.

The brakes

A run-off encounters three brakes on its way to the allocation tracks; the brakes consist of steel beams squeezing the wagons' wheels against the rail, creating friction and hence the braking force. The three brake types, shown in Figure 2.4, are:

1. The two main brakes consisting of two segments of four sections, totalling eight sections controlled separately. The brakes have a total length of about 27 meters and brake the wagon on both rails to provide enough braking force. Figure 2.5 schematizes a segment of brakes.
2. The six bundle brakes are only one segment of brakes consisting of five sections, and they are about 16.5 meters long, again applying force on both rails.

3. The final brakes on each of the 43 allocation tracks only brake the wagon at one of the rails (so only on one side of the wagon). The brakes consist of four separate sections and are 12.5 meters long.

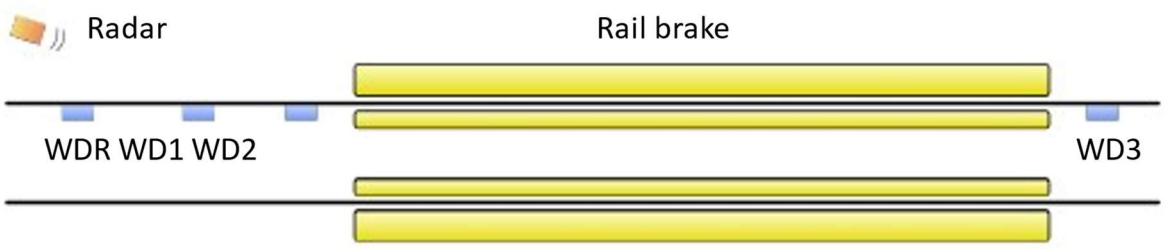

Figure 2.5: Schematization of the brakes (Lenssen, 2018)*, here the brakes are shown on both its track rails.*

The above figure shows a schematization of the braking system. Once a wagon is detected by the wheel detector WDR, the radar starts measuring the velocity of the run-of. Following these radar measurements, the control system continuously updates the braking force. Furthermore, the axle detectors WD1 and WD2 measure the initial velocity as a check on the radar system. At the same time, WD2 and WD3 form a sector loop to detect whether a run-off is inside the braking area. Once the run-off has passed WD3, the radar is switched off. WD3 can be used as a velocity measuring device as a final check on the radar measurements.

The switches

MSR32 also operates the switches; the switches direct the wagon to the correct allocation track. The system can change a switch in an average of half a second, enabling the system to redirect a wagon quickly if it detects a possible rear-end collision within the brakes.

The pushing systems

At the allocation tracks, multiple systems finalize the automated humping process. The diagram in Figure 2.6 is a schematization of these different elements. Once the run-off has left the final brakes, the “clearance system” pushes the run-offs, if needed, further forward onto the allocation tracks, clearing the track for the subsequent potential run-off. The pushing system consists of two small carts between the rails connected to a steel rod and a winch. The carts are equipped with small retractable arms; when extended, the arms push against a wagon’s wheels. Further on the allocation track is the “joining system”, which operates similar to the clearance system, except for its function is to combine the separate run-offs to form a train.

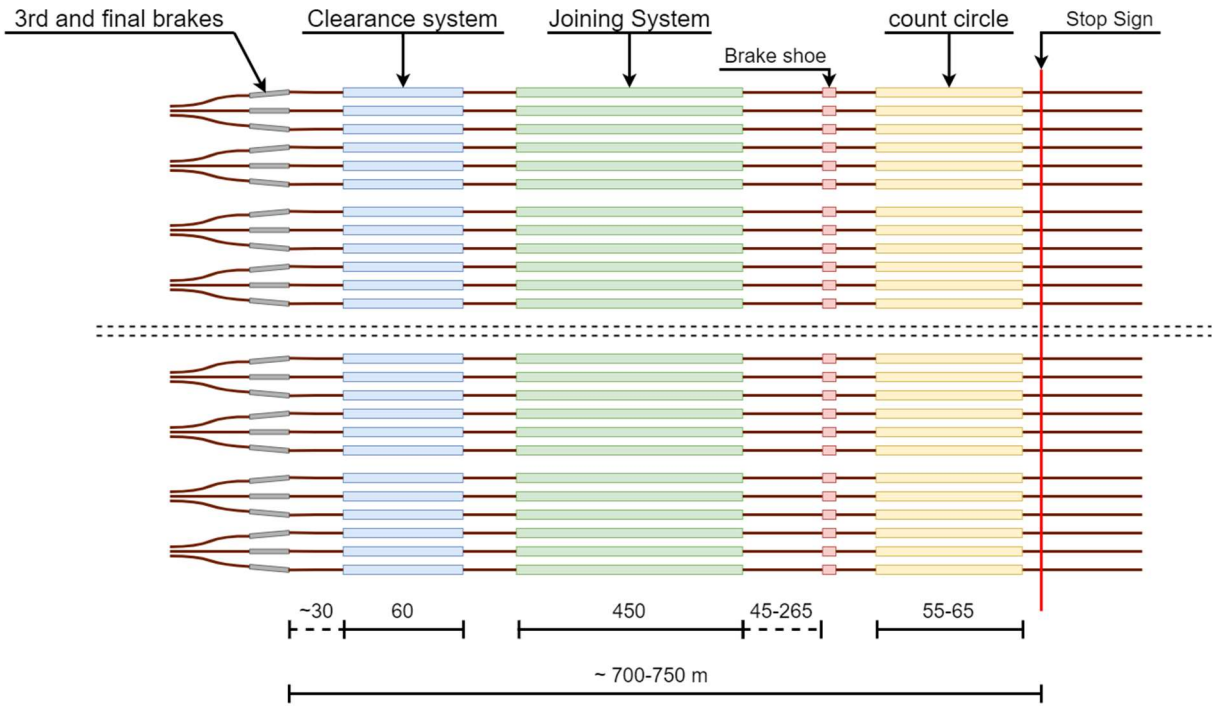

Figure 2.6: Diagram of the elements on the allocation track.

The brake shoe

The brake shoe's task is to prevent the wagons from moving through the stop sign at the end of the tracks. Figure 2.7 shows pictures of a brake shoe. It brakes the wagons utilizing sliding friction between the track and the shoe. The magnitude of the friction force is directly related to the normal force of the front axle.

Figure 2.7: The brake shoe at the end of the allocation tracks (Hendrikx, 2019).

The 'count circle'

A 'count circle' is a simple system of two separate axle detectors at each end of this 'circle' (section), counting the number of axles between these detectors. This system aims to prevent the wagons from rolling through the stop sign at the end of the tracks. Once a wagon passes the last wheel detector, the traffic control leader receives a warning, and the system automatically interrupts the joining system. The protocol requires the wagons to be pushed back in front of the count circle before he may restart operations.

2.2.2 Process description at Kijfhoek

This paragraph describes the processes from arrival to departure at Kijfhoek. An information graphic regarding the processes is found in Appendix B. The figure below shows the traffic flow in a simple schematization; together with Figure 2.4, they clarify the processes described below.

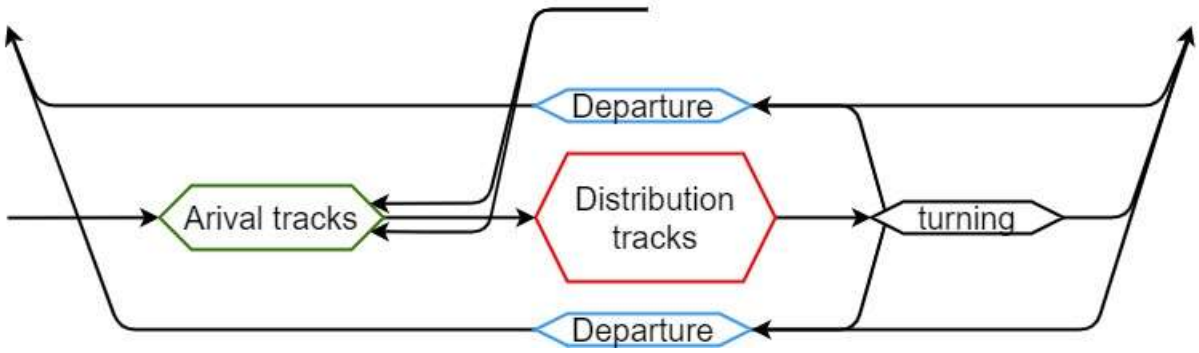

Figure 2.8: Schematization of the traffic flow and the different sections at Kijfhoek.

Arrival process

Arriving trains park their wagons at one of the 14 arrival tracks at the North-side of the emplacement. They are accessible from both the North and the South. The tracks leading to the arrival area are equipped with a weighing system, measuring each wagon's weight. Staff members check the arrived wagons for any irregularities that could interrupt the humping process (e.g. damages). All necessary information on the arrived wagons is now available in the electronic traffic planning system. The planning system uses the wagons destination and the wagons' weight to make a detailed plan for the humping process. The wagons stay coupled until they reach the top of the hump. Wagons with the same destination stay coupled during the whole humping process and thus form a run-off unless their total weight or length exceeds 360 tonnes or 80 metres. If either of these restrictions is exceeded, the relative run-off will be split. Once the plan is completed and no abnormalities occurred, a staff member drives a unique diesel locomotive behind the wagons. The train is now ready for the humping process.

Humping process

The driver of the diesel locomotive hands over the controls of the locomotive to the traffic process leader; the locomotive is now automatically controlled by the system. The system now pushes the train onto the hump with a velocity of around $1.5\ m/s$. On the top of the hill platform, a staff member uncouples the separate run-offs while the train is still moving. The run-off's weight is measured one last time before it runs down the hump to one of the 43 allocation tracks.

On its way down the hill, the run-off passes numerous automated switches and three sets of brakes. Just before and during braking, a radar measures the velocity. The system's algorithm determines the braking force using the velocity and mass of the run-off. It alters the force if the velocity from the radar is not the same as the algorithm predicted. The system is designed so that the run-offs exist the final brakes with a velocity of $1.5\ m/s$, the so-called 'Exit'-velocity.

On the allocation track, there is an automatic clearance system, followed by the joining system. If the run-offs Exit-velocity is below $1.5\ m/s$, the clearance system pushes the run-offs down the first 70 m of the allocation track. The joining system pushes the various run-offs together against the brake shoe at the end of the track.

Departure

Once all run-offs have arrived on the allocation track, the joining system pushes all the wagons against the brake shoe. A staff member couples the various run-offs and checks the wagons and their loads for irregularities. The individual brakes of the separate wagons are

activated and tested. After the wagons' inspection, a train driver attaches a locomotive to the front of the wagons. For the electrified allocation tracks, the trains are ready to leave for departure. For some unelectrified tracks, a diesel locomotive takes the train to the departure tracks, and the train leaves from there after changing to an electrified locomotive.

2.3 Calculation method for determining External Safety

The calculation method requires a Quantitative Risk Assessment to determine the probability of Loss of Containment of Dangerous Goods specific to certain sections within the institution. The calculated risk quantities are then used in a software model called 'Safeti-NL', which determines the consequences by modelling the spreading of the Dangerous Goods in the surroundings. This software package eventually determines the Site-Specific Risk and Group Risk.

- Site-Specific Risk is governed by the probability of one person dying because of an accident considering Dangerous Goods. This risk may not be greater than one in a million per year (10^{-6}), and is expressed by probability contours around the institution. In principle, it means that the 10^{-6} contours should not extent to other establishments or residential areas. Figure 2.9 shows the Site-Specific risk contours for the Kijfhoek emplacement, calculated using the calculation method (SAVE, 2009).
- Group Risk is governed by relating the number of fatalities in case of a disaster (Rijksoverheid, n.d.) and is expressed in a FN-curve (an FN-curve displays the cumulative frequency F of the number of fatalities N, as a function of N). The target reliability for Group Risk is $10^{-3}/N^2$ per year. Figure 2.10 shows the results for Kijfhoek calculated in 2009.

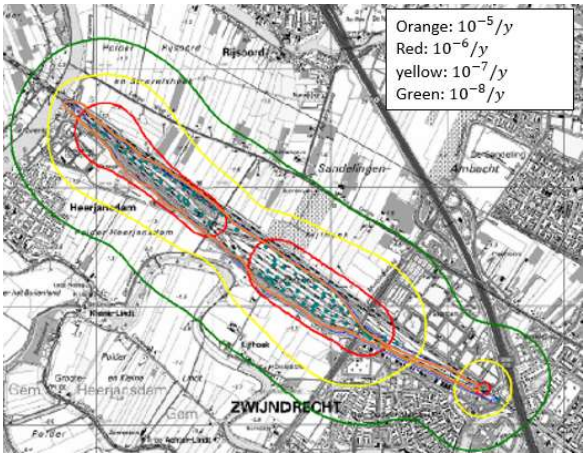

Figure 2.9: Risk contours of the results regarding Site-Specific Risk at Kijfhoek. The red contour may not extent to residential areas (SAVE, 2009).

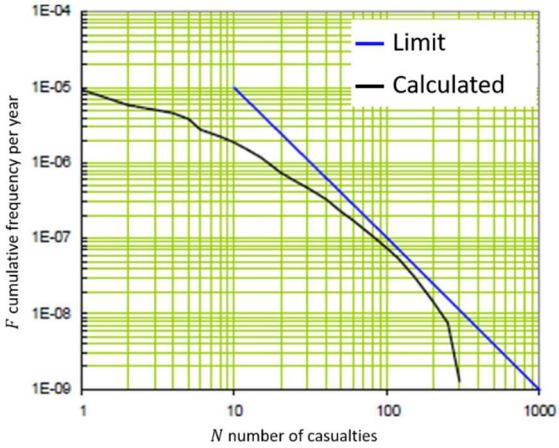

Figure 2.10: FN-curve of the group risk calculated using the Software Safeti-NL (SAVE, 2009).

'Safeti-NL', is not further investigated or used in this thesis, and the rest of this section focusses on the QRA in determining LOC.

The targets for the QRA are risk-based (Site-Specific and Group Risk) and in terms of failure probabilities and the number of fatalities. Providing results in a manner of quantifiable risks may suggest a reliability-based assessment as the basis of the calculation method. However, the assessment is deterministic, and the emplacement's reliability remains ambiguous.

The 'disclaimer' of the calculation method clearly state that, with the use of their method, the correctness of the results are certainly not guaranteed, since there are no specific failure

values for marshalling emplacements and deviation of an 'average' emplacement is likely, without even specifying what 'average' means (SAVE, 2006).

2.3.1 The QRA

Before examining the deterministic values further, it is necessary to describe the setup of the QRA. In this QRA, not all Dangerous Goods are considered a risk to External Safety, and a distinction is made into six different types of DG affecting External Safety. Table 2.1 shows the different categories with some examples. Institutions handling Dangerous Goods need to document them properly.

Table 2.1: List of DG categories and their index number, also some examples are given.

DG Category		Examples	Danger index nr.
A	Flammable gas	Propane or butadiene	23, 263, 239
B2	Toxic Gas	Ammoniac	268, 26,265
B3	Very Taxic Gas	Chlorine	268 (UN1017)
C3	Very flammable liquid	Hexane	33, 33*, X33*, 336
D3	Toxic liquid	Acrylonitrile	336(UN 1093)
D4	Very toxic liquid	Hydrogen fluoride or Acrolein	66, 663, 668, 886, 88, X886

Furthermore, the QRA distinguishes eight different scenarios for which a failure frequency needs to be determined. The eight scenarios are listed in Table 2.2 together with their deterministic failure probabilities. These probabilities are used in further calculations described in Appendix C. The calculation for scenario six, the humping process, which is of interest in this thesis, is as follows:

$$F_{humping} = F_{basic} * P_{leakage} * N * P_{leak,type} * \left(P_{flame}\right) \quad 2.1$$

In which $P_{leakage}$ describes the probability of a leak given an incident, N the number of wagons in category A-D, $P_{leak,type}$ describes whether the leakage is instantaneous or continuous and P_{flame} describes the probability for flammable goods and how they set fire, The values to be used in the QRA are found in Appendix C.[4]

[4] The leakage probability, $P_{leakage}$, is multiplied by a factor 0.1 in the Government's method, because it is assumed that only 10% of the cases are important for External Safety. This assumption may be counted double since N is only considering tank wagons in the calculation, but this is unclear.

Table 2.2: Failure scenarios and their generic failure frequencies used in the QRA for External Safety (SAVE, 2006).

		F_{basic} (failure frequency per interaction)
1	Interaction of trains with ongoing traffic during arrival and departure	5.50E-07 per train
2	Interaction of trains (A/D) with the emplaced trains	2.12E-05 per train
3	Unilateral accident	2.75E-05 per train
4	Interaction with the locomotive and the trains on the emplacements	1.00E-06 per locomotive change
5	Incidents through reordering	2.12E-05 per train
6	Humping process (automated)	1.76E-05 per wagon
7	Intrinsic Failure	5.00E-07 per wagon per year
8	Warm Bleve	3.10E-07 (see Appendix C)

Furthermore, the emplacement must be divided into sections at which accidents could occur, these sections are either 100x100 m or 25x25 m. In total, the emplacement at Kijfhoek was divided into 74 sections, of which about 40 are located on the allocation tracks. A probability for LOC of 10^{-8} for a scenario per section per year is considered negligible, and no further calculation is necessary. If a potential incident has equal probability anywhere on the allocation tracks, the negligible probability for LOC on the allocation tracks is $40x10^{-8}$ per year.

2.3.2 The problem with the Government's proposed approach

Several problems arise with the Government's proposed QRA assessment for emplacement.

1. As specified in the method, the failure frequencies of points 1-5, 7 and 8 are not specific for rail emplacements.
2. The basic frequencies are deterministic, no matter what risk-reduction methods are applied at a specific emplacement.
3. The frequencies are based on incidents dating back to pre-1995 (Y.S. Kok-Palma & P.G.J. Timmers, 2014). Especially significant for the automated humping process, which have improved massively since then, and it includes the Shunting process which is banned in Europe since 2005.
4. The failure frequency for scenario 6 is described as a probability of an 'irregular event'. Without specifying the word irregular, or what irregular events are. Scenarios 1-5 it at least specifies the probability of a collision, although not at which velocities or what exactly is considered a collision. Furthermore, the probability of leakage used in the collision scenarios is the same as for an 'irregular event'.

The proposed QRA method allows emplacements to deviate from the calculation method, provided that approval is obtained from the inspectorate. However, without being more specific in the current method, it is difficult to determine in which areas deviation from the method is beneficial and accepted.

Structural design codes often provide a Level-I method using several (partial) safety factors, depending on a Reliability Index, which in turn describe the reliability of the design. Although, determining a structures safety using a level-I method is not a full-probabilistic approach, the explanation of the safety factors often describes under which circumstances

they need to be applied, and the user of the manual gets inside in the background of the approach. This background is important because one can determine the relevance of certain parameters in specific situations, and where deviation from the method is possible. This is exactly what is lacking in the current QRA for External Safety since it only provides generic failure probabilities without any background information. Furthermore, safety factors can provide insight into areas in which risk-reduction measures are beneficial.

2.4 The problem at Kijfhoek

Since the ethanol fire in 2011, the national and local authorities are on top of the processes and safety at Kijfhoek, and since 2018, Kijfhoek is under the supervision of the 'Human Environment and Transport Inspectorate' (Lamé, 2018). The main issue is the comprehensibility of the calculations determining External Safety. ProRail is unable to prove, with enough certainty, that Kijfhoek is safe enough. Over the last ten years, several external agencies, including Horvat & Partners, could ***not*** prove that the systems at Kijfhoek were unsafe. However, all of them concluded that the transparency and knowledge regarding the safety at Kijfhoek should be improved.

The ILT demands a safe enough automated process as one of the requirements before lifting its supervision. From 2006-2009, SAVE, in name of ProRail, performed a QRA according to the prescribed calculation method at Kijfhoek (2009). However, for the automated humping process scenario six, they decided to deviate from the method. They assumed that rear-end collisions in the automated process could only lead to LOC if velocities above $11\ m/s$ were reached, and this probability was calculated at 10^{-1} per year, negligible for further calculation. However, the 2011 incident and several other incidents showed that LOC can occur at lower velocities, and the primary assumption is proven false. This does not necessarily mean that the overall External Safety is at risk.

This thesis focuses on rear-end collisions on the allocation track during the automated process, using a reliability-based analysis. And aims to find improvements for the calculation method.

3. The theoretical framework

This chapter presents an outline of the investigation and the methods used in this thesis. First, the investigated problem is elaborated. Second, some theory about energy dissipation in a collision is presented. Third, the dynamic model is explained, justified, and verified. Finally, the approach used to determine the probability of damage in a rear-end collision is explained.

3.1 The investigated rear-end collisions

This thesis limits its investigation to the collisions on the allocation track. The allocation tracks are straight, resulting in a 'straight' collision, which allows for a model in one dimension. Figure 3.1 shows a schematization of such a collision.
At Kijfhoek, the number of wagons, their masses and types vary constantly. The run-off can consist of up to 5 wagons, whereas the wagons of the already allocated wagons can consist of about 28 wagons. All these variations result in many different configurations in case of a possible collision. Moreover, different buffer types, explained in section 4.4.2, need to protect the wagons from damage.

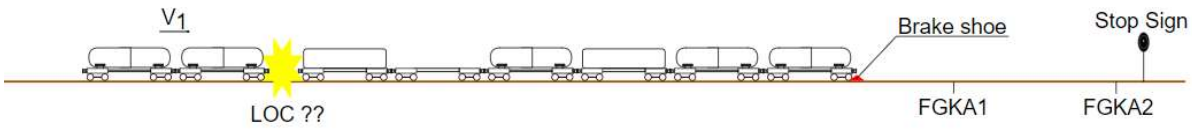

Figure 3.1: A schematization of the collision on the allocation track and the situation at Kijfhoek.

For a collision to happen on the allocation track, a run-off must have an impact velocity much higher than the systems designed Exit-velocity ($1.5\ m/s$). Several causes could lead to a high Exit-velocity and the fault tree in Figure 3.2 shows most of them. This thesis limits itself to the 'normal' operations, obviously it is not normal that a run-off has a too high Exit-velocity, but sometimes errors occur under regular operations of the system, such as wagon measuring errors, radar errors, software errors, sloshing of a fluid or factors affecting the braking performance, such as greasy wheels or bad weather. Human errors caused the fire incident in 2011 and another incident in 2018, and these are not considered 'normal' operations. The data provided by ProRail is from 2012-2020, and these are considered normal operations apart from the incident in 2018. From this data, the probability of a high Exit-velocity is determined, ***not*** by assessing the events in the fault tree.

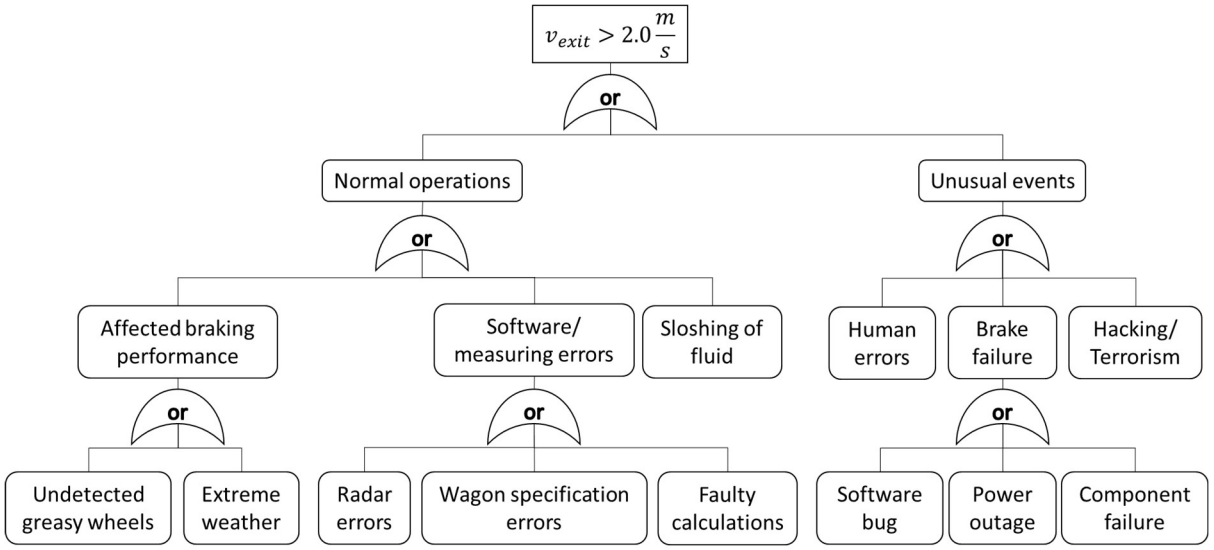

Figure 3.2: Fault tree leading to a high Exit-velocity. This thesis limits its investigation to normal operations.

A high Exit-velocity does not automatically lead to LOC of Dangerous Goods. Going from a high Exit-velocity to LOC is explained by an Event tree in Figure 3.3. The events are investigated in this thesis to determine the probability of LOC of Dangerous Goods due to rear-end collisions, considering External Safety on the allocation track. The event tree also shows where the description of each event's probabilities is found in this document. The probability for LOC considering DG with the risk of affecting External Safety is estimated by multiplying the probabilities in Figure 3.3 and summing over the six different DG categories explained in section 2.3.1.

$$P(LOC_{ES}) = P(v_{exit} > threshold) * P(collision)P(D|v_{exit} > threshold)P(DG)\sum_{i=1}^{i=6} P_i(leakage)P_i(cat.) \quad 3.1$$

In which $P(v_{exit} > threshold)$ represents the probability that a run-off has an Exit-velocity higher than a chosen threshold. $P(collision)$ represents the probability that a run-off runs into a stationary wagon, $P(D|v_{exit} > threshold)$ represents the probability of damage to a tank wagon given an Exit-velocity above the chosen threshold, $P(DG)$ the probability of the given tank wagon containing a dangerous good. $P_i(cat.)$ represents the probability that a Dangerous Good is one of the DG categories, i, from Table 2.2 constituting to External Safety. $P_i(leakage)$ represents the leakage factor per category, describing the probability that the damage is severe enough to result in Loss of containment.

High exit velocity P(v>threshold)	Collision with a stationary wagon P(collision)	Damage to a tankwagon P(D|v>threshold)	Contains a Dangerous Good P(DG)	Damage leads to leakage/LOC P(leakage)	DG concerns External Safety P(cat.)	Result LOC considering ES $P(LOC_{ES})$
From data, Section 4.1	From reports, Section 4.4.5	Simulation of collision section 4.5 & Ch. 5	From data & MC-sim. Section 4.2.4 & 4.6.1	From literature Section 4.6.1	From data & MC-sim. Section 4.2.4 & 4.6.2	Result Section 4.6.2 & Ch. 5

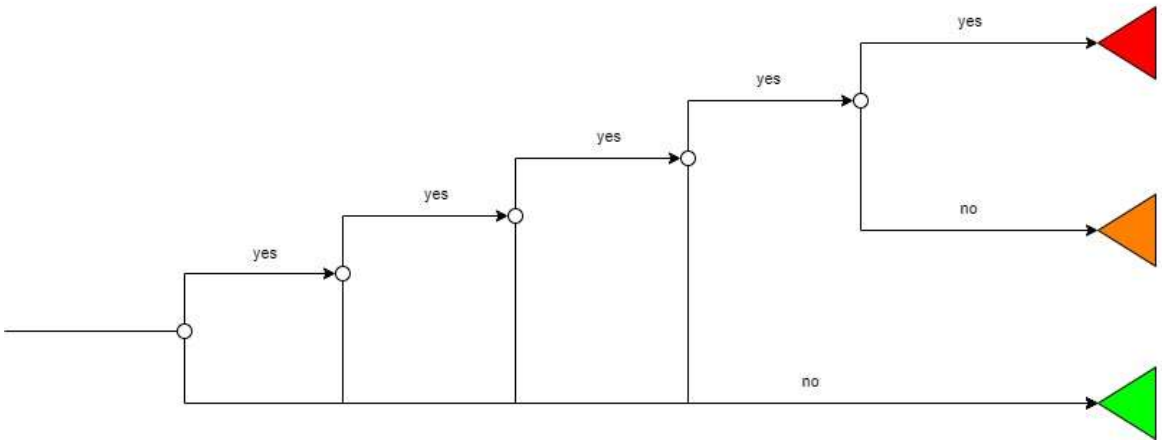

Figure 3.3: Event tree, starting with a high Exit-velocity leading to LOC, the red triangle is LOC considering External Safety, the orange triangle is LOC not considering External Safety and at the green triangle there is no LOC.

In the literature, damage in a collision is often investigated through energy absorption ($E_{absorbed}$) in a collision. This absorbed energy is then compared to the energy absorption capacity ($E_{absorption\ capacity}$) of the absorbing elements, such as buffers. Both these variables depend on other stochastic variables, and a combination of these variables could lead to damage. In a reliability analysis, the reliability is investigated by means of a failure probability. The probability of wagon damage is the probability that the absorbed energy is higher than the absorption capacity:

$$P(D) = P(E_{absorption\ capacity} < E_{absorbed}) \quad 3.2$$

In this study the reliability of the system against a rear-end collision on the allocation track is investigated using a Limit State Function (LSF), described with the letter Z:

$$Z = E_{absorption\ capacity} - E_{absorbed} \quad 3.3$$

When $Z < 0$, there is damage to a wagon.

3.2 Energy dissipation

Many investigations into train collisions are performed in literature over the last decades; most of these studies involve passenger trains. Zhu et al. (2020) provides an overview of many papers focusing on collision energy management. The overall consensus of these papers is similar; design the energy-absorbing parts and the vehicles' structure to orderly control the forces and deformations in a collision (Zhu et al., 2020). He further categorized these papers into the following different approaches to solving the problem at hand:

1. Theoretical study of collision dynamics,
2. Finite element models (FEM),
3. Multi-body dynamic model,
4. Test analysis.

A list of each method's advantages and disadvantages (Zhu et al., 2020) is found in Appendix D. The approach used in this dissertation is a non-linear MBD model, explained in section 3.3.

Wagons that run off the hill at Kijfhoek contain kinetic energy ($E_k = 0.5mv^2$) and momentum ($p = mv$). Through the well known physical laws for conservation of momentum and conservation of energy, Scholes (1987) and Scholes and Lewis (1993) derived what they called the collision energy:

$$E_{\mathrm{C}} = \frac{M_1 M_2}{2(M_1 + M_2)}(v_1 - v_2)^2 \qquad 3.4$$

In which M_1 and M_2 are respectively the masses of the two objects (in this case trains) colliding; v_1 and v_2 their respective velocities.

The collision energy in rear-end collisions on the allocation track is the energy transfer from the original run-off's kinetic energy into other forms of energy. One could call this the dissipated energy. For instance, these other energy forms are the energy absorbed by the wagons' buffers, the deformation of material and heat. Ideally, the buffers are designed to absorb enough energy to prevent damage to the wagons.

Lu (2002) investigated five different projects in which he simulates moving passenger trains' colliding with an identical stationary train. As a result, he was able to find a relation between the absorbed energy at the impact interface, and the kinetic energy of solely the front vehicle of the moving train; the relation is shown in equation 3.5.

$$E_{\mathrm{d}} = \frac{R_1}{2f_{\mathrm{d}}} E_{k,1} \qquad 3.5$$

E_d represents the design value of the absorbed energy at the impact interface, R_1 (=0.9) the ratio factor between the absorbed energy and the front vehicle's kinetic energy $E_{k,1}$. The number '2' assumes that both vehicles shared the same amount of energy absorption and f_d (=1,2) represents the dynamic factor. Lu (2002) further suggested that impact collisions of rakes of 3 to 4 vehicles are sufficient to present longer rakes.

The situation at Kijfhoek and other humping yards is particular and differs from what is investigated in the literature. In fact, the relation stated in equation 3.5 changes significantly under certain circumstances at Kijfhoek. Because of the differences at Kijfhoek a dynamic model is designed in this thesis and explained in the next section.

3.3 The Dynamic Model

The situation shown in Figure 3.1 is simplified to a multi-body system composed of several mass-damper-spring systems. Figure 3.4 shows a diagram of this model, and equation 3.6 describes the Equations of Motion (EOM) of this model. The wagons are modelled as lumped masses connected to massless non-linear spring-dashpot elements (Kelvin-Voigt elements). A spring-dashpot element represents the coupler in tension and the buffers in compression. Eventually, the deformation of the wagons' structure is also included in the spring-dashpot element. The EOM of this system reads:

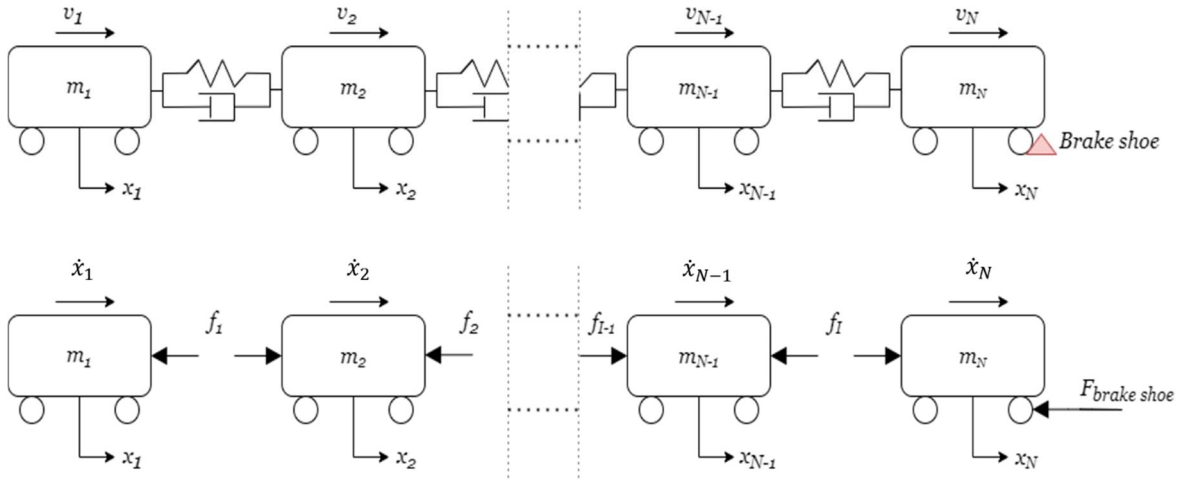

Figure 3.4 Schematization of the dynamic model that represents the collision between two trains.

$$m_n\ddot{x}_n = f_{i-1}(x_{n-1}, \dot{x}_{n-1}, x_n, \dot{x}_n) - f_i(x_n, \dot{x}_n, x_{n+1}, \dot{x}_{n+1}), \qquad for\ i = n \tag{3.6}$$

$$f_i = f_{i_{spring}}(x_n, \dot{x}_n, x_{n+1}, \dot{x}_{n+1}) + f_{i_{dashpot}}(x_n, \dot{x}_n, x_{n+1}, \dot{x}_{n+1}), \tag{3.7}$$

in which f describes the force function of a non-linear equivalent spring and dashpot, both explained in section 4.4.4, behind and in front of the wagon. The mass of the wagon is represented by m. The quantities $x, \dot{x}$ and $\ddot{x}$ represent respectively, displacement, velocity, and acceleration. The number of each wagon is given by n, and N is the total number of wagons. Whereas the number of the interfaces is presented by i; I represents the total number of interfaces and is equal to $N - 1$. The EOM in 3.6 does not apply to the first and last wagon; for these wagons, one of the two force functions drops from the equation, and the constant brake shoe force is added to the final equation.

Solving this system of differential equations is performed by transforming the 2nd order differential equations from equation 3.6 into a set of first-order differential equations by using the state-space representation. This system of first-order ODEs is solved in the time domain by using a time-stepping scheme. More specifically, 'ode45' in MATLAB (MathWorks, 2020) is used.

3.3.1 Interface force f

The interface's force function describes the non-linear elastoplastic behaviour of multiple elements: the coupler, the buffers, and the wagon's structure. The magnitude of the force depends on the stochastic nature of each of these elements and is further explained in the reliability section 4.4.

3.3.2 The brake shoe force

At the end of the allocation tracks, a brake shoe prevents the wagons from rolling through the stop sign. The brake shoe is not attached to the track and slides along the track, creating friction and braking the vehicle. The braking force depends on the front wagon's axle-load, investigated by Hendrikx (2019) in the name of Dekra Rail at Kijfhoek. The force applied by the brake-shoe to the last wagon is defined by equation 3.8.

$$F_{brake\ shoe} = \frac{\mu m_{last} g}{n_{axles}}, \tag{3.8}$$

in which μ represents the friction coefficient, g the gravitational acceleration, m_{last} the mass of the last wagon and n_{axles} the number of axles of the last wagon.

Through experimental testing and using the Coulombs friction law, Hendrikx (2019) found a friction coefficient[5] $\mu = 0.25$ for the brake shoe. Neither the track condition (wet or dry) nor the condition (old or new) of the brake shoe affects the braking capacity of the brake shoe.

The collision impact and the energy absorption of the buffers occur almost instantly, whereas the energy absorption of the brake shoe needs a long distance and time (the force of the brake shoe is relatively small compared to the forces in the buffers during impact). Because of these different time scales, the brake shoe force has minimal effect on the absorbed energy at the interfaces. Therefore, the friction coefficient and the number of axles ($n_{axles} = 4$) are considered deterministic.

3.3.3 Justification and the necessity of the dynamic model

Much research into train collisions can be found in the literature. The energy relation (Lu, 2002) in equation 3.5 would be beneficial for a probabilistic study. However, the situation at Kijfhoek is particular and deviates from the investigations performed in the literature. This thesis requires a model that allows for these differences. The following points at Kijfhoek are different from Lu's (2002) investigation:

- The difference in mass between carriages/wagons is more significant at Kijfhoek,
- The buffer types are different
- The configuration of the moving versus the stationary train is hardly ever the same on multiple levels, such as the number of wagons, the mass of the wagons, and the buffer types.
- The performance of each of the interfaces (the buffers) is assumed deterministic in Lu's studies.
- A force is acting on the stationary train at the end of the allocation track from the brake shoe.
- The impact velocities are much lower.
- The high-velocity run-offs consist mainly of a single wagon.

Apart from the influence of the brake-shoe, which has a negligible influence on the energy absorption at the interfaces, the above points have a significant effect on the constant R_1 in equation 3.5. Especially a combination of the above points, which frequently occurs at Kijfhoek, could lead to a doubling of the constant R_1. On the contrary, the constant R_1 is often much lower for a single wagon impacting the stationary wagons, overestimating the failure probability. The above points justify the need to abandon Lu's energy absorption relation and use the newly developed dynamic model. An updated energy relation applicable in Lu's investigation as well as in Kijfhoek is found in section 4.5.4. This updated energy relation is determined with the dynamic model developed in this thesis.

Investigation into the strength of a tank wagon against loss of containment would suit a finite element method (FEM). An excellent example of such investigation is performed by Šťastniak, Moravčík and Smetanka (2019), who investigate the design of a single type tank-

[5] Due to an error in the Dekra report, the value used in this thesis is 0.35, however after collaboration with the author 0.25 was the correct value. Luckily, the brake shoe force is negligible, and the value did not alter the results.

wagon. However, at Kijfhoek there are many different types of wagons and many different possible configurations of how these wagons are arranged. Setting up a FEM for all these configurations would take months of investigation and preparation. Furthermore, due to the probabilistic approach in this paper and the number of simulations required, a FEM analysis, which requires a great deal of computation power, would take days, if not months, of simulation. The multi-body dynamic model allows for the possibility to vary the essential parameters probabilistically, and the computation time is limited compared to a FEM model.

3.3.4 Verification of the dynamic model

Verifying the model is performed by looking at two versions of a limit case and by comparing the results to those found in Lu's (2002) investigation. The limit case is a single wagon impacting another single wagon.

Verifying in the limit cases

The buffers are modelled as a constant spring, without damping and no brake shoe present. In this case, the collision is elastic; the spring stores energy in compression and then rereleases the energy when it unloads. No energy is dissipated in the system. The MBD model in this thesis uses non-linear springs to represent different elements capable of absorbing energy, explained in section 4.4.4. All these spring stiffnesses during loading and unloading are set to an equal value in the model. If both wagons have the same mass, the impact wagon comes to a complete stop and transfers all its kinetic to the stationary wagon. The stationary wagon has the initial impact velocity after the contact between the wagons is broken. Figure 3.5 shows the velocity-time diagram of this collision.

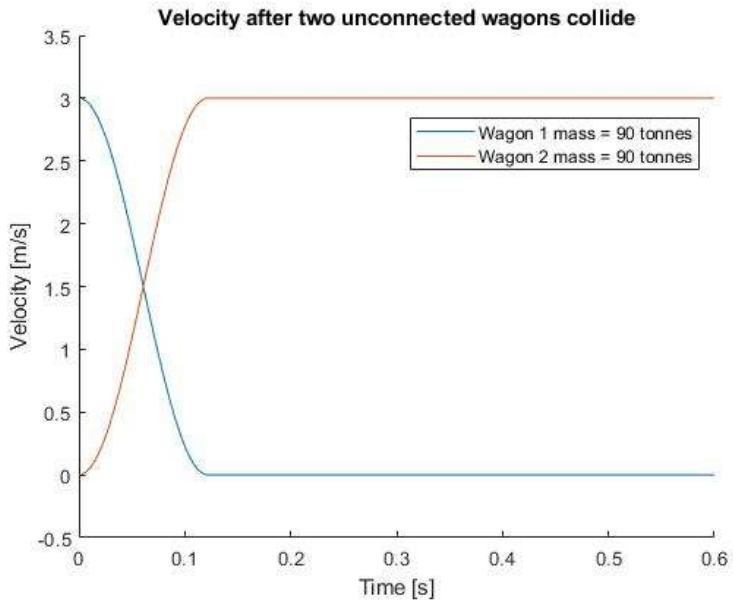

Figure 3.5: Velocity-time diagram of two wagons unconnected wagons in an elastic collision; the spring-stiffness is constant. No energy dissipates the system.

Linear limit case

Another extreme case is when the above example is performed with coupled wagons, where the coupler also works in compression with the same spring stiffness. Equation 3.9 represents the equation of motion for this coupled two degree of freedom system.

$$\mathbf{M\ddot{x} + Kx = 0} \qquad 3.9$$

$$\begin{bmatrix} m_1 & 0 \\ 0 & m_2 \end{bmatrix}\begin{bmatrix} \ddot{x}_1 \\ \ddot{x}_2 \end{bmatrix} + \begin{bmatrix} k & -k \\ -k & k \end{bmatrix}\begin{bmatrix} x_1 \\ x_2 \end{bmatrix} = \begin{bmatrix} 0 \\ 0 \end{bmatrix}$$

The natural frequencies are found by transforming equation 3.9 into the frequency domain by substituting equation 3.10 into 3.9, forming an eigenvalue problem in equation 3.11.

$$\begin{aligned} x_1(t) &= X_1 \sin(\omega t) \\ \mathrm{x}_2(t) &= X_2 \sin(\omega t) \end{aligned} \qquad 3.10$$

$$(-\mathbf{M}\omega^2 + \mathbf{K})\begin{bmatrix} X_1 \\ X_2 \end{bmatrix} = \mathbf{0} \qquad 3.11$$

The non-trivial solution is retrieved by setting the determinant of the eigenvalue problem to zero. Resulting in four eigenvalues in equation 3.12, of which two are repeated roots and zero. The unrestrained rigid body movement physically explains the repeated roots.

$$\begin{vmatrix} -\omega^2 m_1 + k & -k \\ -k & -\omega^2 m_2 + k \end{vmatrix} = (-\omega^2 m_1 + k)(-\omega^2 m_2 + k) - k^2 = 0$$

$$\omega_{1,2} = \pm\sqrt{\frac{m_1 + m_2}{m_1 m_2}k}\,, \quad \omega_{3,4} = 0, \qquad 3.12$$

The period T and corresponding eigenvector $\boldsymbol{e}$ to the first two eigenvalues are (the eigenvector of the zero eigenvalues is simply $\begin{bmatrix} 1 \\ 1 \end{bmatrix}$ and not further elaborated):

$$T = \frac{2\pi}{|\omega|}$$

$$\boldsymbol{e} = \begin{bmatrix} 1 \\ \dfrac{-\omega^2 m_1 + k}{k} \end{bmatrix} = \begin{bmatrix} e_1 \\ e_2 \end{bmatrix}, \qquad for \begin{bmatrix} x_1 \\ x_2 \end{bmatrix} \qquad 3.13$$

A general solution is then:

$$\begin{bmatrix} x_1 \\ x_2 \end{bmatrix} = At + B + \{C\sin(\omega_{n1}t) + D\cos(\omega_{n1}t)\}\boldsymbol{e} \qquad 3.14$$

The four unknown constants are found by solving equation 3.14 with the initial conditions.

$$A = \dot{x_2}(0) - C\omega e_2$$

$$B = x_1(0) - D$$

$$C = \frac{\dot{x_1}(0) - \dot{x_2}(0)}{\omega - e_2\omega} \qquad 3.15$$

$$D = \frac{x_2(0) - x_1(0)}{e2 - 1}$$

Figure 3.6 shows the analytical solution compared with the model, in which the velocity of the impact wagon is the only non-zero initial condition. The model shows a very good match with the analytical solution and verifies the model in this extreme case.

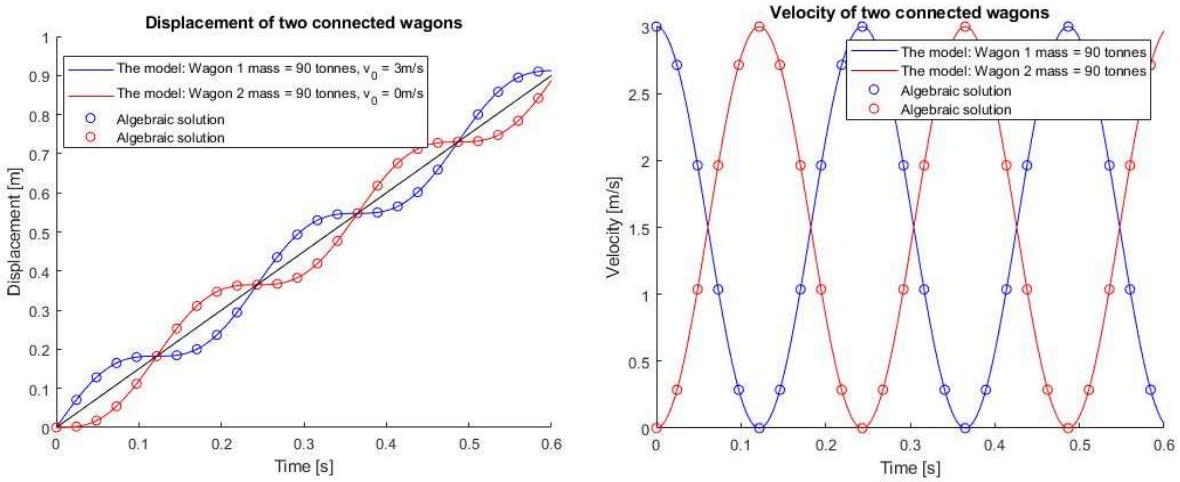

Figure 3.6: Diagrams showing the results and the algebraic solution of two connected wagons, where only one has an initial velocity. Left: Displacement-time diagram. Right: velocity-time diagram.

Verifying with the literature

To verify with literature, the model is compared with the simulations performed by Lu (2002) at an impact velocity of 16.67 m/s. In his paper, he addresses the similarity of the five various projects' crashworthiness and that the differences in force-stroke diagrams at the interfaces (e.g. buffers) were minor. One of his earlier papers showed detailed examples of such buffers and force- stroke diagrams (Lu, 1999). These diagrams are replicated with linear springs (see Appendix E), similarly to what is done in section 4.4.4.

The definition of the interfaces is shown in Figure 3.7. The absorbed energy in this thesis MBD model is found numerically through integration of the Force-Stroke diagram (explained in section 4.4.4) over the stroke, using 'trapz' in MATLAB (MathWorks, 2020).

Although the exact force-stroke diagrams of the projects in Lu's (2002) papers are unknown, the model results in Table 3.1 match the results of Lu's simulations very well, especially in the interfaces of interest, verifying the model used in this thesis[6]. The discrepancy in interface 4 and 4s, has little effect on damaging tank wagons since it is only a minor percentage of the total absorbed energy. Since both trains in this collision are identical, the total absorbed energy should equal 50% of the initial kinetic energy according to the collision energy from equation 3.4 with identical masses and $v_2 = 0$. The deviation from 50% in this thesis model is due to numerical reasons, whereas the deviation in Lu's model is partly caused by the included friction force of the brakes from the parked train.

[6] The model showed similar results for the other three projects that Lu (2002) investigated. Only two projects are shown here, to keep clarity in the report.

Table 3.1: Comparison of this thesis dynamic model and two of Lu's simulations. The absorbed energy per interface, including the percentage from the moving vehicle's kinetic energy before impact.

	Arlanda train				SWT train			
	Lu's model		Thesis model		Lu's model		Thesis model	
	kJ	%	kJ	%	kJ	%	kJ	%
Interface 4	164.8	0.6	33.5	0.1	188.0	0.8	35.7	0.2
Interface 3	1447.7	5.1	1052.7	3.7	806.7	3.5	648.9	2.8
Interface 2	2658.1	9.3	3068.8	10.8	2278.6	10.0	2418.2	10.6
Impact interface 1	6500.1	22.8	5916.2	20.8	5541.6	24.3	5176.5	22.7
Interface 2s	2661.2	9.3	3068.8	10.8	2275.8	10.0	2418.2	10.6
Interface 3s	1452.2	5.1	1052.7	3.7	804.0	3.5	648.9	2.8
Interface 4s	162.5	0.6	33.5	0.1	187.7	0.8	35.7	0.2
		52.8		49.9		53.0		49.9

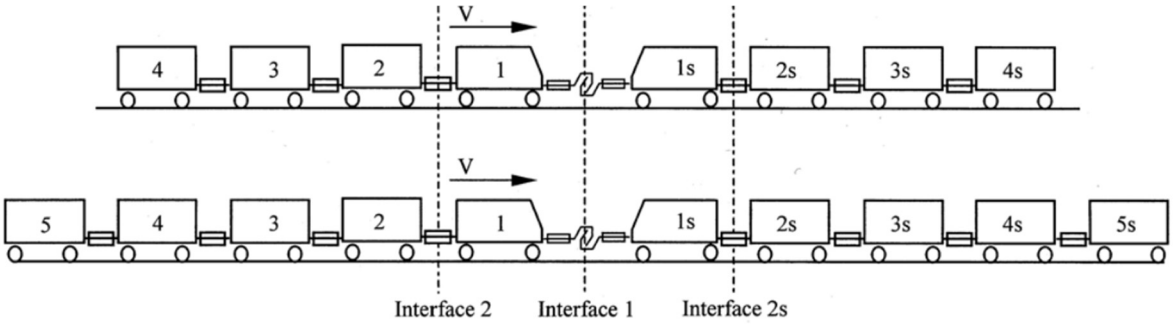

Figure 3.7: Description of the wagons and the interfaces (Lu, 2002).

3.4 Approach to determine the probability of damage in a rear-end collision

Due to the deviation from the energy relations found in the literature, the energy absorption in the Limit State Function in equation 3.3 needs to be solved utilizing the MBD-model. A suitable way to determine the failure probability is to use a Monte Carlo (MC) simulation.

3.4.1 Monte Carlo simulation

In a regular Monte Carlo simulation, the stochastic variables are determined randomly (in case of independence), and all the variables are filled in the LSF to determine failure. By repeating this experiment N times and documenting the number of failures (n_f) the failure probability is determined as follows

$$P_f = \frac{n_f}{N} \tag{3.16}$$

However, in this thesis, to determine damage in rear-end collisions, the LSF in equation 3.3 is no longer analytically solvable, and all the variables are to be implemented in the MBD model.

The Coefficient of Variation (COV) of the failure probability is estimated according to equation 3.17 (Jonkman et al., 2017):

$$V_{P_f} \approx \frac{1}{\sqrt{NP_f}} \tag{3.17}$$

3.4.2 Assessing damage

Since the MBD model is used inside the Monte Carlo simulation (section 4.5) it is no longer necessary to determine the damage criteria using energy. The energy absorption capacity of buffers is directly related to the maximum stroke of the buffers (explained in section 4.4.2). If the maximum stroke of the buffers is exceeded, the buffers energy capacity is reached, and the wagon's structure starts absorbing energy, which is called "Type 1 damage". Type 1 damage is written in a LSF as follows:

$$Z_{type1} = Length\ of\ the\ buffers' stroke - The\ maximum\ reached\ stroke. \quad 3.18$$

Calculating the energy capacity of the buffers from equation 3.3 using the MBD-model is challenging because of its dependence with the relative velocity explained in section 4.4.4. Using the LSF from equation 3.18 avoids this problem. This LSF is performed at each interface, and MBD-model determines the maximum reached stroke.

Another way to determine damage is by using the wagons strength. If the wagon's plastic deformation force (explained in section 4.4.1) is exceeded, damage to the wagon is assumed; this is called "Type 2 damage". The LSF for Type 2 damage is as follows:

$$Z_{type2} = F_{wagon,pl} - F_{max,occuring}, \quad 3.19$$

in which $F_{wagon,pl}$ represents the force needed to reach plastic deformation of the wagon, and $F_{max,occuring}$ represents the maximum occurred force at an interface calculated by the MBD model. Type 2 damage can occur in two possible ways:

- The usual way: first, the buffer capacity is entirely depleted, after which the linear deformation of the wagons continues and eventually resulting in plastic deformation of the weakest wagon on either side of the interface (This probability should therefore be lower than Type 1 damage).
- The 'unusual' way: The wagons strength (see section 4.4.1) is smaller than the mean force of the plastic region of the buffers (see section 4.4.2). This is possible due to the probabilistic distributions of both parameters and is visually described in Figure 3.8. The choice of distributions for both parameters is chosen such that equal force occurs at $\mu \pm 2\sigma$ respectively.
  Since the wagon and the buffers work in series, the buffers cannot absorb energy when the wagons strength is smaller. So instead, the wagon is absorbing the energy and 'protecting' the buffers from damage. The buffers plastic deformation is never engaged, instead the wagon starts to deform plasticly if the collision forces are high enough.
  This type of failure may also be called: 'malfunctioning of the buffers plastic absorption capacity.'

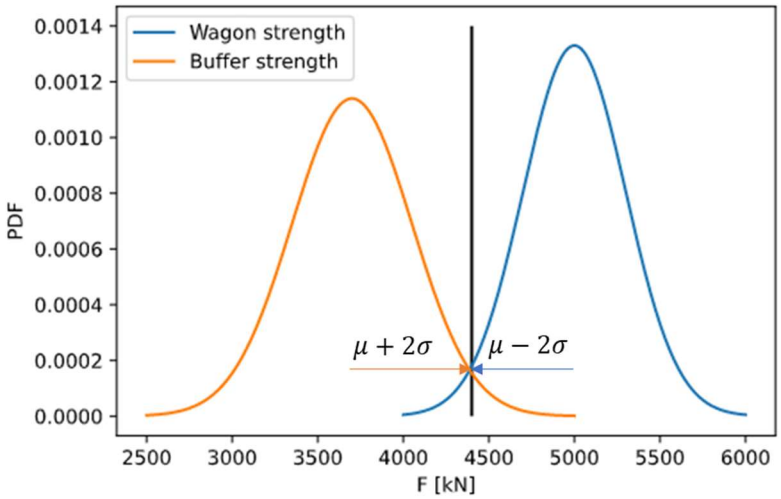

Figure 3.8: Two overlapping normal distributions. Which can lead to Type 2 failure, where the plastic region of the buffers is never engaged.

Finally, applying a Monte Carlo simulation utilizing the MBD model is time-consuming, and a simplified model is proposed in section 4.5.4 using an improved energy relation. This approach is further evaluated in chapter 5, where a First Order Reliability Method (FORM) is applied.

3.4.3 FORM-calculation

In a FORM calculation all the variables in the LSF are transformed from the original 'X-space' to the (independent) standard Normal 'U-space', as is the LSF itself. The calculations of the FORM are performed using the OpenTURNS software in Python (Baudin et al., 2015); it uses an "equiprobabilistic transformation" in the design point. Furthermore, FORM linearizes the LSF in the design point, and the shortest distance between the tangent of the LSF in the design point and the origin in the U-space describes the Hasofer-Lind Reliability Index β_{HL}. This whole process is visually described in Figure 3.9 for an arbitrary LSF $Z(X)$. The design point is the point on the LSF at which the probability density is the highest, and thus where failure is most probable (Jonkman et al., 2017).

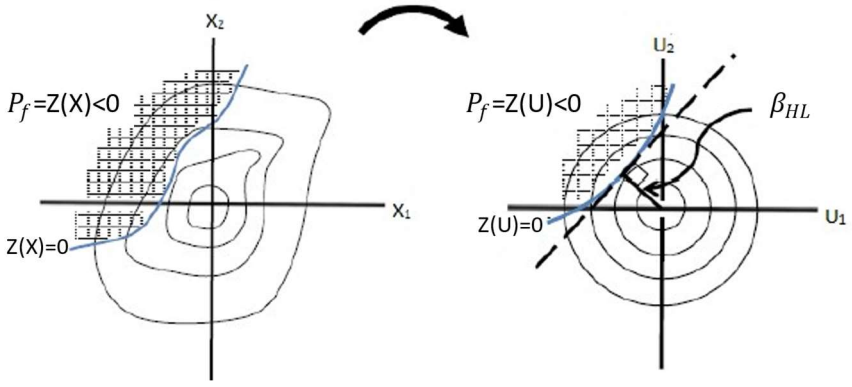

Figure 3.9: The transformation of the original X-space to the standard Normal U-space. Also showing the definition of the Reliability Index in the U-space (Moss, 2020).

In a FORM calculation the design point is found in the U-space and the α-values are determined from the U-space. In the design point in the U-space the following holds:

$$Z(a_1\beta, \dots, a_i\beta) = 0 \quad 3.20$$

It does not necessarily mean that the corresponding design point in the X-space is also the most probable failure point (Orlin, 2020). However, if the LSF is not too non-linear and the variables in X-space do not deviate too much in the tails of the Normal Distributions, the design point in the X-space should approximate closely using the found α-values. For the independent case, these values are found using the following equation:

$$x_i^* = F_{X_i}^{-1}[\Phi(-\alpha_i\beta)] \quad 3.21$$

In which x_i^* corresponds to any of the parameters in a Limit State function (Jonkman et al., 2017).

4. Reliability-based assessment

The main goal of this chapter is to answer the following questions:

- What are the model parameters, and what are their distributions?
- What influences the model parameters, and how are they dependent?
- How reliable is the system against a collision on the allocation track?
- Which parameters are dominant in the results?
- What are the influences of the assumptions and uncertainties?

In the reliability-based approach, the uncertainty of the parameters needs to be determined. The field data obtained are used to derive parametric distributions to the stochastic variables, or when appropriate, an empirical distribution is used. Additionally, the data processed in this thesis are from 2012 until 2020, because the ethanol fire in January 2011 has led to some alterations in the system process at Kijfhoek, to make the emplacement safer. Through a new warning system, the possibility of a similar accident was eliminated. From 2012-2020, ProRail registered a little over 712 thousand run-offs, for which the system recorded crucial information required for smooth operation.

This chapter explains and justifies the selections made for each of the parameters important in the risk of Loss of Containment. Once all these stochastic variables are determined, a Monte Carlo simulation (section 4.5) is performed using the multi-body dynamic model explained in section 3.3. As explained in section 3.2, the run-off's kinetic energy, determined by the mass and velocity, is essential for investigating a possible collision. Since ProRail has little control over each wagon's mass, the Exit-velocity measurements of the run-offs are assessed first in section 4.1. The remainder of this chapter is best described by the figure below and shows a reader's guide through this chapter for the discussed design parameters, and Table 4.1 gives a summary of each of the design parameters. Assumptions are made throughout this chapter. At the end of some sections, important assumptions and possibly relevant assumptions are highlighted. The main assumptions are evaluated in the section 4.7. Finally, this chapter finishes with a summary and discussion in section 4.8.

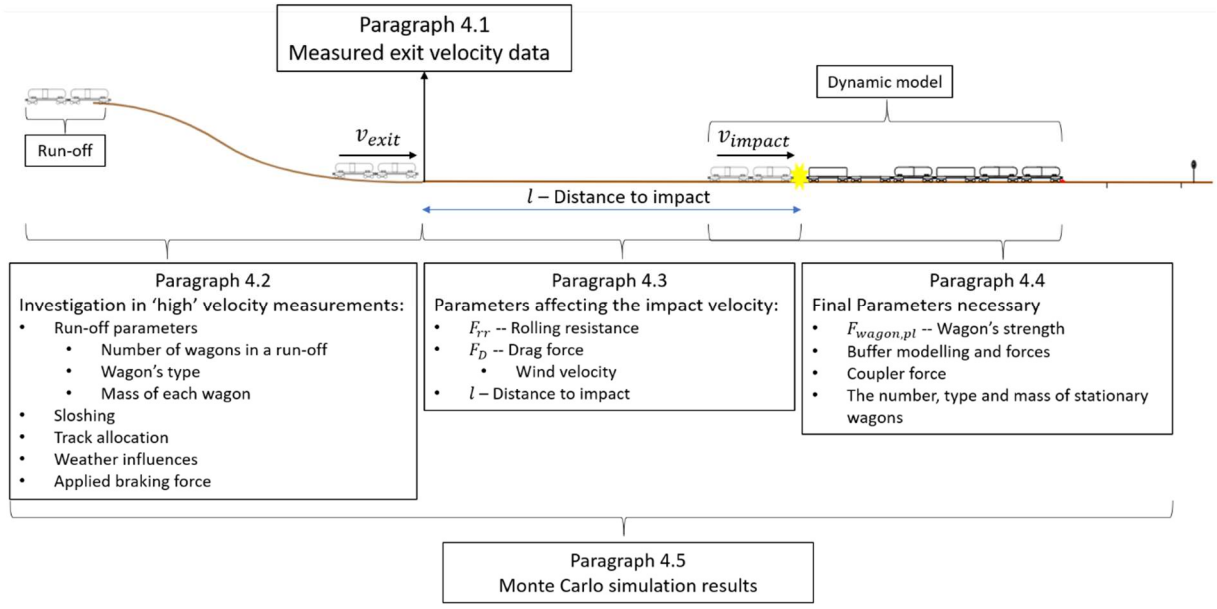

Figure 4.1: Diagram served as a reading guide for this chapter.

Table 4.1: The variables of interest in the Monte Carlo simulation, including a short description and the distribution type.

Parameter	Description	Distribution type	Section
v_{exit}	The measured velocity of the run-off when it exits the final brakes and enters the allocation tracks.	$GPD(\mu = 2.0, \sigma = 0.23, \zeta = 0.19)$ $[\frac{m}{s}]$	4.1
Parameters influencing the high Exit-velocity measurements			4.2
$n_{run-off}$	The number of wagons in a run-off with an Exit-velocity higher than 2 m/s. Is depended on the Exit-velocity.	Empirical	4.2.1
Wagon type (run-off)	The type of wagon, whether it is a tank wagon ('Z') (possible containing dangerous goods) or not. P('Z') depends on the number of wagons in a run-off and the Exit-velocity.	$Bern(p = 0.965)$ $(P('Z'\|nr.wagons = 1 \cap v > 2.0) = 0.965)$	4.2.1
m	The mass of any given wagon depends on the number of wagons in a run-off and its type. In a run-off, it also depends on the Exit-velocity.	Empirical	4.2.2 & 4.4.5
$e_{sloshing}$	The imposed error in the Exit-velocity measurements of wagons containing a fluid, due to the effect of sloshing.	$Arcsine\ distribution$ $(-0.5,0.5)$ $[m/s]$	4.2.3
Substance	The substance a tank wagon carries	Empirical	4.2.3
	Non-parametric extra information, such as track allocation or weather influence.		4.2.5-4.2.6
Parameters affecting the impact velocity			4.3
c_{rr}	The dimensionless rolling resistance coefficient. This determines the force resisting rolling. $F_{rr} = Nc_{rr}$	$N(0.0015, 0.00015))$ [-]	4.3.1
C_D	Drag force coefficient. Affects the drag force ($F_D = \frac{1}{2}\rho v^2 C_D A$).	$N(1,0.1)$[-]	4.3.2
Wind direction	The direction of the wind	Empirical	4.3.2
v_{wind}	The wind velocity, depended on the wind direction.	Weibull/Gumbel	4.3.2
l	The total distance the run-off is resisted to motion before impact. This is a function of the number of wagons on the allocation track.	Deterministic	4.3.3
v_{impact}	This is dependent on parameters described above.		4.3.4
Final parameters			4.4
$F_{wagon,pl}$	The force to reach plastic deformation of a wagon.	$N(5000,300)$ $[kN]$	4.4.1

Parameters affecting the buffer force: this chapter also describes the modelling of the buffers and the regulations to which the buffers need to comply.			4.4.2
F_1	The force at the end of the elastic region of two combined buffers in parallel.	Dependent: $N(1700,150)$ $[kN]$ Independent: $N(1700,106)$ $[kN]$	
a_1	Length of the elastic region	$N(105,5.25)[mm]$	
F_2	The mean force in the plastic region for two combined buffers.	Dependent: $N(3700,350)$ $[kN]$ Independent: $N(3700,247)$ $[kN]$	
a_2	The length of the plastic region	$N(215,10.75)[mm]$	
c_{cw}	Damping coefficient of a crashworthy buffer	$N(8 * 10^5, 1.2 * 10^5)$ $[kg/s]$	
$c_{standard}$	Damping coefficient of a standard buffer	$N(2 * 10^5, 3 * 10^4)[kg/s]$	
$k_{tension}$	This is the tension stiffness of the coupling device between connected wagons.	Deterministic	4.4.3
$n_{stationary}$	The number of wagons on the allocation track when impact occurs	Discrete uniform $U_d(0,27)$	4.4.5
Wagon type (stationary wagons)	The type of wagon, whether it is a tank wagon (possible containing dangerous goods) or not.	$Bern(P('Z') = 0.649)$	4.4.5
E_{cap}	Simplified buffers using energy capacity	$N(960,80)$ or $N(36,3)$ $[kJ]$	4.4.2
R_E	Normalized energy factor	$L(\sigma = 0.63, \theta = 0.48, m = 0.064)$	4.5.4

4.1 Exit-velocity data

As is illustrated in chapter 2, a run-off passes three brakes on its way to an allocation track. The velocity at which a run-off exits the final brakes and enters the allocation track is called the 'Exit-velocity'. The data provide measurements at two different locations/times, separated by 1~1.2 m, at which the Exit-velocity is logged, just when it leaves the final brakes and when passing the final axle detector. Under normal circumstances, this velocity is measured by the radar system at both locations/times. However, if the system detects an error in the radar system, the system uses the velocity measured by the axle detector. Thus, each allocation track has a separate radar system and axle detector, leading to $43x2$ measuring devices.

The measurements at these two locations/times show significant differences in the high-velocity tail ($v > 2.0\ m/s$) *if* the measurements are not identical[7]. The following four points illustrate why the measurements at the axle detector are used in this thesis.

1. The incorrect radar measurements are filtered out at the axle detector and replaced with the 'correct' axle measurements.

[7] About halve of the measurements at the two different locations, show the exact same value. It is unlikely that the velocity is indeed exactly the same at two moments in time/locations, but according to Siemens this is due to the way the algorithm interprets the radar signal.

2. A Kolmogorov-Smirnov (KS) test is performed among the high-velocities ($v > 2.0\ m/s$), between the identical measurements and the measurements at both locations respectively. The results of the KS-test are found in Appendix F, and the measurements at the location of the axle detector are likely to come from the same distribution as the identical measurements (P-value $= 0.3$).
3. Fitting the Generalized Pareto Distribution (GPD) to the Exit-velocity measurements at the axle detector leads to similar results whether or not the identical data are included or excluded. Whereas, at the location before the axle detector, these distributions showed significant differences.
4. Siemens suggested using the data measured at the second location because these are more accurate than the first location.

According to the above points, the data at the second measurement location are more representative and thus used in this thesis.

4.1.1 The measurements

To limit the chance of an accident, the system targets an Exit-velocity of 1.5 m/s. Consequent to the system specifications (Vrijling et al., 2012), 97,5% of the run-offs Exit-velocity needs to be below 1,65 m/s ($v < \mu + 2\sigma = 1{,}65$); it does not specify an upper limit for the velocity. ProRail assumes that the Exit-velocity follows a normal distribution with a mean of 1.5 m/s, and the standard deviation is therefore required to be smaller than 0.075 m/s. According to the measurements, a little over 99% of the run-offs have an Exit-velocity below 1.65 m/s. Figure 4.2 displays the axle measurements and the best fitted normal distribution with $\mu = 1.467$ and $\sigma = 0.077$, which corresponds to the system specifications. However, the figure clearly shows that the normal distribution does not correctly fit the tails of the measurements.

When the radar[8] measures a velocity higher than 2.0 m/s, the system should give a warning and stop the humping process. ProRail considers this an unwanted event, and the protocol requires an investigation into the cause of such a high velocity.
In the last nine years (from 2012-2020), the system registered 121 run-offs with $v > 2.0\ m/s$. However, the data at the axle measurement system registered 319 events[9], a rate of 0.49 per thousand when averaged over the 9-year data set.

4.1.2 Fitting distributions to the high Exit-velocity tail data

Before fitting distributions to the Exit-velocity data, the following is assumed regarding the run-off's data:

- all the measurements of all the run-offs from 2012-2020 are in the obtained dataset,
- the measurements are independent of one another,
- the system was operating under regular circumstances[10],
- the radar measurement system is an appropriate system to determine the velocity.

Since the data contains the entire time series, Coles (2001) thinks it is "natural" to regard extreme events, such that the measurements exceed a certain high threshold. Furthermore,

[8] These are the radar measurements at the first location on the allocation track, and not at the axle detector.
[9] The system also registers a so called 'radar error' and does not consider this an unwanted event. However, most data point show exact the same result at both measurement locations.
[10] The maximum measured Exit-velocity was 8.25 m/s by the axle measurement. At this time the system was not running, and someone pushed a run-off down the hill without ProRail's knowledge. This value is dropped from the data and is not considered being normal operations.

he recognizes the use of the Generalized Pareto Distribution as an appropriate choice. Several other distributions are also fitted, but the Generalized Pareto Distribution is indeed the most promising.

Fitting 't-distribution'

The Exit-velocity measurements with the fitted normal distribution in Figure 4.2 show heavier tails (a high kurtosis) than the normal distribution. The well-known 't-distribution' fits this high kurtosis generally better. The probability density function (PDF) of the non-standardized form of the 't-distribution' is given in equation 4.1.

$$f_t(x;\hat{\mu},\hat{\sigma},\nu) = \frac{\Gamma\left(\frac{\nu+1}{2}\right)}{\Gamma\left(\frac{\nu}{2}\right)\sqrt{\pi\nu}\hat{\sigma}}\left(1+\frac{1}{\nu}\left(\frac{x-\hat{\mu}}{\hat{\sigma}}\right)^2\right)^{-\frac{\nu+1}{2}} \qquad 4.1$$

in which $\hat{\mu}$ indicates the location parameter, $\hat{\sigma}$ the scale parameter, ν the degrees of freedom or shape parameter and Γ represents the gamma function.

The best fit t-distribution ($\hat{\mu} = 1.47$, $\hat{\sigma} = 0.038$ and $\nu = 2.69$) in the same figure indeed shows much more promising results compared to the normal distribution. However, the t-distribution overestimates the probability of the high Exit-velocity measurements slightly. Therefore, it potentially serves as a safe upper bound in the Monte-Carlo simulation.

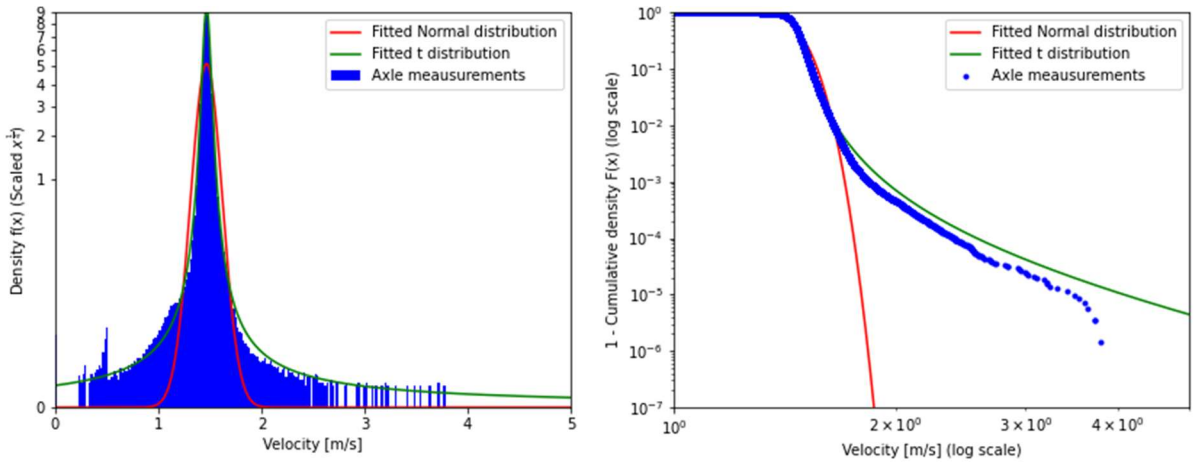

Figure 4.2: The PDF (left) and 1-CDF (right) of the fitted with the t- and Normal distribution, together with the empirical Exit-velocity measurements (axes are scaled).

The Generalized Pareto Distribution

The cumulative distribution function (CDF) of the Generalized Pareto distribution is given by (Coles, 2001):

$$F_{GPD}(x;\mu,\sigma,\xi) = \begin{cases} 1-\left(1+\frac{\xi(x-\mu)}{\sigma}\right)^{-1/\xi} & \text{for } \xi \neq 0 \\ 1-\exp\left(-\frac{x-\mu}{\sigma}\right) & \text{for } \xi = 0, \end{cases} \qquad 4.2$$

in which μ is the location parameter, σ the scale parameter and ξ the shape parameter. The generalized Pareto has, like the Generalized Extreme Value (GEV) distribution, three types:

- Distributions with exponentially decreasing tails ($\xi = 0$)
- Distributions with tails decreasing polynomially ($\xi > 0$, concave)
- Distributions of finite tails ($\xi < 0$, convex)

Since the GPD contains only a subset (values above a threshold) of the complete dataset, the probability of exceedance is given by (Jonkman et al., 2017):

$$P(X > x|X > u) = 1 - F_{GPD}(x) = \frac{P(X > x)}{P(X > u)}, \quad 4.3$$

in which X represents a stochastic variable, x represents a particular value and u the threshold value. $P(X > u)$ can be estimated with the empirical CDF according to:

$$P(X > u) = 1 - \ P(X < u) \approx 1 - F_{emp}(u), \quad 4.4$$

in which F_{emp} represents the CDF of the empirical distribution. For the case at Kijfhoek where the threshold Exit-velocity is $2.0\ m/s$. The probability for a run-off to exceed this threshold is: $P(v_{exit} > 2.0\ m/s) \approx 1 - F_{emp}(v_{exit} = 2.0) = 4.48 * 10^{-4}$.

Fitting the GPD

The data in the high Exit-velocity tail is also fitted using the GPD. Finding a proper threshold value for the GPD is a balance between bias and variance (Coles, 2001), where a higher threshold leads to fewer measurements and higher variance, whereas a lower threshold leads to a higher bias toward the lower measurements. To determine the threshold, Coles (2001) suggest two methods, and both are applied in this thesis.

1. Assessing the mean of the excesses of a threshold, in which the sample's mean is above the threshold, gives an empirical estimate. This mean of excesses should increase linearly for increasing threshold levels if the GPD is a suitable model. This method advantage is that it can be used before performing a model estimate.
2. The second method requires the estimates of the parameters of the GPD for different thresholds. These estimates are then evaluated, in which the shape parameter should be somewhat constant and the scale parameter linear.

The first method, applied to the Exit-velocity data, indicates a linear increase of the mean excesses between roughly 2.0 and 2.4 m/s, as is shown in the so-called 'mean residual life plot' in Figure 4.3. Therefore, choosing a threshold between 2.0 and $2.2\ m/s$ is a good option since the linearity is preserved for larger threshold values.

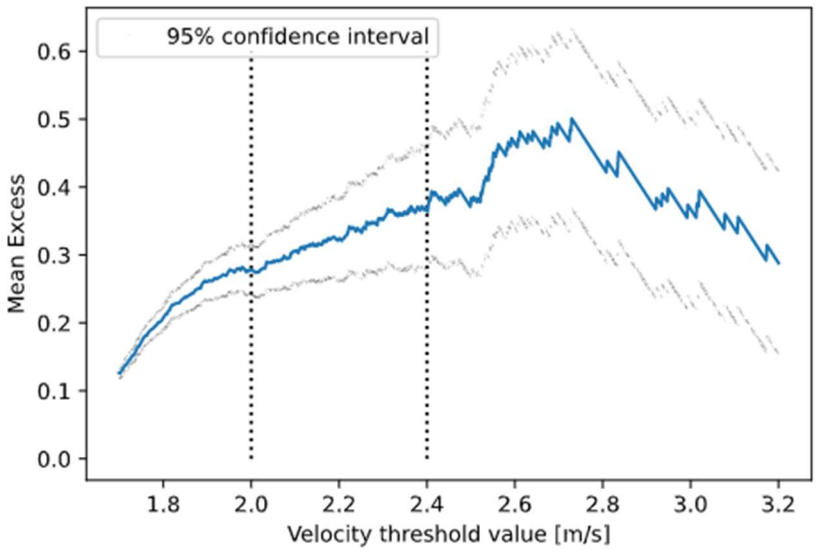

Figure 4.3: Mean Residual life plot for the Exit-velocity data.

Figure 4.4 graphically shows the second method. Again, these plots show promising results for the GPD since the shape parameter is relatively constant for velocities between 2.0 and $2.4\ m/s$, and the scale parameter linearly increases in this region.

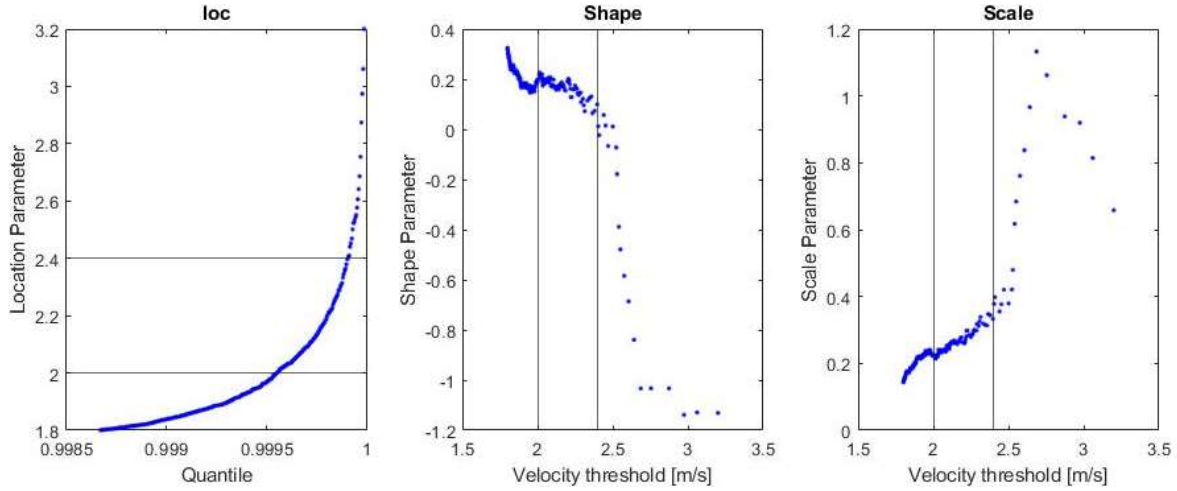

Figure 4.4. The Location μ, Shape ζ and Scale σ parameters for different thresholds. The black lines indicate the threshold Exit-velocity 2.0 and 2.4 m/s.

Since both methods give similar results for the threshold values, any value between 2.0 and 2.2 is a good choice. Because the threshold value of $2.0\ m/s$ has a lower variance, this is the threshold of choice. The best fit to this threshold is shown in Figure 4.5 with $\mu = 2.0,\ \xi = 0.186$ and $\sigma = 0.228$, and indeed it reveals a reasonably good fit for the high Exit-velocity measurements. Especially when considering that the run-offs possibly consist of several configurations and the measurements come from 43 (every allocation track) different devices. Furthermore, the figure shows the 95% confidence interval of the Maximum Likelihood estimators (MLE) of the GPD parameters. The upper bound of the 95% confidence interval of the GPD is close to the t-distribution fit.

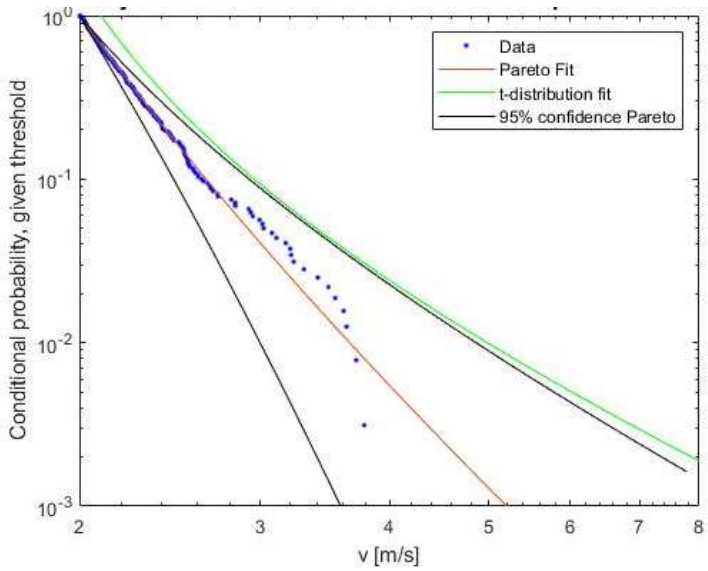

Figure 4.5: Best GPD fit, including the 95% confidence interval and the t-distribution fit to all the high Exit-velocity measurements, with a threshold value of 2.0 m/s. Both axes are in log-scale.

A two-sample KS-test is performed 100 times, comparing the measurements with the same number of randomly picked values from the best fit GPD, and it was never rejected at an $\alpha = 0.05$, with the lowest P-value at 0.07. The PP- and QQ-plot in Figure 4.6 and Figure 4.7

also show the compatibility of the fitted distribution and the measurements. However, the last measurement deviates slightly in the quantile plot. An attempt was made in Appendix G to improve the GPD fits by singling out the full or partially filled and single tank wagons (possibly sloshing) from all the other possible run-off configurations. These fits are not better and only lead to a higher spread of the confidence intervals.

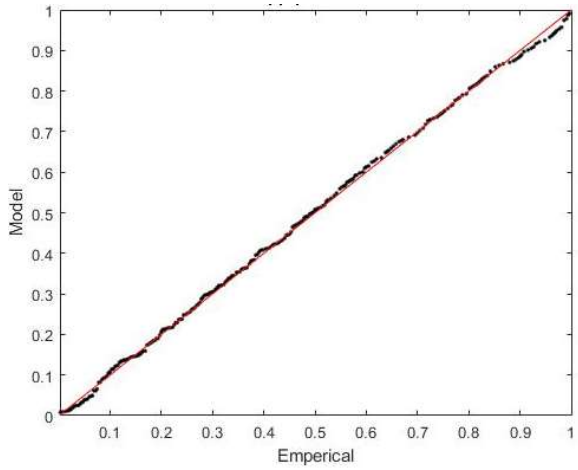

Figure 4.6: PP-plot of the best-fit GPD and the Exit-velocity measurements.

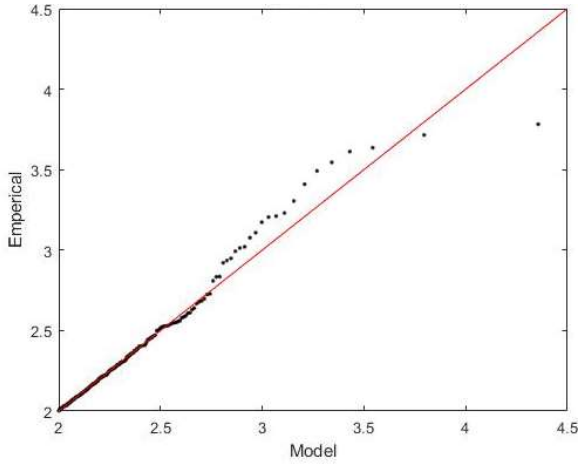

Figure 4.7: QQ-plot of the best-fit GPD and the Exit-velocity measurements.

Because the run-offs are governed by gravity, the Exit-velocity at which the wagons come down the hump likely has a maximum value; the potential energy limits the maximum gain in energy. Since this value is not found in the measurements, and the fitted distribution does not account for this physical maximum the maximum Exit-velocity is determined using the laws of physics. Figure 4.8 shows a cross-section of the hump and the allocation tracks; the height difference is about 5.5 meters. Assuming that a run-off has a maximum initial velocity of around $3.0\ m/s$ on top of the hump and neglecting the resistance to motion and wind, the maximum Exit-velocity is found using the energy relation in equation 4.5.

$$\frac{1}{2}mv_{initial}^2 + mgh = \frac{1}{2}mv_{exit}^2 \rightarrow v_{exit,max} = \sqrt{(2g * 5.5 + 3.0^2)} \approx \mathbf{11.0}\,\frac{\boldsymbol{m}}{\boldsymbol{s}} \qquad 4.5$$

<u>Assumption:</u> The maximum Exit-velocity is likely lower than $11\ m/s$, due to rolling resistance and drag forces. The influence of tailwind could potentially increase this velocity but is less probable.

Figure 4.8: Height profile of the hump at Kijfhoek (Home | AHN, n.d.).

4.2 Investigation into the high Exit-velocity measurements.

This section investigates the 319 run-offs with a high Exit-velocity ($> 2.0\ m/s$) measurement and compares them with all run-offs. This investigation has two objectives. First, to better understand the system and find patterns or causes for these high-velocity run-offs. Second, to get a better prediction of the parameters used in the probabilistic assessments. The following parameters are investigated and listed in order of importance:

1. the type of wagon, whether it is a tank wagon or not,
2. the number of wagons in a run-off,
3. the wagons' mass,
4. the 'sloshing' effect.
5. the substance (gas or liquid) a tank wagon contains,
6. the allocation track to which the run-offs are directed,
7. the influence of the weather,

Because this section has two objectives, the following paragraphs explain the causes and patterns that are found, and they describe the implementation of the parameters as used in the probabilistic assessment.

4.2.1 The type of wagon and the number of wagons in a run-off

Among the high Exit-velocity run-offs, the number of tank wagons is significantly higher. Usually, about 65% of the run-offs are tank wagons, whereas, in the high Exit-velocity run-offs, this amount increases to over 94%. This substantial increase is visible in Figure 4.9; tank wagons are labelled with the letter 'Z', per the UIC classification (DB Schenker Rail AG, 2011). Appendix A displays more information regarding the letter codes and the types of wagons.

According to Vrijling (2012), the fluid sloshing (see section 4.2.3) inside the tank wagons causes a high percentage of tank wagons in the extreme velocity measurements. Due to the fluid's inertia, the fluid moves forward inside the tank when the brake force is applied to the run-off. The applied braking force causes the wagon's body to slow down quicker than calculated by the system, triggering the system to adjusts the braking force according to the radar's velocity measurement. Since the fluid is inside the tank, the radar does not 'see' the fluid, and the adjusted braking force is undesirable. Once the wagon picks up speed again, it is too late to alter the velocity to the desired 1.5 m/s.

The sloshing phenomenon is mainly present in single tank wagons, explaining the significant change in the distribution of the number of wagons in high Exit-velocity run-offs. In general, about 46% of the run-offs consist of a single wagon, whereas this value is almost doubled in

the high Exit-velocity measurements, namely 89% (286 of 319 measurements, of which only 10 are no tank wagon), visible in Figure 4.10.

Together, a high Exit-velocity run-off consisting of a single tank wagon amounts to 86.5% (276 of 319) of all the high Exit-velocity run-offs, three times higher than the 29.5% in general.

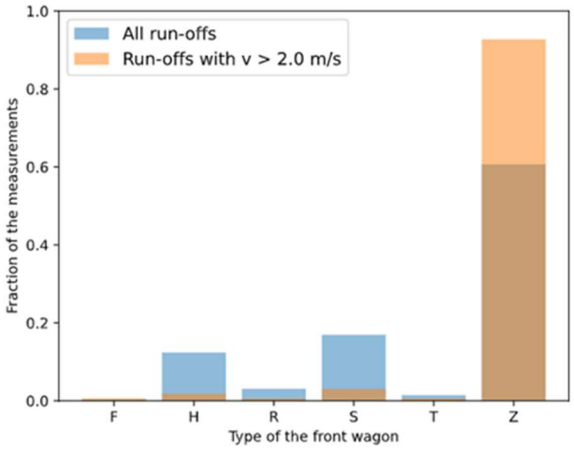

Figure 4.9: The distribution of the number of wagons for all measurements compared to the high Exit-velocity cases.

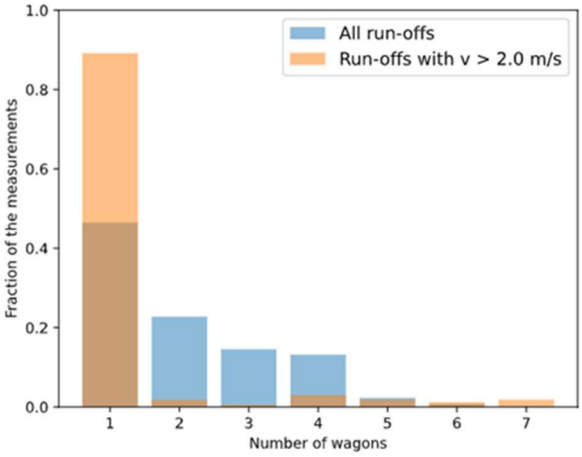

Figure 4.10: The distribution of the type of wagon for all measurements compared to the high Exit-velocity cases.

In the probabilistic assessment (only looking at $v > 2.0\ m/s$), firstly, the number of wagons in a run-off is determined from the empirical discrete distribution[11] in Table 4.2 and Figure 4.10.

Table 4.2: The empirical probability of the number of wagons in a run-off, considering a velocity of the run-off above 2.0 m/s.

Number of wagons in a run-off	1	2	3	4	5
Empirical probability, given $v > 2.0$ $P(n_{run-off} \mid v > 2.0\frac{m}{s})$	0.89375	0.026565	0.01719	0.03594	0.02344

Secondly, the wagon type is selected based on the number of wagons in a run-off. The types are separated into two categories: a tank wagon or any other type of wagon. Given that the number of wagons is equal to one, the conditional probability is found from the empirical measurements with a Bernoulli distribution $P('Z' \mid nr.wagons = 1\ \&\ v > 2.0) = 0.965$ $(276/286$ measurements).[12] For more than one wagon in a run-off, the general empirical probability for the type is used and considered independent from the number of wagons: $P('Z')_{general} = P('Z' \mid n_{run-off} \neq 1\ \&\ v > 2.0) = 0.649$.

[11] The empirical distribution in Figure 4.10 also shows 6 and 7 wagons, in 2014 the maximum allowed length of a run-off was adjusted to 80 meters, roughly 4 to 5 tank wagons. The fraction of the 6 and 7 wagons is therefore evenly distributed over the 2-5 wagons.

[12] Since there are only two possible outcomes the probability for not being a tank wagon is given as follows: $P(\ not\ 'Z' \mid nr.wagons = 1) = 1 - P('Z' \mid nr.wagons = 1) = 1 - 0.965$.

4.2.2 The mass of the wagons

The mass of the wagons is determined from three different empirical distributions because the following conditions showed significant differences:

1. single wagons with an Exit-velocity $v > 2.0\ m/s$.
2. single tank wagons
3. single wagons of any other kind

The empirical density distribution of the wagon's mass for the three different conditions is shown in Figure 4.11, indicating dependency between the type of wagon, velocity of the run-off and the mass of the wagons.

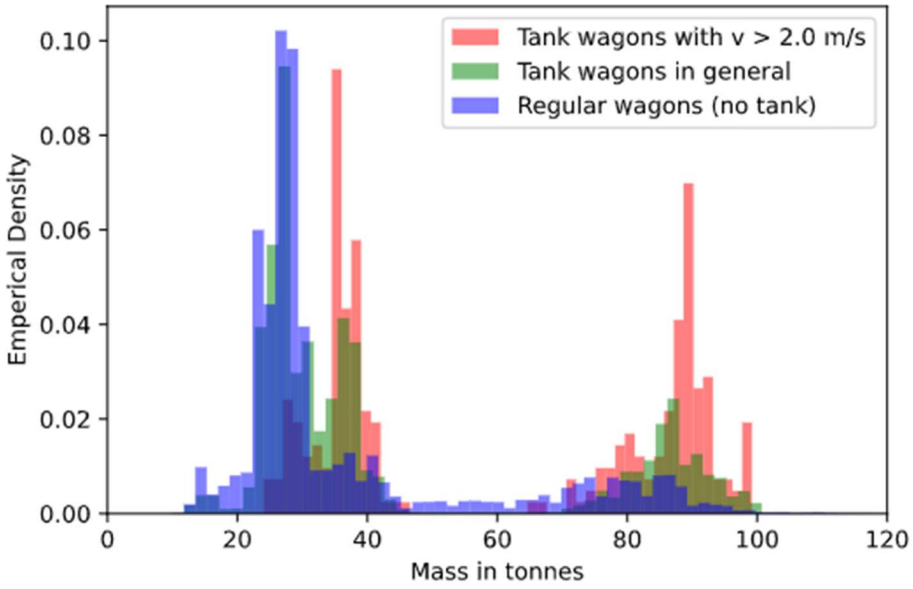

Figure 4.11: The empirical density of the mass distribution given for three different conditions.

Interestingly, the mass distribution for tank wagons with v>2.0 m/s shows that about 50% of the wagons have a mass below 50 tonnes, suggesting they are empty or contain hardly any fluid. Therefore, the sloshing effect is not causing the high velocity of these low mass wagons, suggesting an alternative hypothesis for the high abundance of these empty wagons. It may be possible that the radar is affected by the shape of the tank wagons and not measuring a correct velocity. If the radar measures a low velocity, the braking force is low, but if this radar measurement is incorrect, the Exit-velocity measured by the axle will show a higher velocity (and vice-versa). The above hypothesis is not tested and requires further investigation. Although the effect of these faulty radar measurements is not explicitly investigated, it is assumed to be absorbed in the investigations into the exit-velocity data and the fitted distributions because faulty measurements are replaced with the 'correct' axle measurements.

<u>Assumptions:</u> The values or distributions determined in the last two sections, based on the data, and based on the condition that the run-off has an exit-velocity $> 2.0\ m/s$, are assumed to also hold for higher velocities not measured in the data. (This assumption is continued in the following paragraphs for conditional distributions/probabilities)

4.2.3 Sloshing of tank wagons

Sloshing is the movement of fluid inside a closed container, in this case, a tank wagon. The sloshing potentially increases the wagons velocity, increasing the collision energy. However,

once the impact velocity is known, the fluid inside the tank has a damping effect on the crash (Razaghi et al., 2015). Razaghi et al. (2015) showed that the fluid's damping effect reduces when its volume increases. Under the assumption that fluid is incompressible[13], a full tank is not sloshing. Thus, any fluid sloshing has a positive effect on the energy absorption capacity of the system. Therefore, the fluid's motion is not considered in the dynamic model resulting in a conservative approach.

However, for the impact velocity the sloshing can have a negative effect. Since there are only two measurement locations within 1.2 m from one another in the provided data, the sloshing effect is not easily detected, and it could potentially alter the velocity at a later moment in time. Furthermore, Siemens pointed out that sometimes the high measurements are caused by radar error, and the values are replaced by the axle detectors measurement. It is difficult to know which measurements are faulty and which are caused by the sloshing effect. However, an attempt is made to incorporate sloshing in the impact velocity. In the figures below, the difference in measured velocity between the 2 locations is given for all the measurement points and single-'full'[14] tank wagons for the measurements $v_{exit} > 2.0\ m/s$. In the high measured velocities one can see a tendency of an increased velocity at the second measurement point. This possibly indicates that the wagons are accelerating after the first measurement and the fluid is sloshing. It may also be caused by radar errors

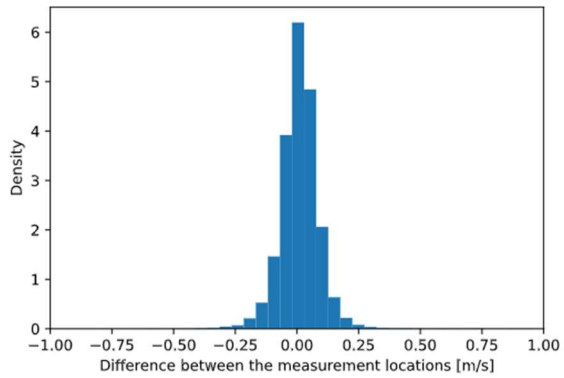

Figure 4.12: The density distribution of the difference in the measured velocity, for all the data points.

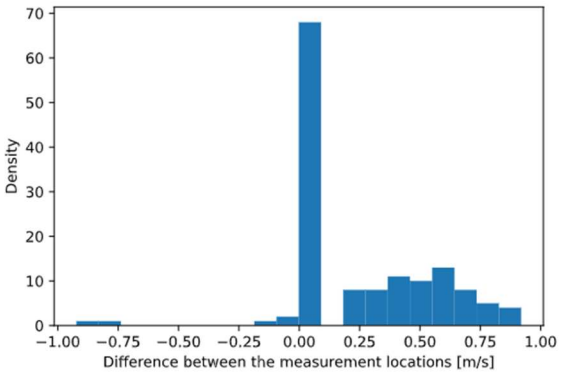

Figure 4.13: The density distribution of the difference in the measured velocity, for single 'full' tank wagons with a measured velocity higher than 2 m/s.

Since the exact movement inside the tank is unknown and not investigated in this thesis, the following is assumed: mainly the primary mode of oscillation is exercised in the braking zones, resulting in a velocity pattern that can be described by a single sine wave around the mean velocity (Figure 4.14 shows a sine wave around zero mean). If in the measurements the velocity is measured in the 'upper region' of the sine wave, the measurements are distorted, and the fitted distribution has a tendency toward higher measurements. On the other hand, if the measurements are not in the upper region, the velocities may even be larger at impact. However, it is assumed that the moment of measuring is randomly on a sinusoidal curve with an amplitude of $0.5\ m/s$ around its measured velocity value. This amplitude is chosen from the figures above.

[13] Assuming the fluid is incompressible is also a conservative approach because compressible fluid will also absorb energy in case of a collision.

[14] Full in this case means a wagons mass above 50 tonnes and thus containing a fluid, can also be partially filled.

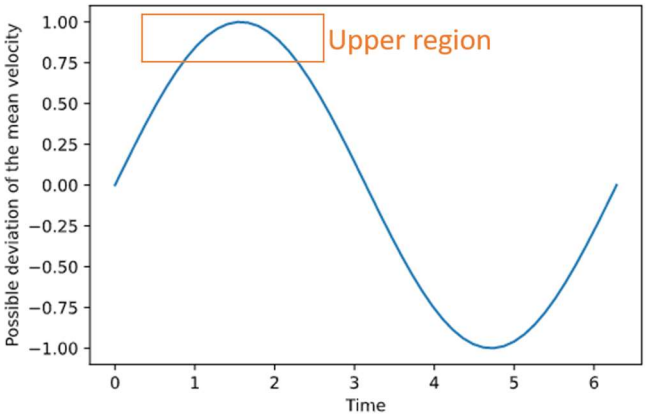

Figure 4.14: Simple sine wav with the description of upper region.

Since the collision happens at a different moment in time, the impact velocity could be determined using the distance from the measurement to the collision together with the period of oscillation. However, the period of oscillation differs per type of good and is not investigated. Therefore, the relation between the impact velocity and the moment of measuring are considered independent. However, sloshing tank wagons cover more distance when the velocity is high, increasing the probability of impact at this higher velocity. This is, however, not considered, and the impact is considered possible at any moment on the sine wave. This results in a probability according to the arcsine distribution, one for the moment of measurement and one for the moment of impact. The impact velocity needs adjustment of twice the error due to sloshing.

$$v = v_{exit} + 2e_{sloshing} \qquad 4.6$$

In which $e_{sloshing} \sim Arcsine\ distribution(-0.5,0.5)$ is the error due to sloshing. This impact velocity is only considered for single tank wagons that actually contain a fluid. For empty tank wagons and other wagons, the sloshing effect is not taken into account. To conclude, the adjusted velocity for 'full' tank wagons is somewhere between $\pm\ 1\ m/s$ of the measured velocity coinciding with the values found in Figure 4.13.

<u>Assumptions</u>: The sloshing is based on several assumptions and is certainly not appropriately investigated. For convenience, these assumptions are listed:

- *Only the primary mode of oscillation is engaged,*
- *The amplitude of this primary mode is chosen at 0.5 m/s,*
- *The moment of impact is independent of the wagon's velocity due to sloshing.*
- *The measuring moment is assumed randomly on the sinusoidal curve.*

4.2.4 The types of tank wagons and the substance it contains

This section focuses on the 276 single tank wagons with a velocity above 2.0 m/s. Tank wagons, indicated with the letter 'Z', are designed to carry certain substances based on their composition, resulting in many different types of Z-wagons. Moreover, the type of wagon has a close relationship with the type of liquid or gas it contains. Figure 4.15 shows the distribution of the 276 measurements compared to all the single tank wagons divided over their United Nations (UN) number. The UN labelled all the dangerous goods and specified them with a number; the goods corresponding to the numbers presented in Figure 4.15 are found in Appendix H. The highest three contributors to the high Exit-velocity data are the following substances in their corresponding wagon type:

- UN-number 1040: Ethelene oxide, including nitrogen. This substance is mainly carried in type *'Zagns'*, which has a load capacity of more than 50 tonnes and is designed for transporting compressed or liquified gases, or gases under dissolved pressure.
- UN-number 1888: Chloroform. Chloroform is mainly carried in types *'Zacns'* and *'Zacens'*, which have a load capacity exceeding 50 tonnes and are unloaded using compressed gas. The difference between the two types is the letter *'e'*, which specifies that a heating system is present.
- UN-number 1965: A mixture of liquified hydrocarbon gasses (LHG or LPG). Substance 1965 is mainly carried in type 'Zags', which has a load capacity lower than 50 tonnes and is designed for transporting compressed or liquefied gasses, or gases under dissolved pressure.

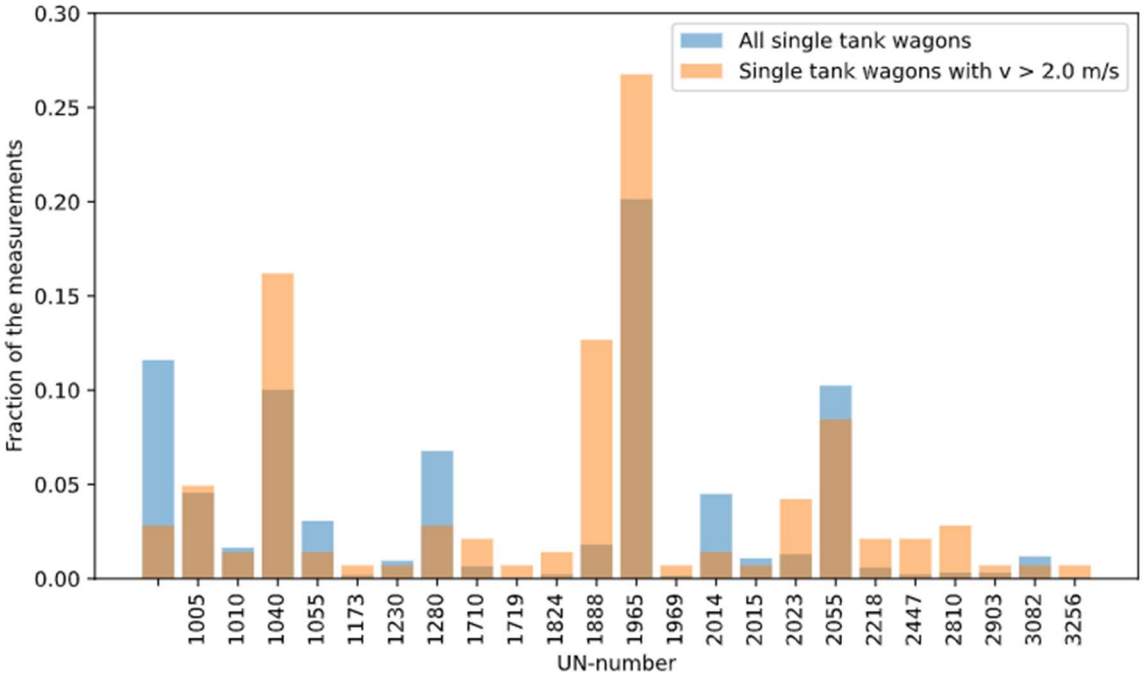

Figure 4.15: High Exit-velocity single wagons compared to all single wagons, divided by UN-numbers, which indicates the type of gas or liquid.

As was described in chapter 2, not all dangerous goods affect External Safety. Figure 4.16 shows the distribution of the goods affecting External Safety at Kijfhoek separated for all the tank wagons in the left panel and 'full' tank wagons in the right panel with a velocity above $2.0\ m/s$. In the high Exit-velocity measurements, when the tank wagon is 'full', there is about a 32% chance it affects External Safety, compared to 60% in general. The rest is not relevant for External Safety. Furthermore, there is a high abundance of empty wagons of category A in the high Exit-velocity measurements, which is not further investigated.

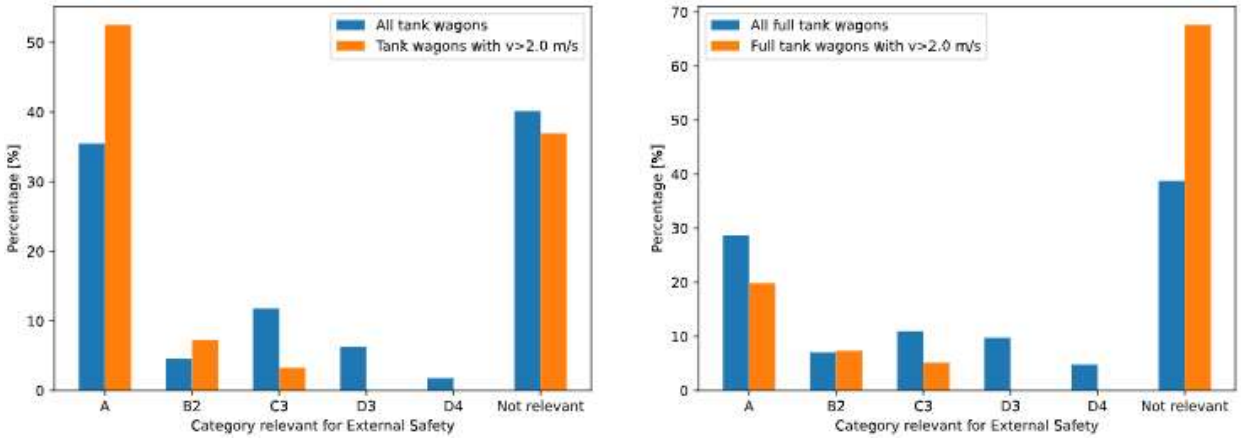

Figure 4.16:The distribution of the tank wagons according to the classification category for External Safety, in the high Exit-velocity measurements for 'full' tank wagons this distribution changes significantly.

4.2.5 Distribution over the different allocation tracks.

This part investigates whether the brake number (these are numbered based on the allocation track) influences the high Exit-velocity measurements. Figure 4.17 clearly shows that on certain allocation tracks, more high Exit-velocity measurements were measured. This could have a couple of reasons:

- The performance of the brakes is different
- The performance of the measurement systems is different
- The lay-out of the tracks to these brakes, which could for instance amplify the sloshing effect.

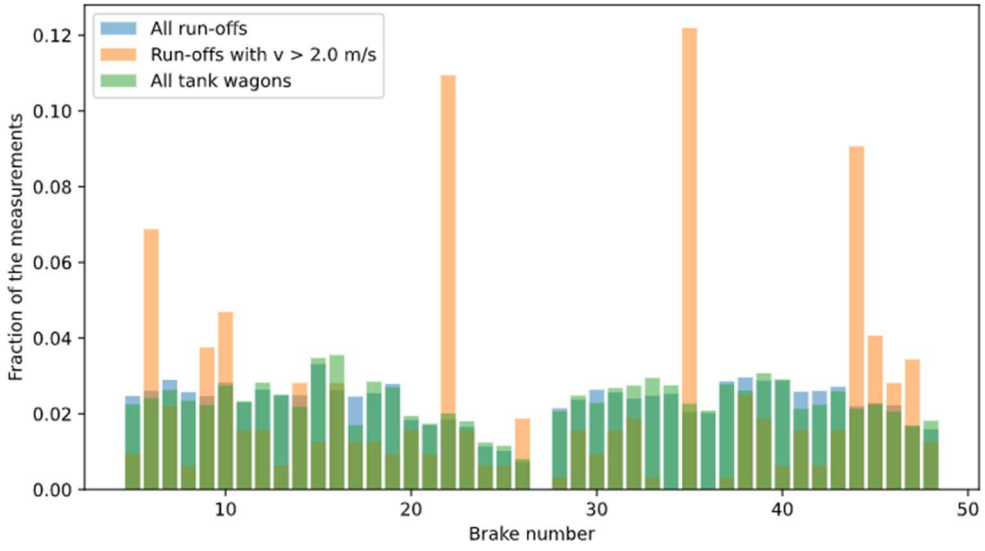

Figure 4.17: High Exit-velocity run-offs divided over their allocation track compared to all the run-offs and all tank wagons.

Although the above figure may certainly be of interest for ProRail, it had little effect on the best fit GPD for velocity measurements whether brake number 6, 22 or 35 were included or excluded from the data. Therefore, no further investigation is deemed necessary. Appendix I shows a couple extra plots that may be useful to ProRail.

4.2.6 Influence of the weather

To find the influence of the weather, the hourly weather information from KNMI (*KNMI - Uurgegevens van Het Weer in Nederland*, n.d.) of the nearest station in Rotterdam is combined with the data from ProRail. The following hourly weather information is assessed:

- Ice – if it was freezing,
- Snow – if and how much it was snowing,
- Rain – the amount of rainfall,
- Wind – the maximum velocity of the wind in a given hour.

The weather, especially rainfall, can be very local, so the data from Rotterdam may not be very accurate for Kijfhoek, but no other data is available.

Only 5% of the assessed high-velocity data showed an Ice, Snow, Rain, or relatively higher wind velocity. This was no significant increase compared with all the measurements.

4.3 Parameters affecting the impact velocity

This section describes the parameters that influence the impact velocity after the run-off's have exited the final brakes.

4.3.1 Rolling resistance

In most moving train simulations, the resistance to motion is generalized in a single formula, for which usually the Davis equation forms the basis:

$$R = A + Bv + Cv^2 \qquad 4.7$$

In which R is the resistance force, v the velocity of the train or wagon, and A, B, C are constants (Szanto, 2016). There are many different values used for these constants in different papers, mainly depending on the specifications of the train. The first term is related to the constant part of the rolling resistance, the second term to the variable part of the rolling resistance (or damping) and the third to the aerodynamic resistance (Newman, 2017). The first term forms the most significant part of the total resistance force at low velocities, and the second constant B could be considered zero (Szanto, 2016).

Like the brake shoe's energy absorption, the energy absorption in a collision due to rolling resistance happens on a much larger timescale and is negligibly small compared to the buffers' energy absorption.

On the contrary, the rolling resistance has a significant effect on the velocity if the travel distance is large enough. As an example, a wagon entering the allocation track with a velocity of 3 m/s will come to a complete stop after about 300 meters, only due to the rolling resistance. Thus, the rolling resistance is considered when determining the impact velocity on the allocation track.

The constant term A in equation 4.7 is related to the Normal force and is often described with a single coefficient, as was done in the Dekra (Hendrikx, 2019) report for Kijfhoek. The rolling resistance formula is given by[15]:

$$F_{rr} = Nc_{rr} \qquad 4.8$$

[15] Actually, this is not the formula as shown in the Dekra report, because the formula in the report was incomplete. After contact with the author, the correct formula is given here.

In which F_{rr} is now the rolling resistance force and is used instead of the constant A in the Davis equation, c_{rr} is the rolling resistant coefficient and N is the normal force, which on a flat track is given by mg. The value of this coefficient for freight trains is usually between 0.001 and 0.002 (Hendrikx, 2019). In this thesis, c_{rr} is considered normally distributed with a mean of 0.0015 and a coefficient of variation of 10%.

4.3.2 The drag force and wind velocity

The aerodynamic resistance or 'drag' is given in the Davis equation (4.7) by the third term and depends on the squared velocity of the wagon relative to the surrounding air. An equation for the drag force from fluid dynamics is given by (Elger et al., 2013):

$$F_D = \frac{1}{2}\rho v^2 C_D A \qquad 4.9$$

In which ρ is the density of the fluid (for air $\rho = 1.2\ kg/m^3$), v the relative velocity of the object to the air, C_d the drag coefficient and A the area subject to the direction of motion. To determine the area facing motion, Figure 2.2 is used, and only the circular area of the tank is considered leading to: $A = \frac{\pi D^2}{4}$, with $D = 3.035$.

The drag coefficient depends on the Reynolds number, the surface roughness, and the object's shape, making it hard to determine. Therefore, it is usually determined through experiments (Elger et al., 2013). The wagons at Kijfhoek have many different shapes and sizes, although the tank wagons all have a similar cylindrical shape. Elger et al. (2013) found a drag coefficient for a cylinder (with an axis parallel to the flow) of roughly 0.95 (with a length/width ratio of 6, similar to the tank wagon). In contrast, Bhagya Lakshmi Nageswari & Jyothi (2020) investigated a regular 'rectangular box shaped' transport wagon and found a drag coefficient of around 1.05. Since the tank wagons are not perfectly cylindrical, this thesis assumes a Normally Distributed drag coefficient $C_D \sim N(1.0,0.1)$. The uncertainty in this drag coefficient also considers the uncertainty of the area of influence (A).

To illustrate the importance of the drag force compared to the rolling resistance force, Figure 4.18 shows F_{rr} on a flat track for different values of wagon's mass, and F_D for different values of relative velocity. The dotted lines indicate the area in which the forces have similar magnitudes. It clarifies that a relative velocity of below $7\ m/s$ has negligible influence compared to the rolling resistance, whereas above $19\ m/s$ (depending on the mass of the wagon), the drag force takes the upper hand.

In order to determine the relative velocity of the wagon with the air, the wind velocity, the wind direction and the emplacement's orientation become important. For a 90 tonnes wagon to increase its velocity due to wind and to overpower the rolling resistance, a severe wind (close to a storm) must blow from a suitable direction.

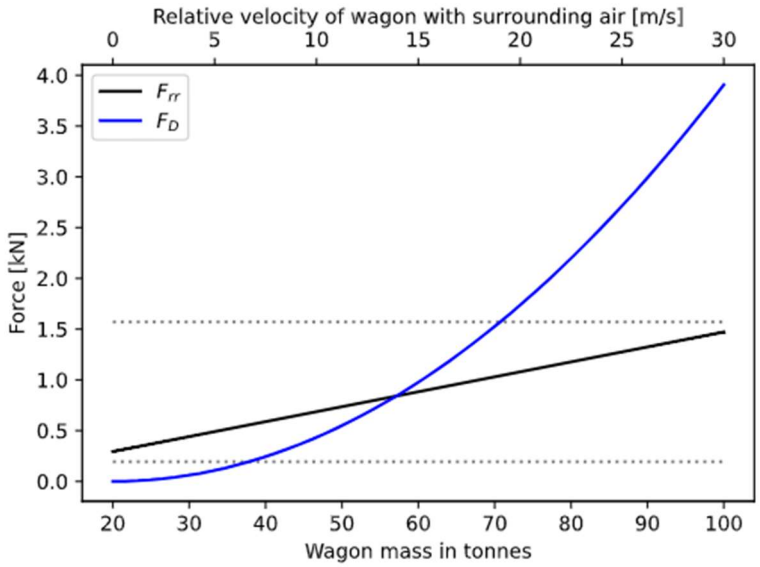

Figure 4.18: An indication of the magnitude of the rolling resistance force (on a flat track) and the drag force. The rolling resistance is linearly dependent on the wagon's mass, whereas the drag force is quadratically dependent on the relative velocity of the wagon.

A wagon must travel quite some distance (a minimum of about 200-300 meters, and a maximum of about 600 meters) from the moment it exits the brakes to the first stationary wagon of impact. At the relatively low wagon velocities at Kijfhoek the travel time is significant. Since wind gusts only last for a maximum of about 20 seconds (Erasmus, 2020), much shorter than the travel time on the track, a mean wind speed over a short interval of, say, ten minutes is more desirable. However, the wind data with the shortest interval available is an hourly[16] average from the KNMI weather station in Rotterdam (*KNMI - Uurgegevens van Het Weer in Nederland*, n.d.).

Figure 4.19 shows the hourly average wind climate at the station of Rotterdam, in which the distribution of wind velocities in m/s are separated into sixteen direction sections of each $22.5°$. The arrow in Figure 4.20 shows the orientation and the direction in which the wagons are moving at Kijfhoek. Furthermore, only the wind directions shown in this figure are considered to influence the velocity of the wagons. Side winds from the other directions possibly push the wagon to the rail on the leeward side, potentially increasing the rolling resistance. This effect is deemed minor and is not further considered.

[16] The hourly mean wind velocities are likely not independent, as is also noted by Wieringa and Rijkvoort (1983), an uncomplicated way to cope with this issue is not available. Therefore, in Appendix J the data is separated into 4-hour segments to obtain more independence, but the parameters of the distributions did not alter significantly compared to the hourly parameters. Hence, the hourly data is used and assumed independent since a shorter interval is more desirable for the effect on the run-offs.

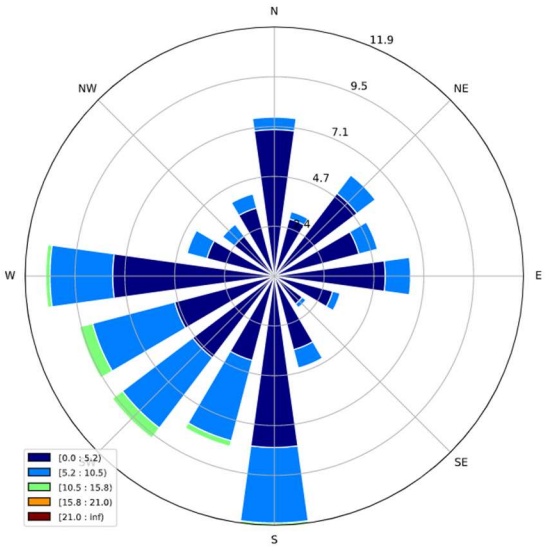

Figure 4.19: The hourly mean wind climate in Rotterdam over the last 20 years. The values in the legend are in m/s.

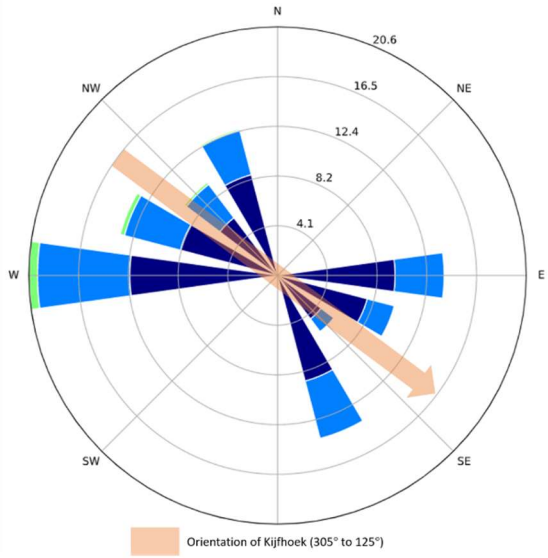

Figure 4.20: The wind directions considered in this thesis due to the orientation of the emplacement at Kijfhoek.

In Hydraulic Engineering, wind velocity is studied widely because of the influence on the water levels and wave height. Especially in the Netherlands it is essential since most of the country lies below sea level and is susceptible to flood risk. Investigations into the wind climate in the Netherlands have been performed for years. Wieringa and Rijkoort (1983) found that a Weibull distribution, with a shape parameter of around two, fits the distribution of the hourly mean wind velocities in the Netherlands well, for wind velocities between 4 to $16\ m/s$. From theory, if the parent distribution is a Weibull distribution, the extremes are often Gumbel distributed (Nápoles, 2019; Wieringa & Rijkoort, 1983). Therefore, these two distributions are fitted to the average hourly measurements of the last twenty years (2001-2020) from the Rotterdam weather station in Figure 4.21 and Figure 4.22. The data is separated into two different sections, the headwind and tailwind (directions $\geq 90°$ and $< 170°$ and directions $\geq 270°$ and $< 350°$ respectively). To determine the wind direction, the empirical distribution from Figure 4.19 is used.

The wind velocities are determined using fitted distributions. The headwinds are fitted well with just the (shifted) Weibull distribution[17] ($W(2.19, 0.17, 4.33)$, whereas the tailwinds are fitted better with a combination of the Gumbel ($G(3.02, 1.82)$ and Weibull ($W(1.89, -0.09, 4.70)$ distribution. In this case, just the average (each distribution has an equal weight factor) of the two distributions is selected and deemed suitable. Van Gelder (2008) made a similar choice of distribution based on averages on the river discharges of the American River (CA, USA).

[17] Statistical goodness-of-fit tests do not show promising results because the hourly wind velocity data are rounded values to whole numbers in m/s and is thus not a continuous distribution. The best fit is therefore determined based on the writers engineering judgement and looking at the figures.

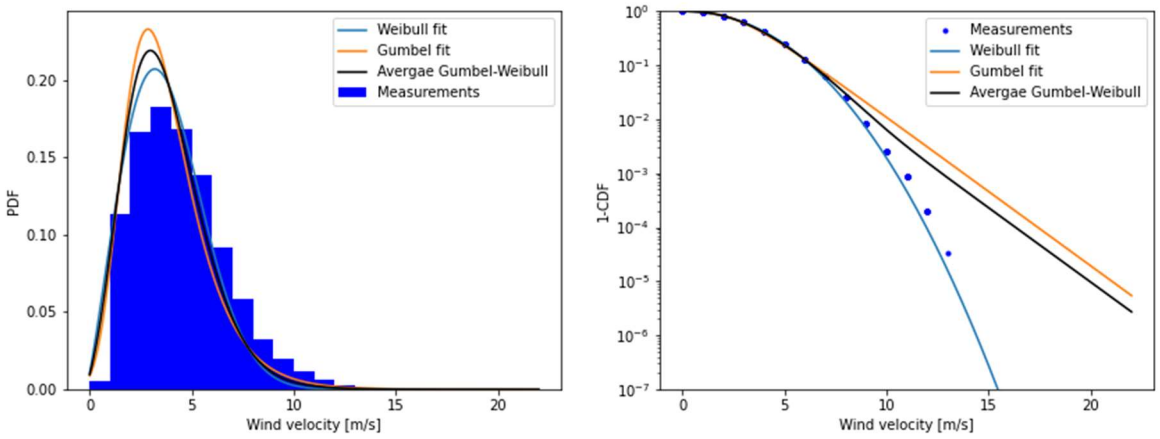

Figure 4.21: The wind velocity measurements and fitted distributions for the run-offs' headwinds at Kijfhoek. Weibull is the chosen distribution.

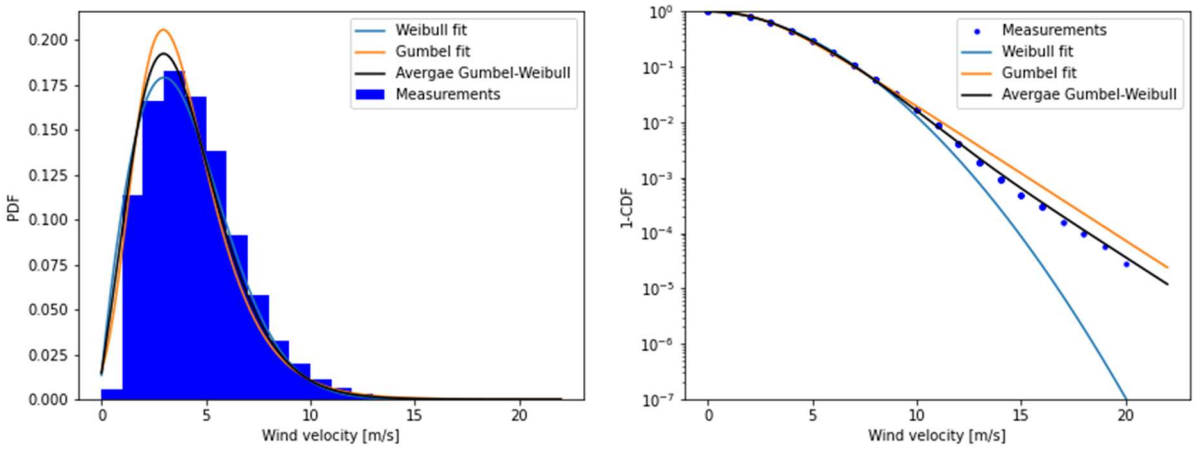

Figure 4.22: Best fitted distributions to the tailwind measurements at Kijfhoek. The average distribution between the Weibull and Gumbel is the chosen distribution.

The PDF of the Gumbel distribution is:

$$f_G(x;\mu,\beta) = \frac{1}{\beta}\exp\left(-\left(\frac{x-\mu}{\beta} + e^{-\frac{x-\mu}{\beta}}\right)\right), \qquad 4.10$$

in which μ is the location parameter and β the scale parameter.

The PDF of the (shifted) Weibull distribution is:

$$f_W(x;k,u,\alpha) = -\left(\frac{k}{\alpha}\right)\left(\frac{x-u}{\alpha}\right)^{k+1}\exp\left\{\left(\frac{-(x-u)}{\alpha}\right)^{k}\right\} \qquad 4.11$$

in which k is the shape parameter, u the location parameter and α the scale parameter.

4.3.3 The distance 'l' from axle-detector (velocity measurement) to impact.

The distance from the axle detector to the stationary wagons is necessary for determining the impact velocity. The longer the distance before impact, the more the rolling resistance and the drag force influence the velocity. The distance $'l'$ is determined using the total distance from the axle detector to the brake shoe minus the number of stationary wagons (section 4.4.5) multiplied by the average length of a wagon. Wagons come in different

lengths for many different types; the average length over the buffers is estimated at 17.5 meters and considered as deterministic (DB Schenker Rail AG, 2011; Greenbrier Europe, n.d.). The total distance to the brake shoe is estimated and deterministic, from Figure 2.6, at 600 meters[18].

4.3.4 Impact velocity

The impact velocity is calculated using the energy dissipation over the travelled distance l, according to equation 4.12. The drag force is related to the velocity, and this calculation is therefore performed iteratively over 20 sections ($dl = l/20$).

$$\frac{1}{2}mv_{impact}^2 = \frac{1}{2}mv_{exit}^2 + l(F_{rr} + F_{drag}) \qquad 4.12$$

Remember that rolling resistance is negative and the drag force can either be positive or negative dependent on the relative velocity of the wagon with the surrounding air. Furthermore, the maximum Exit-velocity from equation 4.5 is $11\ m/s$, and adjusted for sloshing according to equation 4.6.

4.4 Final parameters

Apart from the parameters explained in the previous paragraph, this paragraph describes the final variables which are necessary in determining a failure probability using the Dynamic model.

4.4.1 Strength of a wagon's structure

Many different wagons exist at Kijfhoek, which is described in section 2.1. All these different types are likely to have different strengths. This section describes the overall strength of the wagon's structure and does not determine the strength of the tank (this is handled in section 4.6.1). Besides the different types, a wagon consists of many different components, and determining its overall strength in longitudinal direction depends on the force distribution through all these components and the accumulation of stresses in critical points. This investigation is not performed in this thesis, and the wagon's strength[19] is estimated following the regulations of the crashworthy buffers (NEN, 2017), and no distinction is made between wagon types.

The maximum mean force in the plastic region of the buffers is not allowed to exceed $2200\ kN$ (see the next section), since a wagon consist of two side buffers at each end, the combined force is possibly doubled to $4400\ kN$. For these buffers to perform correctly in a collision, the wagons strength needs to exceed this value, else the wagon damages before the buffers do. Therefore, the wagons mean strength in plastic deformation is estimated at $5000\ kN$, and two standard deviations away from the $4400\ kN$, leading to: $F_{wagon,pl} \sim N(5000,300)[kN]$. The relatively large probability (2.3%) of a wagon's strength being lower than $4400\ kN$ is also based on investigations by Boyko (2012) in which he states that fatigue causes cracks in the structure of a tank wagon already visible after eight years of normal operations.

[18] Deterministic values are considered good enough since the forces resisting motion need a long distance; being of by 50 meters will not influence the velocity much.

[19] The regulations and strength of wagons could be obtained from NEN-EN 12663-2:2010, but the TU Delft nor ProRail has excess to this document, and therefore an estimation is made based on the maximum allowable strength of the buffers.

<u>Assumption</u>: Not enough information regarding the wagon's strength was found in literature. Basing the wagon's strength on the regulations of the maximum buffer's plastic force is a large assumption. This assumption is expected to have a significant influence in determining Type 2 damage.

4.4.2 Buffers

Buffers are elements placed at the longitudinal ends of a wagon or train carriage capable of absorbing energy. The buffers on transport wagons are called 'side buffers.' These side buffers are the most critical energy-absorbing devices in preventing damage to the main structure of the wagon and preventing possible Loss of Containment in case of collision.

Therefore, these buffers are subject to specific regulations. For example, in order for these side buffers to function correctly in a series of connected wagons, European regulations (NEN, 2020) require the buffers of all wagons to be located on the same level with respect to the surface and the centreline of the wagon. Figure 4.23 shows a schematization of two coupled wagons, showing the coupler and the side buffers, with the buffer location according to European regulations. In addition to the location, the buffer's energy absorption capacity must comply to several standards.

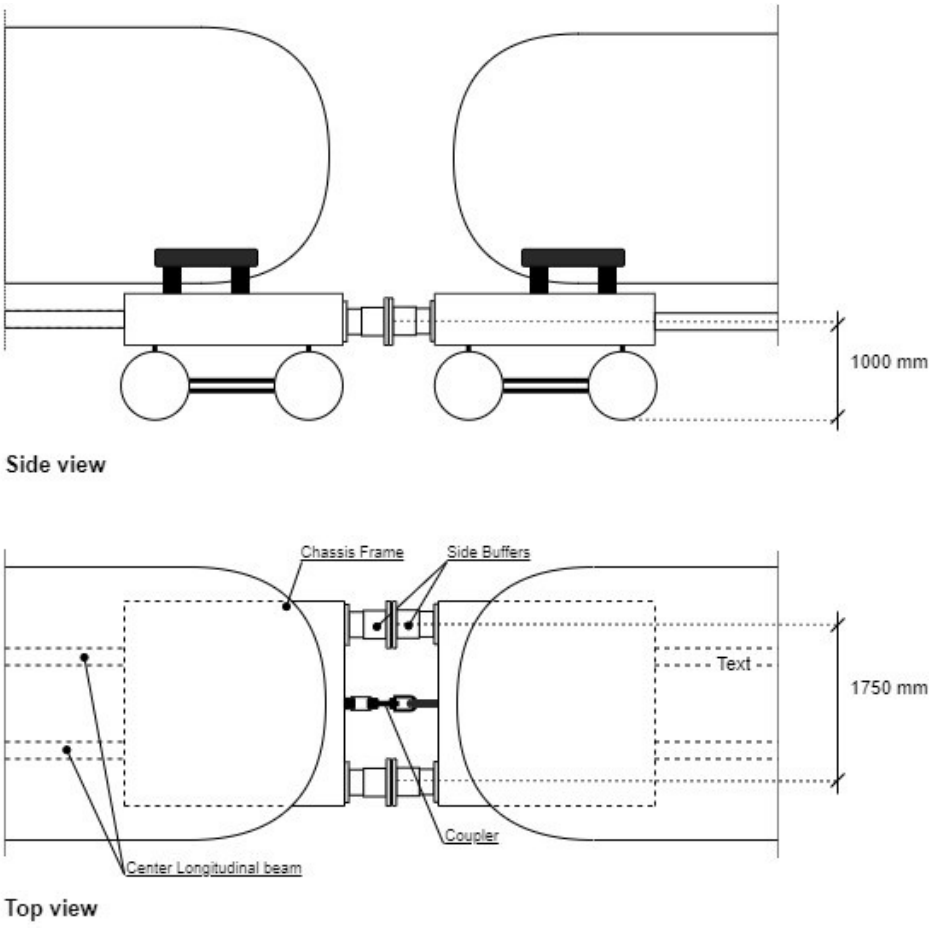

Figure 4.23 Schematization of the connection between two wagons. The dimensions are from NEN 15227 (2020).

The NEN (2017) has categorized side buffers into three different categories according to their dynamic energy capacity, shown in Table 4.3. Damage to the buffers or the wagon shall not occur below these energy levels.
Category A buffers, with a maximum buffer stroke of 105 mm, are the required buffers for

traditional freight wagons. The 'stroke' is the amount the buffers are compressed. Before reaching the maximum stroke, a buffer needs to have an energy absorption capacity according to Table 4.3, and no permanent damage or deformation may occur (it should return to its original state, this is called elastic deformation).

Table 4.3: Energy capacity per buffer category (NEN, 2017).

Buffer Category	Dynamic Energy Capacity kJ
A	≥ 30
B	≥ 50
C	≥ 70

According to the "Regulations concerning the International Carriage of Dangerous Goods by Rail" (RID, 2019), side buffers on tank wagons have to comply with much stronger standards. Therefore, tank wagons need to be fitted with so-called 'crashworthy buffers' as is described in the NEN-EN 15551 (2017). Crashworthy buffers are categorized in the same manner as Table 4.3, but they have an extra letter 'X' behind their original category name (AX, BX or CX), describing an extra absorption capacity in the plastic deformation of the buffers. Plastic deformation refers to deformations that are non-reversible and thus causing damage to the buffers. Moreover, the crashworthy buffers have to comply with the following three conditions (NEN, 2017):

1. velocities of under $12\,\frac{km}{h}$ $(3.3\ m/s)$ shall not trigger the plastic deformation of the buffers,
2. the total energy absorption capacity must be $\geq 400\ kJ$. For buffers on wagons built before 2005, this capacity should be $\geq 250\ kJ$,
3. plastic deformation to the tank body is not allowed if the energy absorption is below respectively 400 or $250\ kJ$.

Further requirements that are of interest:

a. The force to trigger the plastic deformation should be $\geq 1500\ kN$.
b. During the plastic deformation, the mean force in the plastic region should be $\leq$ $2200\ kN$.

Buffer modelling

The wagon's buffers are modelled with distributions for its parameters based on the following points:

- The regulations explained in the previous paragraph,
- The literature, moreover in the next paragraph,
- It should be implementable in the multi-body dynamic model explained in section 3.3,
- The product guides of buffer manufacturers in Appendix K.

Buffer modelling in literature

The crashworthiness in trains has been of interest in the literature for many years. However, most of these studies are primarily focused on passenger safety and passenger trains. Whereas investigations into collisions of transport wagons and tank wagons are limited, even though the transporting of dangerous goods via rail also concerns public safety. Moreover, the investigated collisions in the literature are performed with higher impact velocities than commonly present at Kijfhoek. Despite these differences, the way the buffers are modelled is helpful, and done similarly for many years in papers using a multi-body dynamic model (Cole & Sun, 2006; Lu, 1999; Sun et al., 2012, 2014; Xu et al., 2019).

Figure 4.24 shows a few examples from the literature. The two most right panels separate the force-stroke diagram into several linear segments, using 'a piecewise-linear spring', modelling the non-linear behaviour of the buffer. The Cole & Sun (2006) model (middle panel) describes a similar draw hook system with two side buffers as is used on wagons at Kijfhoek and demonstrated in Figure 4.23.

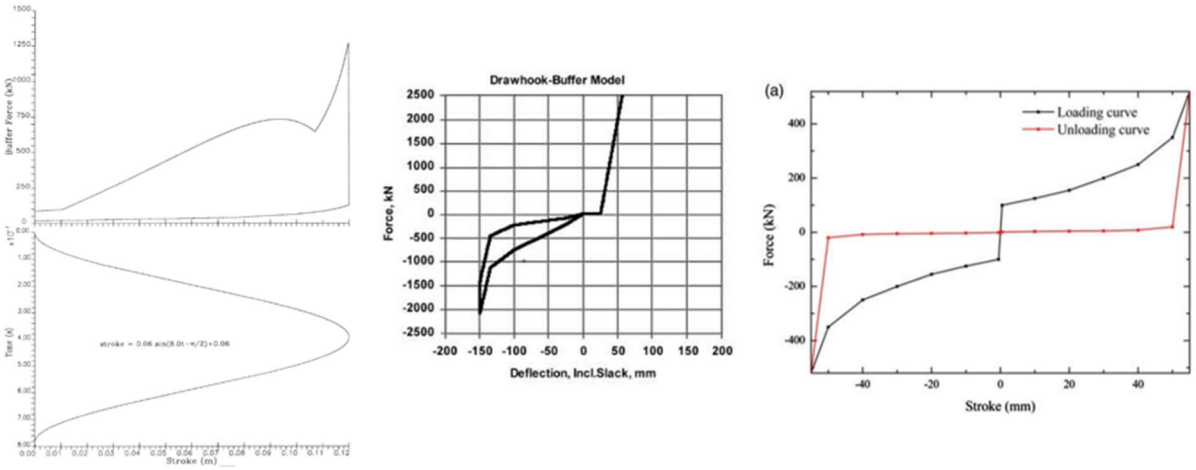

Figure 4.24: Several examples from the literature show the loading and unloading curves in the elastic region of the buffers using a force-stroke diagram. From left to right Lu (1999)*, Cole & Sun* (2006)*, and Xu et al.* (2019)

Energy-absorption of a spring-damper

In this thesis, the buffers are modelled using a non-linear elastoplastic element by applying several non-linear springs and a viscous damper in parallel. A single linear spring element does not have an energy-absorbing capacity[20]. Figure 4.25 and Figure 4.26 show the difference between the loading and unloading of linear spring versus an imposed non-linear spring (or piecewise linear) with different paths for loading and unloading as is done in the literature. This non-linear behaviour depicted in Figure 4.26 is called hysteresis, which results in an energy absorption capacity. The shaded area between the loading and the unloading curve is the energy absorption. Apart from the imposed hysteresis, the viscous damper also absorbs energy, and the influence of viscous damping is visible in Figure 4.30 at the end of section 4.4.4.

[20] A 'perfect' linear spring stores energy as potential energy, if a force is applied in compression or tension. When the force is released, the spring releases its potential energy completely (some energy is always lost in heat, caused by material friction/deformation).

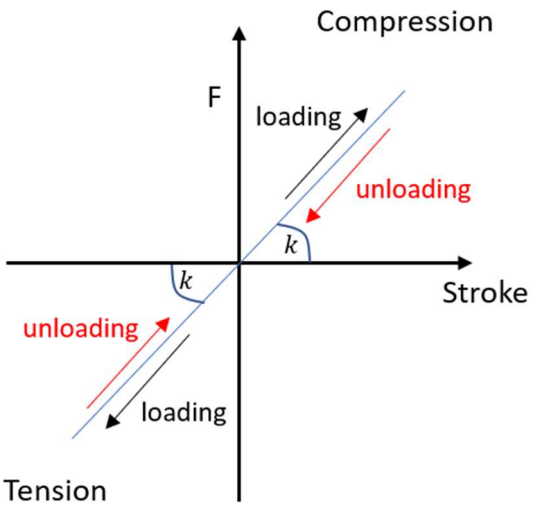

Figure 4.25: Force stroke diagram for the loading and unloading of a linear spring.

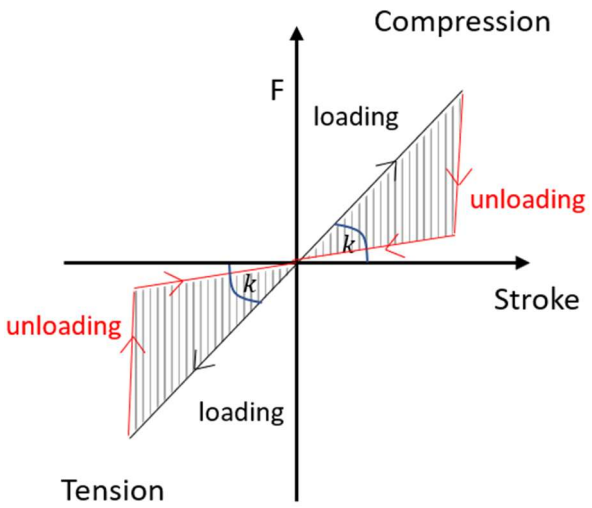

Figure 4.26: Force stroke diagram for a non-linear spring, showing the effect of hysteresis for a different loading and unloading path. The shaded area is the energy absorption.

Modelling of a single buffer in this thesis

Two different buffer types are modelled in this thesis: a standard 'Category A' buffer for regular transport wagons and a crashworthy 'Category AX' for tank wagons. Figure 4.27 shows the linearized quasi-static force-stroke diagram of a crashworthy buffer applied in the dynamic model. The buffer contains two regions: an elastic region and a plastic region. Whereas a regular buffer does not have a plastic region, and the elastic region of the crashworthy buffer describes the complete force-stroke diagram of a standard buffer.
The loading and unloading follow respectively the black and the red line, in which the area between these curves is the energy absorption capacity of the buffer. The unloading curve in the figure is indicated at the end of the respective region. However, unloading happens whenever the exerted force on the buffer is released at any given stroke, resulting in a shift of the unloading curves to the left and reducing the energy absorption. The unloading paths are different in the elastic region and the plastic region, as indicated in the figure. Plastic deformation means that the deformations are permanent, which should result in a force reducing to zero at the point of plastic deformation, indicated by point 1 in Figure 4.27. However, the unloading curve continues on a different path to zero force at zero stroke for numerical reasons.

<u>Assumption</u>: This thesis assumes two buffer types only, while many buffers of many manufacturers are available. However, these buffers must comply to similar standards, and by applying probabilistic distributions to most of these standards, these differences are partly included.

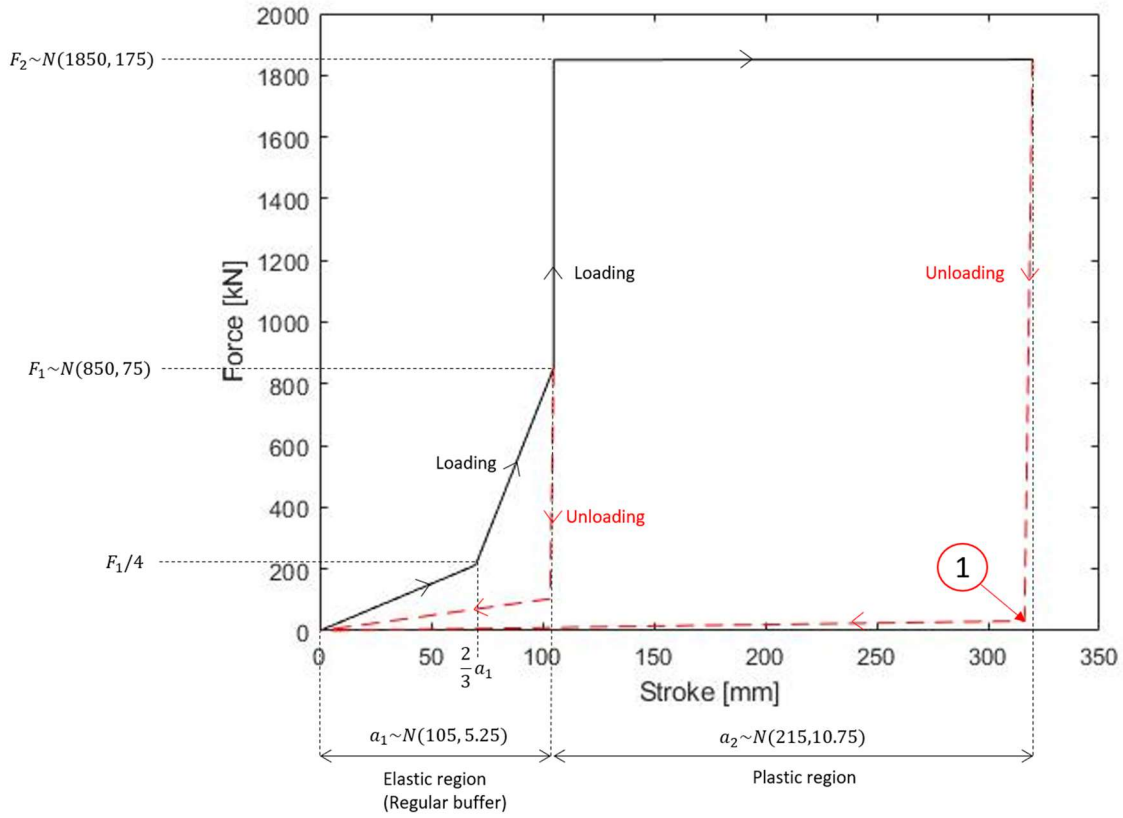

Figure 4.27: The loading and unloading curve of a single crashworthy buffer without the viscous damper. The probabilistic parameters and their values are also shown.

Length of the stroke

From Figure 4.27, the length of the elastic stroke for both buffer types is assumed Normally Distributed ($a_1 \sim N(105, 5.25)\ [mm]$) with a mean, based on the European regulations (NEN, 2017), of $105\ mm$. The crashworthy buffer has a plastic region which is also assumed Normally Distributed ($a_2 \sim N(215, 10.75)[mm]$) with a mean[21] of $215\ mm$. The variance of coefficient for the stroke is relatively small at 5% because it is believed that current production methods are sophisticated enough in developing a minor deviation in the size of the buffers.

The magnitude of the forces

The maximum force F_1 applied by the spring in the elastic region is determined from the manufacturers' product guides in Appendix K. These different guides show a slight variation in the magnitude of this force leading to an assumed Normal Distribution with a more significant standard deviation ($F_1 \sim N(850{,}75)\ [kN]$). To allow for a 'polynomial' shape in the elastic region, the region is divided into two linear segments; the force at two-thirds of the maximum elastic stroke ($\frac{2}{3}a_1$) is equal to $F_1/4$.

[21] This value is determined based on the magnitude of the average force in the plastic region in combination with the requirement of a minimum energy capacity of 400 kJ (NEN, 2017) $F_2 * a_2 = E_{absorbed,plastic}$ and the product guides of the buffer manufacturers in Appendix K.

The force in the buffer's plastic region is assumed constant[22] over the entire stroke a_2, as is done in many papers for components in plastic deformation (Li et al., 2016; Lu, 1999; Pereira, 2006; Scholes & Lewis, 1993). In reality, this force fluctuates due to the plastic behaviour of a material. The value of the constant force F_2 is determined from averaging the values in the following points in the regulations (NEN, 2017):

a. The force to trigger the plastic deformation should be $\geq 1500\ kN$.
b. During the plastic deformation, the mean force in the plastic region should be $\leq 2200\ kN$.

The values $1500\ kN$ and $2200\ kN$ are chosen as the 95% confidence intervals of a Normal Distribution leading to: $F_2 \sim N(1850{,}175)\ [kN]$.

Assumption: A constant mean force in the plastic region is assumed, while this force is known not to be constant. This assumption has little effect on the energy absorption capacity of a single buffer. It may have a more significant effect on the distribution of forces through the system in case of a collision.

Spring stiffness k

The spring stiffness is determined per linear segment by dividing the force difference per segment by the stroke length of the segment.

Simplified buffer capacity

In the description of the buffers as mentioned above, the parameters are chosen such, that these are to be implemented in the dynamic model. In section 4.5.4, a simplified version of the buffers' energy capacity suffices, only describing the energy capacity. The minimum values for energy absorption capacity described in the regulations (NEN, 2017) at the beginning of this section are used as characteristic values with 2.3% non-exceedance. The capacity is assumed normally distributed with about a 10% Coefficient of Variation leading to the following:

- regular buffer energy capacity: $E_{capacity,regular} \sim N(36{,}3)\ [kJ]$,
- crashworthy buffer energy capacity: $E_{capacity,cw} \sim N(480{,}40)\ [kJ]$.

4.4.3 The coupler

The coupler schematized in Figure 4.23 represents a simple screw coupler, shown in Figure 4.28, connected to a hook of the other wagon. The coupler only works in tension and is modelled as a linear spring. With a deterministic spring coefficient $k_{tension} = 3 * 10^4$, determined visually from the force-stroke diagram used for the draw-hook system by Cole & Sun (2006). In a collision, the compression is the part of interest. Once the coupler starts working, the impact has already occurred. Therefore, further investigation into the coupler is deemed unnecessary.

[22] In the dynamic model this force slightly increases by 1kN over the plastic region's length for numerical reasons.

Figure 4.28: Typical screw coupler to connect wagon (SCREW COUPLING 1350 KN: FMC Hidrolik Sistemleri Otomotiv Mak. San. Ve. Tic., n.d.).

4.4.4 Combining the coupler, buffers, and wagon structure

In the above paragraphs, the strength of the wagon structure, a single buffer and the coupler are described. However, in the dynamic model, the complete interface in Figure 4.23, consisting of four side buffers (two on each wagon's end), the coupler, and two wagon structures, is modelled with a non-linear single spring-dashpot element.

Combination of multiple springs

Linear springs in series or parallel are combined using the well-known relations given in equation 4.13. This relation implies that springs in parallel provide twice as much force for the same single spring stroke (increasing the spring stiffness), whereas springs in series provide twice as much stroke before the same force of a single spring is reached (tendency towards the weaker spring).

Parallel	$k_{eq} = k_1 + k_2$	4.13
Series	$\frac{1}{k_{eq}} = \frac{1}{k_1} + \frac{1}{k_2}$	

In which k_{eq} is the equivalent spring stiffness of the combined spring stiffnesses k_1 & k_2.

Figure 4.29 shows a hypothetical force-stroke diagram of a complete interface assuming four identical (deterministic) crashworthy buffers, two same strength wagons and a single coupler[23]. At zero stroke, the buffers and the coupler are assumed in an unloaded condition. This transition point represents zero relative displacements between two subsequent wagons. Thus, the buffers only apply a force on the system when compressed (wagons colliding), whereas the coupler only in tension (wagons moving away from each other).

Once the buffers have reached their total plastic deformation, deformation to the wagon body will continue, ultimately reaching the maximum plastic force of the wagon structure explained in section 4.4.1. The weakest wagon will deform before the more robust wagon.

Loading and unloading follow different paths, describing the element's hysteresis, resulting in energy dissipation. The area between the loading and unloading curves is the energy absorption. Once the plastic region is activated, the unloading and reloading follow the same path until the wagons' relative displacement reaches the previously induced deformation, then following the original loading curve. In the elastic region, no deformation occurs, hence

[23] In Appendix L a figure is shown to illustrate how buffers with different force values are combined into one single force-stroke diagram.

the reloading follows the original loading curve. This process is indicated in the figure below with the different colour lines. In this figure the unloading occurs at the end of the elastic and plastic region, respectively. However, this unloading occurs whenever the relative velocity between two wagons changes sign, and this could happen at any relative displacement.

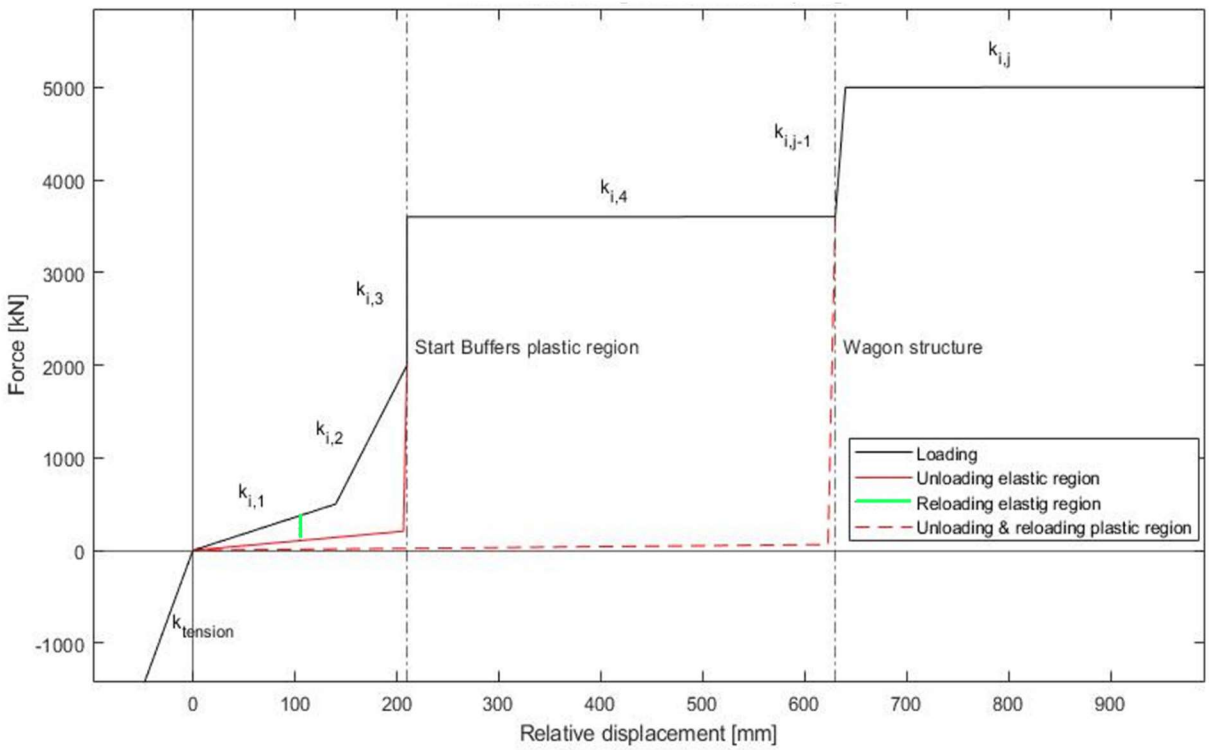

Figure 4.29: A deterministic force-stroke diagram of an interface, consisting of the coupler in tension, the buffers and the wagons' structure in compression, the values in this figure can vary per train or buffer, the viscous damper is not included.

Dependency of the buffers

The buffers on a wagon are likely to show a form of dependency because they are likely the same brand, produced at equal times and have undergone similar wear and tear. The exact dependency is not investigated, but results are found for both independent and fully dependent buffer forces on each wagon. The Normal distribution of two parallel buffers on each wagon's end is shown in Table 4.4 for the independent and dependent cases by summing the Normal distributions of a single buffer. Moreover, in the dependent case, forces and stroke length are the same on both (longitudinal) ends of a wagon.

Table 4.4: Force distribution of two parallel buffers combined; dependent vs independent.

	Description	Dependent $(2\mu, 2\sigma)$ $[kN]$	Independent $(2\mu, \sqrt{2\sigma^2})$ $[kN]$
F_1	Max force elastic region	$N(1700,150)$	$N(1700,106)$
F_2	Mean force plastic region	$N(3700,350)$	$N(3700,247)$

The length of stroke of respectively the elastic and plastic region of two parallel buffers is considered fully dependent. If these are considered independent, it could lead to force

concentration toward one buffer in the lateral direction, which cannot be modelled in a one-dimensional longitudinal model.

Assumption: The use of a MBD model in one dimension prevents the modelling of a concentrated force to a single buffer. This concentrated force is expected to distribute again throughout the width of the wagon's structure behind the buffer. Since the tank wagons are on top of the wagon's structure, it is not expected that these concentrated forces would increase the probability of rupture to the tank wagons significantly.

The viscous damper

The buffer force also depends on impact velocity, as is shown in the difference between the static and dynamic force-stroke diagrams in Appendix K. A non-linear viscous damper models the velocity dependence of the buffers. Damping is active in loading whilst in the elastic region, and the damping equals zero in unloading and once the plastic region is activated.

The damping coefficient in the model is found by performing the impact test for crashworthy buffers according to appendix J of the NEN-EN 15551 (2017). The impact test prescribes an 80t wagon with standard buffers to impact the stationary 90t wagon fitted with the crashworthy type. The damping coefficient is matched to act similarly to the dynamic diagrams from Oleo in Appendix K through trial-and-error. The first 50 mm of the relative displacement, the damping coefficient engages linearly to its total capacity. After which, the dashpot works as a regular viscous damper. The maximum force in the elastic region applied by a single buffer is limited in the model to $1500\ kN$ ($3000\ kN$ for two side buffers in parallel) to prevent the buffers from engaging the plastic region, according to the requirements (NEN, 2017). Figure 4.30 shows the effect of damping on the force stroke diagram in the elastic region, leading to the following equation for the dashpot force, introduced in equation 3.7:

$$f_{i_{dashp}} = \begin{cases} 0, & for\ (\dot{x}_{n-1} - \dot{x}_n) < 0\ or\ (x_{n-1} - x_n) < 0 \\ c(\dot{x}_{n-1} - \dot{x}_n)(x_{n-1} - x_n)/0.05, & for\ 0 \le (x_{n-1} - x_n) \le 0.05 \\ c(\dot{x}_{n-1} - \dot{x}_n), & for\ 0.05 < (x_{n-1} - x_n) \le x_e \\ 0, & for\ (x_{n-1} - x_n) \ge x_e \\ F_{max} - f_{i_{spring}}, & for\ \left(f_{i_{dashpot}} + f_{i_{spring}}\right) \ge F_{max}. \end{cases} \quad 4.14$$

Where x_e is the maximum relative displacement of the elastic region of the combined buffers and F_{max} represents the force at which the plastic region engages.

A damping coefficient of $4 * 10^5\ kg/s$ is used in Figure 4.30 for the whole interface. Because of the trial-and-error method, a coefficient of variation of 15% is assumed. The relation of equivalent springs in series in Equation 4.13 is reversely applied to find the damping coefficient for a single wagon's end, leading to $c_{cw} \sim N(8 * 10^5, 1.2 * 10^5)\ [kg/s]$.

A standard buffer has lower requirements, and a lower damping coefficient is assumed: $c_{standard} \sim N(2 * 10^5, 3 * 10^4)[kg/s]$.

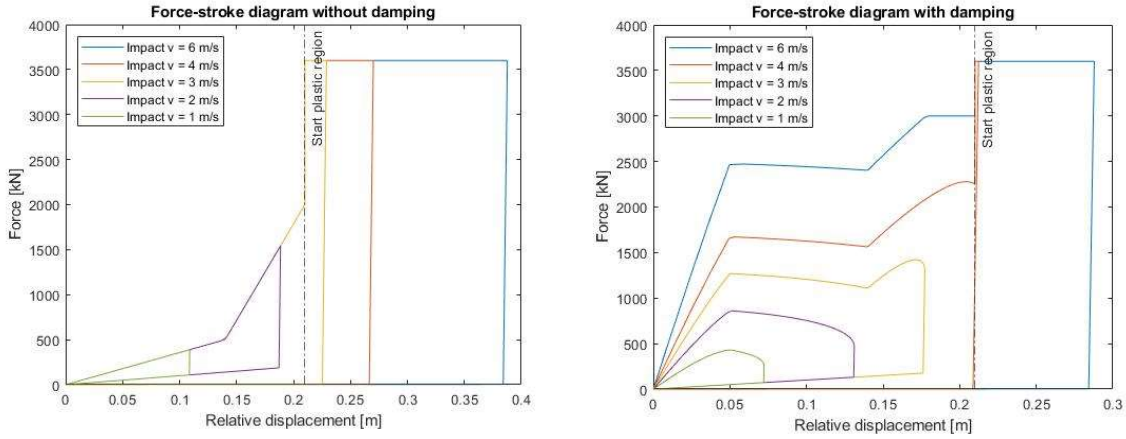

Figure 4.30: Left: The force stroke diagram for different velocities without damping, only showing hysteresis. Right: With damping, showing hysteresis and viscous damping, and the dependence with the velocity.

4.4.5 The number, type, and mass of the stationary wagons

A train (combined of several run-offs) leaving the emplacement is about 28 wagons long. First, this value of 28 wagons is used to determine the number of 'stationary' wagons[24] on the allocation tracks at any given time, with a discrete uniform distribution on the interval $[0,27]$, $U_d(0,27)$. This results in a probability of a rear-end collision $P(collision) \approx \frac{27}{28}$, since once every 28 times the run-off runs into the brake-shoe.
Next, the type of each of these wagons is determined from the empirically found Bernoulli distribution (tank wagon vs any other) $Bern(p = 0.649)$ explained in section 4.2.1 and followed by the determination of the wagons' mass given by the empirical distributions.

<u>Assumption</u>: The wagon's type and mass are considered independent of one another. This assumption is most likely not accurate; one can imagine that a train with a particular destination contains more of the same goods and wagon types. Additionally, this dependency extends to the stationary wagons and the run-off in case of collision. However, a collision between two tank wagons containing energy-absorbing buffers, which is more likely to occur in case of dependency, has more energy-absorbing capacity. Therefore, assuming independence between the wagon types is considered conservative. More investigation into the dependency between wagon types is necessary and leads to more accurate results.

4.4.6 Material Damping

When materials are deformed, some of the mechanical energy transforms into heat. This material damping is considered much smaller than the damping effect of the loading and unloading of the buffers and the chosen damping coefficient. Introducing material damping is possible by re-tuning the damping coefficient in section 4.4.4. However, not considering material damping is a conservative approach because the material damping takes out energy that the buffers absorb in the model. Therefore, adjusting the damping coefficient for material damping is not performed in this thesis.

4.5 Monte Carlo simulation results

In this Monte Carlo simulation, the probability of Loss of Containment is estimated. LOC occurs when the damage of a tank wagon is that severe that it results in rupture of the tank.

[24] Following Lu's (2002) investigation where he suggested 3-4 wagons would be enough to determine the energy absorption in longer rakes. To reduce the computation time in the dynamic model, a maximum of twelve stationary wagons is used, deemed more than enough to represent the collision properly.

Therefore, damage to the wagon's structure is investigated first before rupture of the tank is estimated. As explained in section 3.4, there are two types of damage: Type 1 damage, which uses the buffers stroke and Type 2 damage which uses the wagon's strength.

4.5.1 MC flow chart

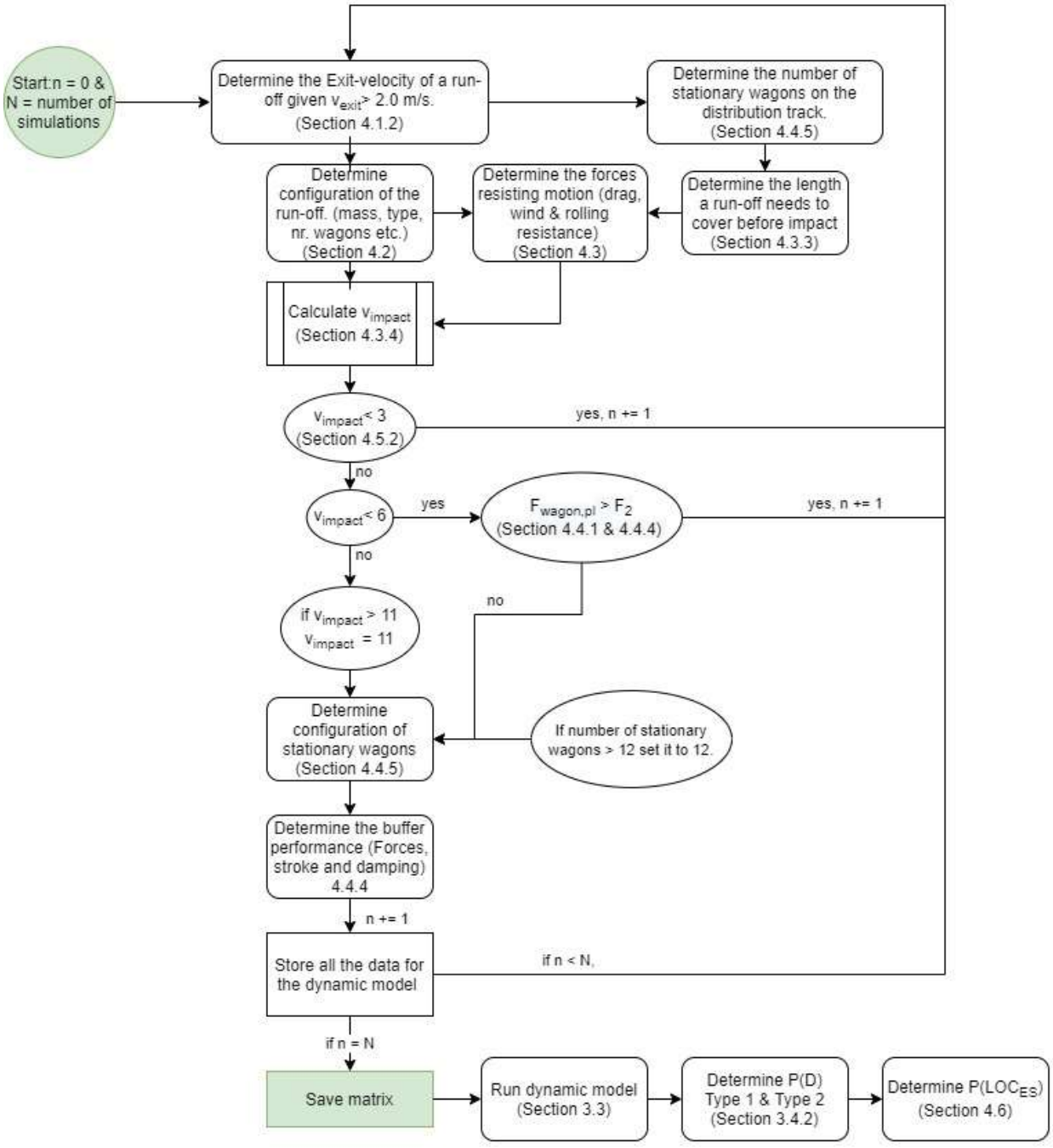

Figure 4.31: Monte Carlo flow chart.

4.5.2 Preliminary MC for different velocities

Before proceeding to the Monte Carlo simulation specific for the Kijfhoek situation, a preliminary MC is performed to determine the impact velocities at which (tank) wagons are damaged in order to limit the computation time. This process could be seen as a kind of 'importance sampling' technique to obtain more simulations in the area where damage

occurs (Jonkman et al., 2017). Since the LSF's in equation 3.18 and 3.19 cannot be solved analytically, a sampling function is hard to find. Therefore, a preliminary MC is performed as follows: 10.000 different configurations of run-offs and stationary wagons, based on the distributions explained in the previous Paragraphs and the MC flow-chart Figure 4.31, are simulated in the dynamic model at ten different velocities (from 2 to 11 m/s, at 1 m/s intervals). These 100.000 simulations are performed for wagons with independent and dependent buffers, resulting in 200.000 simulations for which the results are found in Figure 4.32 and Figure 4.33.

Figure 4.32 shows the results at different velocities of Type 1 damage on a given interface, using the buffer's stroke capacity, involving a tank wagon either in front or behind this interface. Whereas Figure 4.33 present the probability of Type 2 damage to a tank wagon at different velocities. Furthermore, in Appendix M, the damage to any wagon is given (not separating tank wagons), which is of interest in possible damage to a tank wagon for the 'unusual' Type 2 damage, and potentially happens at velocities of 4 m/s. Complete buffer failure (Type 1) of regular wagons is possible at 3 m/s, due to the absence of a buffers plastic region combined with low probabilistic buffer parameters. Furthermore, the dependency of the wagon's buffers, described in section 4.4.4, has little effect on the failure probability.

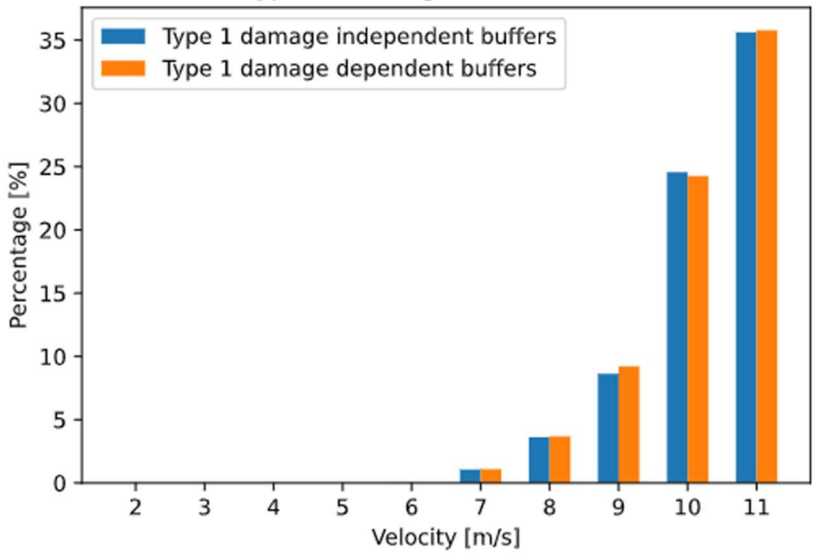

	Type 1 damage [%]: buffers completly damaged	
Impact v [m/s]	Dependent	Independent
2	0	0
3	0	0
4	0	0
5	0	0
6	0	0.01
7	1.09	1.06
8	3.68	3.61
9	9.22	8.63
10	24.26	24.56
11	35.78	35.62

Figure 4.32: Type 1 damage: the percentage per velocity that a tank wagon is involved at interfaces in which the buffers are entirely damaged.

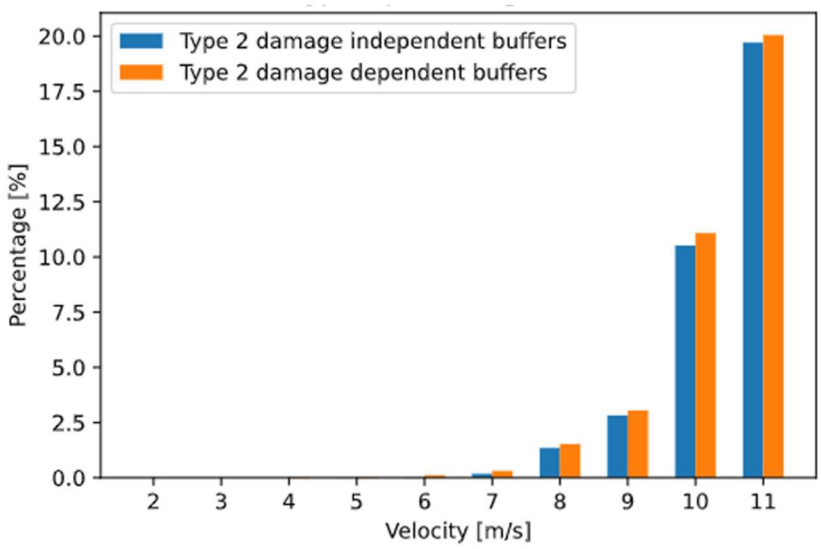

Impact v [m/s]	Type 2 damage [%]: Plastic region of tank wagon reached	
	Dependent	Independent
2	0	0
3	0	0
4	0.03	0
5	0.03	0.01
6	0.11	0.01
7	0.31	0.18
8	1.53	1.35
9	3.05	2.82
10	11.08	10.52
11	20.05	19.71

Figure 4.33: Type 2 damage: the percentage per velocity at which the plastic force of a tank wagon is reached.

4.5.3 MC, Type 2 damage, specific to Kijfhoek

With the above-found results from the preliminary MC, the following list provides the aspects of consideration in the full MC simulation to limit the computation time in the Dynamic model.

- The use of dependent buffers is marginally conservative and provide sufficiently accurate results.
- Impact velocities of $< 3.0\ m/s$ are not leading to damage of a tank wagon, coinciding with the buffer regulations in section 4.4.2.
- Impact velocities between 3 to $6\ m/s$ only lead to damage if the wagon's strength is lower than the mean force of the plastic region of the buffer (unusual Type 2 failure).

The Monte Carlo simulation is performed with four different selections for the Exit-velocity:

1. the best fit Generalized Pareto distribution,
2. the upper bound of the 95% Confidence Interval (CI) of the GPD,
3. the lower bound of the 95% CI,
4. and the best fit t-distribution.

Furthermore, for each of above four choices, another three distinctions for the impact velocity are made.

1. The impact velocity is equal to the Exit-velocity ($v_{impact} = v_{exit}$), the rolling resistance, the drag resistance and the sloshing effect are neglected.
2. The impact velocity is determined using the resistance to motion (section 4.3), but the sloshing effect (section 4.2.3) is not considered.
3. Both the resistance to motion and the sloshing effect are considered to determine the impact velocity.

For each of these 12 (4x3) MC simulations, one million runs are simulated given a velocity higher than $2.0\ m/s$, and the results for Type 2 damage[25] are presented in Figure 4.34. The

[25] A similar graph as Figure 4.34, is presented in Appendix N for Type 1 damage. It also shows that the influence of an increased sloshing amplitude is negligible.

probability of Type 2 damage per run-off is found using equations 3.16, 4.3 and 4.4 into equation 4.15. Furthermore, to estimate the probability per year (for low probabilities), the probability per run-off is multiplied by the total number of run-offs in a year, at Kijfhoek this is averaged at about 80.000 over the last 9 years[26]. The results are shown in Table 4.5. For the best fit GPD, the COV are extremely high, and conclusions regarding these numbers should be handled with care.

$$P(D) \approx P\left(D\middle|v > 2.0\frac{m}{s}\right) P\left(v_{exit} > 2.0\frac{m}{s}\right) = \frac{n_f}{N} 4.48 * 10^{-4} \qquad 4.15$$

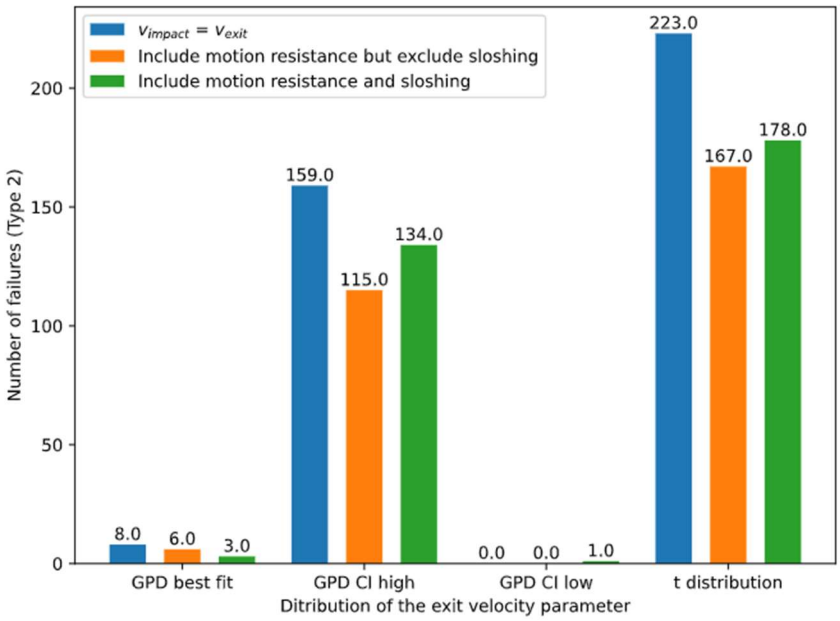

Figure 4.34: Number of Type 2 failures per one million runs, given $v > 2.0\frac{m}{s}$ for the situation at Kijfhoek, with different choices of the Exit-velocity parameter, as well as different determinations of the impact velocity.

[26] **DISCLAIMER:** If the number of run-offs at Kijfhoek changes significantly in the future, the failure probabilities per year are no longer representative.

Table 4.5: Results of the Monte Carlo simulation per run-off and per year.

		Probability of Type 2 damage per *run-off*	Probability of Type 2 damage per *year*	COV V
GPD best fit	$v_{impact} = v_{exit}$	3.59E-09	2.87E-04	0.35
	Include resistance & exclude sloshing	2.69E-09	2.15E-04	0.41
	Include resistance & sloshing	1.35E-09*	1.08E-04*	0.58
GPD 95% confidence interval upper limit	$v_{impact} = v_{exit}$	7.13E-08	5.69E-03	0.08
	Include resistance & exclude sloshing	5.16E-08	4.12E-03	0.09
	Include resistance & sloshing	6.01E-08	4.80E-03	0.09
GPD 95% confidence interval lower limit	$v_{impact} = v_{exit}$	0.00E+00	0.00E+00	-
	Include resistance & exclude sloshing	0.00E+00	0.00E+00	-
	Include resistance & sloshing	4.48E-10	3.59E-05	1.00
Best fit t-distribution	$v_{impact} = v_{exit}$	1.00E-07	7.97E-03	0.07
	Include resistance & exclude sloshing	7.49E-08	5.97E-03	0.08
	Include resistance & sloshing	7.98E-08	6.37E-03	0.07

*Due to the high COV this value is lower than the one above, but it is not likely if you consider the t-distribution and the upper bound GPD.

4.5.4 Simplified MC using an energy relation

The coefficient of variation of the failure probabilities can be reduced by performing more simulations. However, performing more simulation with the extreme demand of computation power inside the MBD model is not efficient, and an alternative approach is favourable. If an analytically solvable LSF is found, the use of the dynamic model can be avoided. The results from the performed simulations are used to find a valuable energy relation for the original LSF in equation 3.3. The energy relation used by Lu (2002) is not sufficient for marshalling yards and needs updating. In order to further simplify the calculation, the following assumptions are used:

1. It is assumed that the impact interface is the interface causing failure, which is very likely.

2. The buffer's energy capacity is simplified using Normal distributions described at the end of section 4.4.2. The buffer's absorption capacity remains similar.
3. The buffers on a wagon are fully dependent from one another, since hardly a difference was visible compared to independent buffers (see Figure 4.32 and Figure 4.33).
4. The resistance to motion and the sloshing effect is neglected, and the Exit-velocity is used as the impact velocity (Figure 4.34 shows this is a conservative approach without being extremely cautious).

Normalized energy factor

The energy absorbed at the impact interface is normalized using a modified version of the collision energy in equation 3.4 and is shown in equation 4.16. This modification uses the masses of solely the front moving wagon and impacted wagon instead of the entire collided trains. If these two wagons have the same mass, as was the case in Lu's investigation, this normalization is similar to Lu's relation.

$$E_{absorbed,impact\ interface} = R_E \frac{m_1 m_{1s}}{m_1 + m_{1s}} v_{impact}^2\ [kJ], \qquad 4.16$$

where R_E represents the dimensionless normalized energy factor, m_1 the mass of the front moving wagon, m_{1s} the impacted stationary wagon, v_{impact} the impact velocity and $E_{absorbed,impact\ interface}$ the absorbed energy at the impact interface.

The results of this normalized energy factor (R_E) from the dynamic model are found in Figure 4.35. It is fitted elegantly (slightly underestimated in the tail) with a scaled lognormal distribution, of which the PDF is shown in equation 4.17, with parameters: shape $\sigma = 0.63$, location $\theta = 0.48$ and scale $m = 0.064$. In Figure 4.35 also a couple of lognormal distributions with an adjusted shape parameter are shown, possibly to fit the tail of the distribution better. In essence, the fitted lognormal distribution used for the normalized energy describes a clustered parameter of all the other parameters described in this chapter[27], except for the parameters specified in equation 4.18.

$$f_L(x;\sigma,\theta,m) = \frac{e^{-\left((\ln((x-\theta)/m))^2/(2\sigma^2)\right)}}{(x-\theta)\sigma\sqrt{2\pi}}, \qquad for\ x > \theta; m, \sigma > 0 \qquad 4.17$$

[27] The normalized energy factor is also depended on the dynamic behavior in the collision and the way the forces are transferred through the rake of wagons.

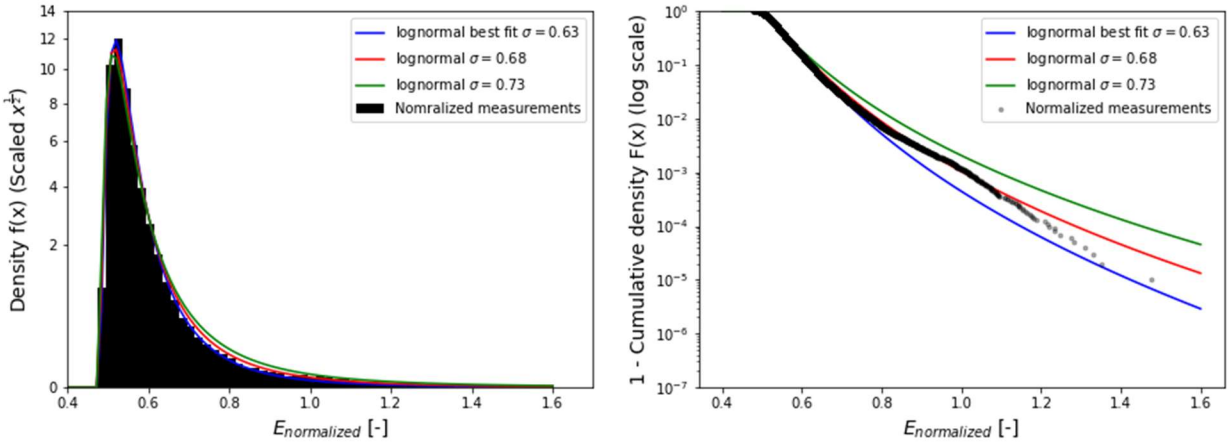

Figure 4.35: Distribution and lognormal fits of the normalized energy.

The failure function of the buffers of the impact interface is then found by combining equation 3.3 and 4.16:

$$Z = E_{cap} - R_E \frac{m_1 m_{1s}}{m_1 + m_{1s}} v_{impact}^2, \qquad 4.18$$

in which E_{cap} represents the Energy absorption capacity of a combination of four buffers, either all crashworthy buffers, two regular and two crashworthy buffers or four regular buffers. There is no tank wagon involved in the last case, so no damage to a tank wagon. The energy absorption capacity of the wagon's structure (before damage to the tank occurs) is *not* considered. Meaning that using the above relation does *not* consider Type 2 damage. Furthermore, the LSF in equation 4.18 is conditionalized on the condition that a collision has occurred (it needs to be multiplied by $P(collision)$ to get the damage probability).

With the use of equation 4.18, the simplified Monte Carlo simulation is performed, as described by the flow chart in Figure 4.36. The results are compared with the Monte Carlo simulation utilizing the dynamic Model for type 1 damage in Figure 4.37. The results are conservative for all the different shape parameters for R_E's lognormal distribution. However, the best fit shape parameter shows promising results with a 'safety factor' between 1.1 and 1.3 and suffices for future calculations at Kijfhoek; changing the shape parameter has minor influence on the failure probabilities. Furthermore, it became obvious that the probability of failure in a tank-no tank collision (TNT) is five times higher than in a tank-tank[28] collision (TT) due to the higher energy absorbing capacity of the buffers.

<u>Assumption</u>: The parameters in the LSF of equation 4.16 are assumed independent (in chapter 5, some attention is paid to the minor influence of dependency)

[28] Tank-tank collision is a collision between two tank wagons, tank-no-tank collisions are collisions consisting of one tank wagon and one regular wagon. NTNT is a collision between two non tank wagons.

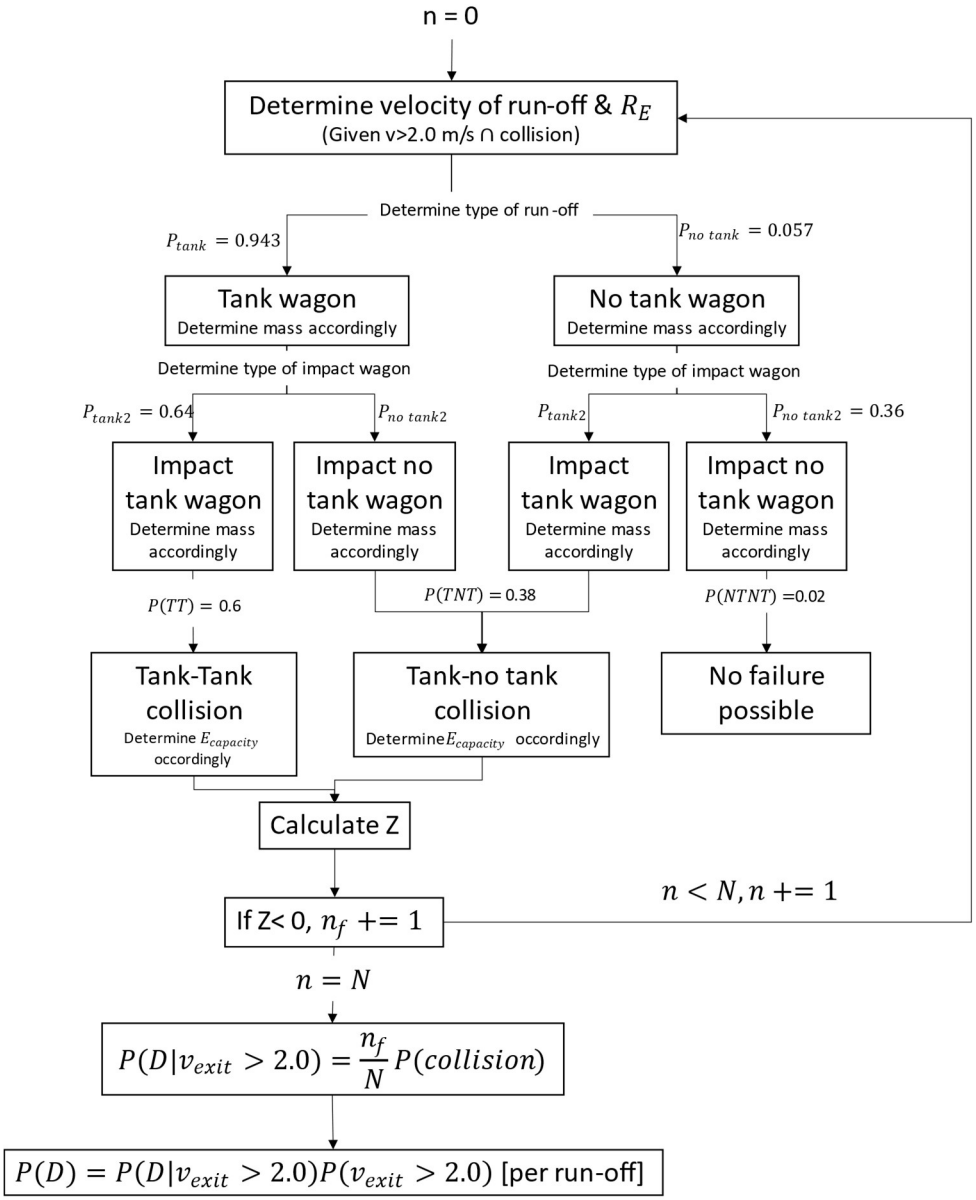

Figure 4.36: Flow chart of the simplified Monte Carlo.

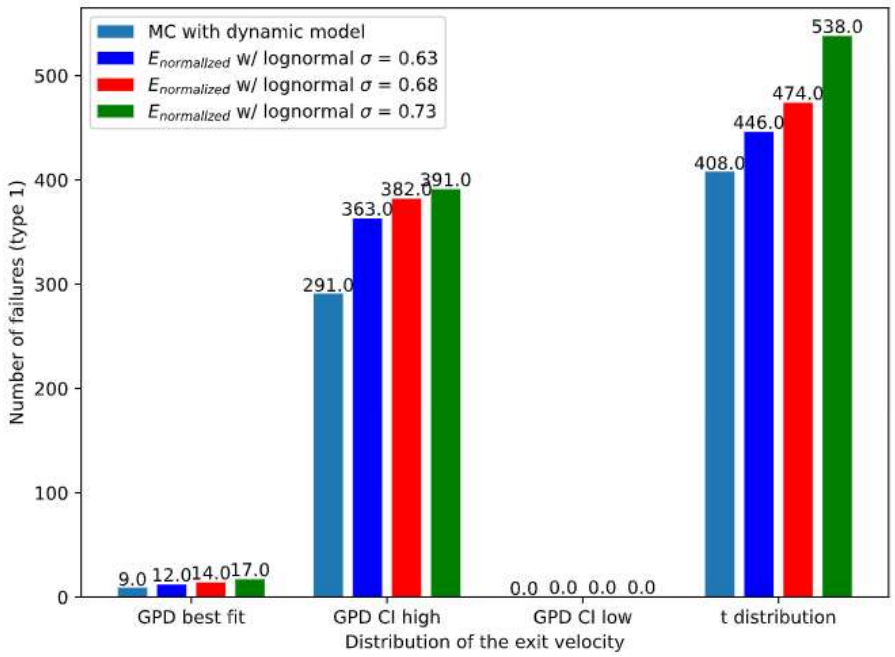

Figure 4.37: The results of the simplified MC applied to 1 million simulations for several shape parameters of the normalized energy's lognormal distribution, compared with the MC using the dynamic model.

4.6 Loss of Containment

Having defined probabilities of damage ($P(D)$) extensively in the previous sections, the following section is focused on determining Loss of Containment. For LOC to occur, the tank wagon's damage needs to result in rupture of the tank; this is explained in the Event tree in Figure 3.3 and by equation 3.1. Identifying LOC moment is complex, and for the scope of this thesis, assumptions are necessary.

4.6.1 Determining $P(DG)$ and $P(leakage)$

The calculation method provided by the government for External Safety (SAVE, 2006), explained in section 2.3, prescribed generic failure probabilities for collisions of the first five scenarios (see Table 2.2). These are multiplied by a probability of a leak based on the thickness of the tank container's wall and are $P(leakage|fluid) = 0.1$ and $P(leakage|gas) = 0.01$. However, the calculation method caused four problems in this thesis.

1. When is a collision considered a collision? As was shown in the previous paragraphs, velocities under $6\ m/s$ do not lead to damage of a tank wagon. Therefore, if collisions at lower velocities are considered collisions, the calculation factor for leakage in this thesis should be higher.
2. The probabilities for the Loss of Containment include the probability of damage (in equation 2.1, they go from collision to LOC, avoiding the intermediate step of damage taken in this thesis), resulting in an increased factor to be used in this thesis.
3. LOC can only occur if the wagon contains a dangerous good (it is partly filled or full). This issue is dealt with separately through $P(DG)$; from the results of the simplified

MC, it is found that in about 78% of the failures, the tank wagons had a mass $>$ $50\ tonnes$, and thus contained a DG.[29] Resulting in $P(DG) = 0.78$.

4. The last difficulty arises in the calculation specific to the automated humping process; the generic failure probability for automated humping, explained in section 2.3, is based on the occurrence of an irregularity, but it fails to specify what an irregularity exactly is. Nevertheless, the regulation requires multiplication of generic failure probability with the same probability of leakage.

Another approach in determining the leakage factor is performed by Kok-Palma & Timmers (2014) using all the reported leakages in Europe from 1996-2005. They found a leakage factor per wagon damage of around 0.074 for gasses and 0.088 for fluids, but this is determined based on all damaged freight wagons, not separated for tank wagons, and not specific to railway emplacements. Indicating, that if only damaged tank wagons are considered in the calculation, the outflow factor would be higher. Furthermore, Kok-Palma & Timmers expect that the outflow factors for gasses used in the current External Safety calculations for emplacements is too low. However, not enough information or data is available to support their claim entirely.

Additionally, the probabilities of LOC should be different for Type 2 and Type 1 damage, and from the found results, the difference in the number of damages between the two types amounts to about a factor of 1.8.

Following the preceding statements, the following is assumed regarding the leakage factors:

- The probability for LOC after type 1 damage has occurred:
$$P(Leakage|fluid \cap Type\ 1\ damage) = 0.25$$
$$P(Leakage|gas \cap Type\ 1\ damage) = 0.025$$
- For type 2, the above are multiplied by a factor of 1.8:
$$P(Leakage|fluid \cap Type\ 2\ damage) = 0.45$$
$$P(Leakage|gas \cap Type\ 2\ damage) = 0.045$$

To determine the overall probability for LOC at Kijfhoek, the distribution of gasses and liquids is required. The investigation into gasses and liquids is limited to DG that contribute to External Safety, described in the next section.

<u>Assumption</u>: This thesis focus lies mainly in determining damage to tank wagons, the assumed leakage factors above are necessary to determine LOC, but research into this factor is not performed during this thesis. However, even if the magnitude of the probability for LOC may change for a more credible leakage factor, the general trend between the probability of damage and the probability of LOC will remain because $P(LOC)$ is linearly dependent on the leakage factor.

4.6.2 Determining $P(cat.)$ and the effect on External Safety at Kijfhoek

As is described in section 2.3, not all Dangerous Goods contribute to External Safety. The distributions per category of 'full'[30] tank wagons in Figure 4.16 are used to determine the probability of LOC per category. It was found in the simplified MC simulation that about 64% of the damages to 'full' tank wagons were to the run-offs front wagon, and the remaining

[29] In the QRA for External Safety is unclear how they deal with this exactly. They mention that in 10% of incidents with tank wagons it leads to LOC concerning External Safety, however they do not multiply by the total number of tank wagons but just the number of tank wagons containing DG.

[30] **<u>Recall</u>**: 'full' can also mean partially filled, it means that it contains a dangerous good.

36% considered a 'full' stationary wagon. The run-offs tank wagons and the stationary tank wagons have different distributions regarding the containment of dangerous goods, according to the graph in Figure 4.16. This graph is normalized with the percentages resulting in a single distribution in Figure 4.38, and the total chance of affecting External Safety is 43%.

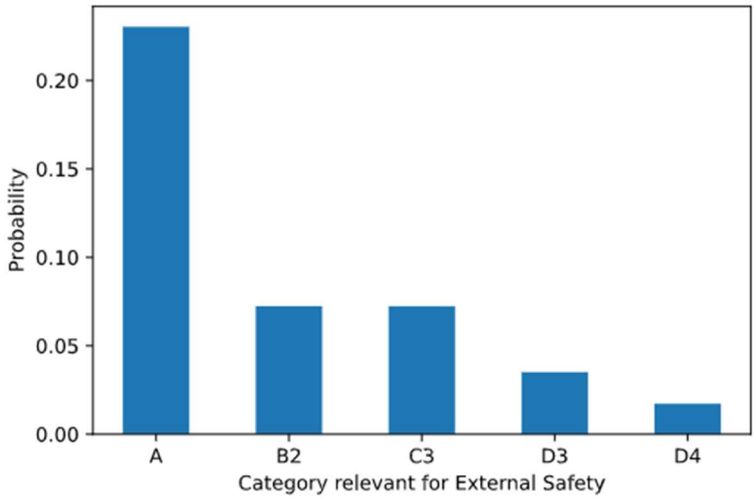

Figure 4.38: The probability that a 'full' tank wagon is in a category, specific for the situation at Kijfhoek. Dangerous Goods not affecting External Safety are not shown in the graph.

Having determined all the necessary probabilities, $P(LOC_{ES})$ can now be determined using equation 3.1. The results per category per year[31] are shown in Table 4.6, for the 95% confidence bounds of the GPD of the Exit-velocity estimate. One must bear in mind that this is ***not*** the risk regarding External Safety. To determine the Site-Specific and Group risk described in section 2.3, the values of $P(LOC_{ES})$ are to be used in further determining External Safety, with the use of the Safeti-NL software.

As is described in section 2.3, further calculations are not necessary if the failure probability calculated below is lower than $4x10^{-7}$ per year, and the risk affecting External Safety is deemed negligible. The results show a failure probability for LOC somewhere between 0 and $3.9x10^{-4}$ and most likely somewhere around 10^{-5}. So, according to the assumption made in this thesis, rear-end collisions should ***not*** be neglected from the QRA assessment. What the exact implication is on the overall External Safety remains unanswered and stays open for future investigation.

[31] **Recall:** to get to a P_f per year the P_f per run-off is multiplied by the number of run-offs per year (80.000) and is susceptive to change in the amount of traffic.

Table 4.6: Results for External Safety per category.

		Probabilities of LOC affecting External safety $P(LOC_{ES})$ per **year**		
External Safety category	GPD for velocity	MC Type 2	MC Type 1	Simplified MC type 1
A (gas)	lower bound	0	0	0
	best fit	2.3E-06	1.5E-06	1.9E-06
	upper bound	4.6E-05	4.7E-05	5.8E-05
B2 (gas)	lower bound	0	0	0
	best fit	7.3E-07	4.6E-07	6.1E-07
	upper bound	1.4E-05	1.5E-05	1.8E-05
C3 (fluid)	lower bound	0	0	0
	best fit	7.3E-06	4.6E-06	6.1E-06
	upper bound	1.4E-04	1.5E-04	1.8E-04
D3 (fluid)	lower bound	0	0	0
	best fit	3.5E-06	2.2E-06	2.9E-06
	upper bound	7.0E-05	7.1E-05	8.9E-05
D4 (fluid)	lower bound	0	0	0
	best fit	1.7E-06	1.1E-06	1.4E-06
	upper bound	3.4E-05	3.5E-05	4.3E-05
Total (sum)	lower bound	**0**	**0**	**0**
	best fit	**1.6E-05** $V = 0.35$	**9.8E-06** $V = 0.33$	**1.3E-05** $V = 0.29$
	upper bound	**3.1E-04** $V = 0.08$	**3.1E-04** $V = 0.06$	**3.9E-04** $V = 0.05$

4.7 Qualitative assessment of the uncertainty in the assumptions

Throughout this chapter, several assumptions were made, and some were highlighted. This section summarizes most assumptions and qualitatively assesses them in Table 4.7. It also indicates whether the probability of LOC with regards to External Safety is expected to go up or down; given more certainty about the assumptions, most of the times this could go either way. Lastly, an indication is given about the expected amount of influence.

Table 4.7: Qualitative assessment on the uncertainty in the assumptions.

Section	Assumption	Remarks	Possible direction and influence level on $P(LOC_{ES})$
4.1.2	The maximum Exit-velocity is based on potential energy only, neglecting drag and rolling resistance.	It is possible that the tailwinds could increase the Exit-velocity, but the drag force and the rolling resistance will always be present.	↓, medium
Throughout this chapter mainly: 4.2.1, 4.2.2, 4.2.4 & 4.6.2	Distributions based on data and on the condition that Exit-velocity of a run-off is > 2 m/s are assumed to hold for higher velocities not encountered in the data.	The influence is mostly visible in the type of wagon, the wagon's mass, and the type of DG. Some have a positive effect of P(LOC) and others a negative. The overall effect is expected to be limited.	↕, low
4.2.3	The assumptions concerning sloshing: 1. only primary mode of oscillation, 2. the magnitude of the velocity amplitude chosen at 0.5 m/s, 3. the moment of impact is independent of the velocity, and 4. The measuring moment is random on a sine curve.	The effect of sloshing would require a separate dynamic model or physical testing and is a study on its own. (Appendix N shows that the influence of the sloshing amplitude is low, keeping the other assumptions the same)	↕, low
4.4.1	The wagons strength is not investigated and based on the buffer strength.	This has a high influence on Type 2 damage, but it has no influence on Type 1 damage since Type 1 only considers the buffers' energy capacity.	↕, high or none
4.4.2	Two buffer types: a regular and a crashworthy one.	There are many different buffer types and manufacturers. It is attempted to consider this uncertainty by using probabilistic values for the buffer parameters.	↕, low
4.4.2	A constant force in the buffer's plastic region.	This has little effect on the energy absorption capacity but may influence the distribution of the forces through the rake of wagons. Indirectly this may lead to change in the normalized energy factor	↕, low

4.4.4	Concentrated forces to a single buffer are not possible to model with the MBD model in this thesis.	These forces are expected to distribute again in the wagon's structure before reaching the tank of the wagon.	↑, low
4.4.5	Assuming independence between the run-off and the stationary wagons.	The mass and type of the wagons are likely dependent. A tank-tank collision lowers the probability of damage significantly.	↓, medium
4.5.4	Using the Exit-velocity as the impact velocity.	This is a conservative approach.	↓, low
4.5.4	Independence between the parameters of the LSF in the simplified approach.	This is investigated in chapter 5 and was deemed to have a minor influence.	↕, low
4.6.1	Determining the leakage factor	This thesis focus lay in mainly finding damage. To determine leakage is a study on its own, and not performed in this thesis. Further, investigation will have a large effect on the leakage factor for gasses. Less so for fluids. (Based on the magnitude of the leakage factors used in this thesis)	↕, high and medium

4.8 Summary and Discussion

This section first summarizes the chapter, followed by the discussion of several findings, the limitations in the approach and uncertainties. With the results found in this chapter and the investigation's set-up, the importance of several parameters can already be discussed without the use of sensitivity factors. The sensitivity analysis is performed in chapter 5.

4.8.1 Summary

The preliminary MC showed that rear-end collisions with an impact velocity $< 3\ m/s$ are not leading to LOC. For impact velocities $< 6\ m/s$, LOC only occurs when either the buffers malfunction or the wagons strength is significantly lower. Furthermore, the dependency between a single wagon's buffers has little effect on the damage levels, and using full dependent buffers is safe and sufficient.

In the full MC utilizing the dynamic model to simulate the rear-end collision, the distinction between the probability distribution of the Exit-velocity is highlighted and had a significant impact on the probability of damage. Also, the effect of the rolling resistance, drag force and sloshing was addressed. Sloshing is challenging to detect in the data, but it affects the distribution of the Exit-velocity, and it affects the impact velocity. The drag force and rolling resistance reduce the failure probabilities by about a third (Figure 4.34). Taking them into account, especially the wind specific drag force, is a time-consuming procedure because it depends on the velocity, and extra iteration steps are necessary. Implementing the rolling resistance is not extremely difficult and deemed reasonably accurate. However, if the resistance to motion and sloshing are both considered, the probability of damage is slightly lower than if the Exit-velocity is used as the impact velocity. Therefore, in the simplified MC approach, the assumption for $v_{exit} = v_{impact}$, is slightly conservative but sufficient.

In the simplified MC approach, an energy relation is found for the absorbed energy at the impact interface. This relation improves the energy relation found by Lu (2002). The absorbed energy relates not only to the first wagon's kinetic energy but also to the mass of the impacted wagon according to the relation found in equation 4.16. The found relation is used in a Limit State function, and it results in a five-parameter problem, significantly lower than the original ± 25 parameters, while keeping the accuracy satisfactory. Furthermore, it is analytically solvable, and the MBD model can be avoided. The following five parameters remain in the LSF:

- the impact velocity,
- the mass of the front wagon in the run-off
- the mass of the impacted wagon,
- the normalized energy factor (clustering the other parameters), and
- the capacity of the buffers.

The results of this simplified MC approach are slightly conservative (giving about 10-30 % higher probability of damage) but same order of magnitude. Using the simplified MC saves a tremendous amount of computation power, going from hours of simulation to several seconds.

The normalized energy factor was fitted well with a lognormal distribution. Adjusting its shape parameter did not affect the probability of damage much (Figure 4.37), suggesting that the normalized energy factor, describing a cluster of parameters, is of less importance.

Finally, the results regarding External Safety ($P(LOC_{ES})$) suggests that rear-end collisions should ***not*** be neglected from the QRA, as was done in 2008. What the effect is on the Site-specific and Group risk is not investigated, but this thesis results can be used to investigate this influence.

4.8.2 Discussion

Throughout this chapter, some assumptions are made that lead to uncertainty. Also, the choice of probability distributions (especially for the exit velocity) has an influence on the probability of damage. This part discusses some of the uncertainties.

The velocity measurements

The largest contributor to the impact velocity is the measured velocity after exiting the brakes, and the impact velocity has a large influence on the probability of damage. Sequentially, the choice of the probability distribution for the Exit-velocity significantly affects the results. Due to the high standards for External Safety, the damage probabilities of 10^{-9}-10^{-10} per run-off are influential. Since the data only provides 712 thousand measurements, the empirical distribution cannot provide these values. Data in the area of interest are missing, and the system's response on these extreme cases is unknown, making the fitted interpolations uncertain. The last two velocity measurements in Figure 4.5 could suggest a velocity ceiling under normal operations, and the results would tend more to the low side of the GPD 95% confidence interval. However, if human error is included in the data, the $8.25\ m/s$ measurement would lay outside the upper 95% Confidence interval. Although this high measurement was excluded from the data under normal operations, it does show that these high velocities can be reached, and that the system did not intervene enough to reduce the velocity to an acceptable level. Whether these velocities are also reached under 'normal' operations remains uncertain.

Furthermore, the assumption of a maximum velocity based on potential energy is fixed at $11\ m/s$ (section 4.1.2). Figure 4.39 shows the distribution, given damage, for different velocities, with the maximum velocity fixed at $11\ m/s$ (remember that all velocities picked from the distributions above $11\ m/s$ are reset to $11\ m/s$, distorting the graph between 10 and $11\ m/s$). In this approach the rolling resistance and drag forces are not considered. However, if this maximum velocity is not 11 but $10\ m/s$, results in many more measurements between 9 and $10\ m/s$, and only reducing the probability of damage by about 10 to $20\ \%$. Reducing it even further to $9\ m/s$, results in a more significant reduction of 30 to $40\ \%$. This maximum velocity should not be too difficult to test physically. If this is tested, one can immediately check the influence of the rolling resistance and drag force. Lower limits are not to be expected because $8.25\ m/s$ has already been measured. Therefore, further investigation into the limit of the Exit-velocity potentially reduces the probability of damage to a maximum of 40%, meaning the order of magnitude stays similar.

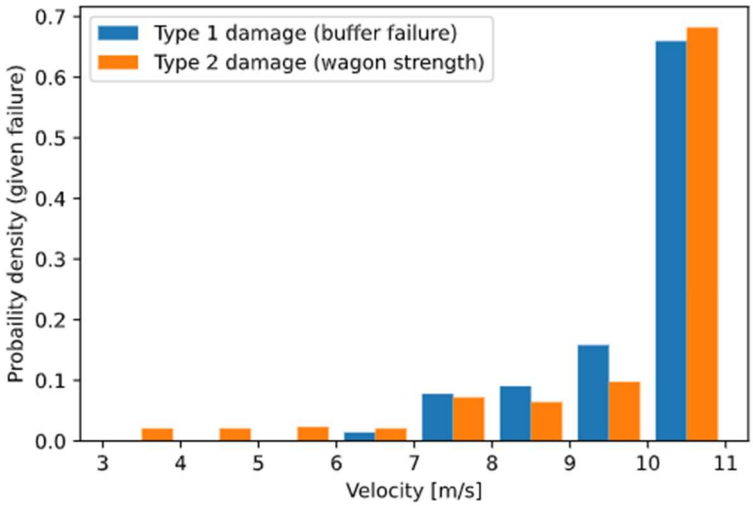

Figure 4.39: The probability density of the velocities given failure, of both damage types. All velocities picked from a distribution above $11\ m/s$ are set to $11\ m/s$, resulting in high abundance in the measurements between 10 and $11\ m/s$.

Sloshing

Sloshing is difficult to detect in the data measurements because there are only two Exit-velocity measurement points within 1.2 meters of each other. This thesis applies several assumptions to apply the sloshing effect into the calculations. One of these assumptions is the magnitude of the amplitude of this sloshing behaviour; the sensitivity of this amplitude to the probability of damage is negligible, as is shown in Appendix N. However, this is only one of the assumptions, while these assumptions are interrelated, and more investigation is certainly necessary. On the contrary, by using the measured Exit-velocity as the impact velocity, a lot of the uncertainty in sloshing diminishes; unless the velocity constantly increases after the measurement, say $> 2\ m/s$, which is highly unlikely. Furthermore, the sloshing is caused due to braking. Damage occurs mainly at high velocities; for these to occur, the braking forces need to be limited, and thus the sloshing effect will also be limited.

Strength of the wagon and the leakage factor

The wagons strength and the leakage factor (the factor to go from damage to leakage) are closely related. Both are not specifically investigated in this thesis. An attempt is made to include the wagon's strength in Type 2 damage. The approach of Type 2 damage is acceptable; however, it is sensitive to the probability distribution and the standard

deviations of the wagon's strength. Since the wagon's strength is uncertain, the results of Type 2 damage are uncertain.

The results of Type 1 damage (using the buffer's capacity) are more certain since the investigation into buffers is extensive in this thesis. However, to determine LOC from Type 1 damage, the uncertainty in the wagon's strength comes back in the form of the leakage factor. Furthermore, the influence of the leakage factor on the probabilities for LOC could be significant if a more credible leakage factor is found.

So, more investigation into the wagon's strength and the leakage factor are necessary. It is recommended to implement this in the leakage factor for Type 1 damage, since Type 1 damage can be determined in the simplified approach and is most accurate in this thesis. However, if it turns out that the wagon's strength is lower or the standard deviation is higher than used in this thesis, more damages occur at impact velocities $< 6.0\ m/s$. These damages are not properly determined in Type 1 damage, but they could be incorporated in the simplified approach through the energy absorption capacity. How to incorporate this may be changeling, and Type 2 damage utilizing the dynamic model may be needed for verification purposes.

Finally, tank wagons from before 2005 have lower buffer capacities. A tank wagon has a lifetime of around 15 years (Boyko, 2012), and are therefore not considered in the calculations in this thesis. Depending on the number of tank wagons before 2005, this could affect the result, but if most of these tank wagons pre-2005 are no longer used, the failure increase is expected to be limited. However, further investigation is necessary.

Dependency of wagon types

In the current assessment, the run-offs are considered independent from the stationary wagons on the allocation track. However, a dependency between wagon types is likely because wagons with similar destinations probably have similarities in the goods they carry. The probability of damage in a tank-tank collision is about five times smaller than in a tank-no-tank collision because of the extra capacity of four crash-worthy buffers. Therefore, if there is a dependency between the wagon types in the run-off and on the allocation track, more tank-tank collisions occur. This dependency will lower the probability of damage.

Domino effect

The domino effect is the effect that an incident with a DG leads to other incidents with other DG, even if the first DG is not considered a Risk to External Safety. This domino effect is not considered in this thesis and needs separate investigation. In the Governmental calculation method for External Safety, the domino effect is also not considered.

NON-straight collisions.

This thesis investigates collisions on a straight track, meaning that both buffers are equally compressed, and both buffers absorb a similar amount of energy. For collisions in a curve, one buffer is more activated than the other. Once its capacity is reached, the wagon's structure starts to absorb energy, and damage occurs. The buffer's energy absorption capacity changes depending on the amount of curvature. This is a geometrical problem that needs investigation before the use of the simplified method is applicable in curved tracks. Furthermore, the normalized energy factor may vary for these types of collisions, although this is not expected to deviate much, because the amount of energy that is needed to absorb the collision remains the same. If no further investigation into the change in energy capacity

for curved tracks is performed, one could assume a single buffer for the energy absorption capacity as a safe upper bound for the probability of damage.

Normalized energy factor

The normalized energy factor is dependent on many parameters. Likely it is also dependent on the wave speed of the forces traveling through the system after impact. Further investigation in the field of collision dynamics is necessary to determine what exactly contributes to the distribution of this parameter. This research can be used to further improvement of the energy absorption relation in case of rear-end train collisions. Furthermore, investigation of this factor when two objects are moving is necessary. It is expected that with the use of relative velocity this factor is similar, but verification is required. Lastly, the normalized energy factor was determined for velocities under $11\ m/s$. Although it is not expected to be dependent on velocity, it should first be verified before using it at higher velocities.

5. Sensitivity analysis

This chapter's main objective is to assess uncertainty using a simple model to gain insight into how the individual parameters affect the probability of failure and what the sensitivity of dependence between variables is. These insights can be used to improve the model, develop a design method, and make systematic operational decisions. The simplified approach introduced in section 4.5.4 is further evaluated, and a Level-II FORM, explained in section 3.4.3, is applied to the Limit State function in equation 4.18. The LSF is repeated here for convenience:

$$Z = E_{cap} - R_E \frac{m_1 m_{1s}}{m_1 + m_{1s}} v_{impact}^2.$$

Two types of collisions could lead to failure of a tank wagon: tank-tank collisions and tank-no tank collisions. This results in two different possible distributions for the buffer capacity (E_{cap}). The analysis should, in general, be performed on both types of collisions. However, there is a way to circumvent this problem and to simplify using only one type of collision. As stated in section 4.5.4, the probability of damage caused by a tank-tank collision is about five times lower than in a tank-no tank collision. This factor 5 is used to rewrite the probability of damage into only damage of a TNT collision:

$$P(D|v_{exit} > 2.0\ m/s) = P(D|TT)P(TT) + P(D|TNT)P(TNT) \approx P(D|TNT)\left(\frac{P(TT)}{5} + P(TNT)\right), \quad 5.1$$

in which $P(TT)$ and $P(TNT)$ represent the probability of occurrence of a tank-tank or tank-no-tank collision respectively; for Kijfhoek, these are found in Figure 4.36. Also, $P(TT)$ and $P(TNT)$ are conditionalized on a collision having occurred when the Exit-velocity is $> 2.0\ m/s$.

By combining equations 3.1 and 5.1, the probability of LOC affecting External Safety can be written in terms of the probability of damage given a TNT collision:

$$P(LOC_{ES}) = P(D|TNT) * X,$$

$$X_L = \underbrace{\left(\frac{P(TT)}{5} + P(TNT)\right)}_{1} \underbrace{P(v_{exit} > 2.0)P(collision)}_{2} \underbrace{P(DG)\sum_{i=1}^{i=6} P_i(cat.)P_i(leakage)}_{3} \quad 5.2$$

in which X_L represents the factor to go from the probability of a tank-no tank collision to the probability of LOC considering External Safety by:

1. Going to $P(D|v_{exit} > 2.0\ m/s)$
2. Going to $P(D)$
3. And the probability of LOC per category regarding External safety to eventually get $P(LOC_{ES})$

$X_L = 6.55 * 10^{-6}$ for Kijfhoek, using all the values found in chapter 4.

Now, to be able to neglect rear-end collisions on the allocation tracks from the QRA according to the regulations; the $P(LOC_{ES})$ should be $< 4\text{E-}07$ per year, as is explained in section 2.3. Under the current amount of traffic at Kijfhoek, this probability is $5\text{E-}12$ per

wagon. With the use of equation 5.2, $P(D|TNT) < 7.64\text{E-}07$ per wagon (given $v_{exit} > 2.0\ m/s$), corresponding to the Hasofer-Lind Reliability Index $\beta_{HL} = -\Phi^{-1}(7.64\text{E-}07) = 4.81$.[32] If the β_{HL} for $P(D|TNT)$ of the system at Kijfhoek is higher than this value; rear-end collisions on the allocation track can be neglected from the QRA.

5.1 FORM results and sensitivity factors

This section applies a FORM calculation using OpenTURNS[33] (Baudin et al., 2015) in Python. First, the method is verified then the results with the corresponding importance factors are presented.

Verification of FORM

The model in OpenTURNS, in which only $P(D|TNT)$ is calculated, is verified using equation 5.1 to compare with the results found in Figure 4.37 of the upper bound of the 95% confidence interval for the Exit-velocity. The upper bound is chosen because the coefficient of variation for the best fit GPD is very large. Furthermore, the FORM results are compared with a MC simulation in OpenTURNS. The verification results are shown in Table 5.1. The failure probabilities for FORM are in the same order of magnitude as the results found in chapter 4, and the MC performed using this simplified approach.

Table 5.1: Verification of the simplified approach for Type 1 damage of OpenTURNS with the results found in chapter 4. The 95% upper bound CI of the GPD for v_{exit} is used.

	$P\left(D\middle\|v_{exit} > 2.0\frac{m}{s}\right)$ [per wagon]	V
MC w/ Dynamic model	2.91E-04	0.059
Simplified MC (MATLAB) section 4.5.4	3.63E-04	0.052
Simplified Approach		
FORM OpenTURNS	4.83E-04	-
MC OpenTURNS	3.83E-04	0.036

Results for LOC regarding External Safety

The simplified approach is now used to determine LOC regarding External Safety for the best fit GPD of v_{exit}, and the coefficient of variation in the MC is reduced by performing 10 million simulations. The results are shown in Table 5.2 and are very close to the MC simulation results found utilizing the dynamic model. The FORM probabilities are slightly conservative compared to the Monte Carlo simulation.

[32] The failure probability and the reliability index are considered given $v_{exit} > 2.0\ m/s$. This target reliability for another distribution without a threshold velocity should be $\beta = 6.17$.

[33] In this thesis the Cobyla optimization algorithm in OpenTURNS is used (*Cobyla — OpenTURNS Documentation*, n.d.)

Table 5.2: Results of the failure probabilities per year for LOC considering External Safety. The best fit GPD of the Exit-velocity is used in this table.

	MC w/ Dynamic model	FORM OpenTURNS	MC OpenTURNS
$P(LOC_{ES})$ [per year]	9.8E-06	3.29E-05	2.2E-05
V	0.33	-	0.049

The sensitivity factors and the Design-Point

From FORM: the sensitivity factors (α-values), the reliability of the current system and the Design Point are found. According to the FORM, the β_{HL} for $P(D|TNT)$ of the current system is 3.79, which is lower than 4.81, and rear-end collisions on the allocation tracks shall thus be considered in the QRA. The α-values[34] are found in Table 5.3, and the results, using equation 3.21 to find the design point, in Table 5.4. From the α-values it becomes clear that the impact velocity is the most crucial parameter in the LSF, as was expected in chapter 4.

Table 5.3: α-values from FORM in OpenTURNS.

	α
E_{cap}	0.11
R_E	-0.15
m_1	-0.11
m_{1s}	-0.29
v_{impact}	-0.93

Table 5.4: Results of the design point using FORM's α-values.

Parameter	Distribution	$\Phi(-\alpha_i\beta)$ $\beta = 3.79$	**Design Point**
E_{cap}	$N(\mu = 1032, \sigma = 80.22)$	0.33	997 kJ
R_E	$L(\sigma = 0.63, \theta = 0.48,\ m = 0.064)$	0.72	0.57
m_1	Empirical	0.67	86 tonnes
m_{1s}	Empirical	0.86	70 tonnes
v_{impact}	GPD$(\mu = 2.0,\ \xi = 0.186, \sigma = 0.228)$	0.9998	6.72 m/s

[34] Similar to footnote 32, the α-values at other emplacement yards is likely to deviate slightly if another distribution or another velocity threshold is chosen. However, the importance of the velocity parameter remains similar.

5.2 Sensitivity to dependency investigated

Until now, the dependency between the parameters in the LSF is not considered. This section investigates the ***sensitivity*** to possible dependencies; it does ***not*** investigate the dependencies.

First, there may be some positive dependence between the run-offs mass and the mass of the impacted wagon (m_1 and m_{1s}) because the wagons with a similar destination may also carry similar goods. Second, the dependency between the impact velocity (v_{impact}) and m_1 is already considered in the choice of distribution for m_1. Third, the correlation between v_{impact} and the mass of the impacted wagon (m_{1s}) is not likely.
Furthermore, the buffer's capacity (E_{cap}) in its elastic region is partly related to the relative velocity between two wagons because of the viscous damper explained in section 4.4.4. However, damage to wagons occurs mainly at relatively high impact velocities, and the capacity in the elastic region at higher velocity is capped, and the dependency is therefore limited. Furthermore, the plastic region absorbs most of the energy, which is independent of the impact velocity. Moreover, the maximum energy absorption capacity described at the end of section 4.4.2 is uncoupled from the MBD model, by using a different approach for the choice of distribution. In conclusion, a minor positive dependency between energy capacity and impact velocity is possible, based on the viscous damping in the buffers.
Lastly, the normalized energy factor (R_E) is a cluster of parameters, and what it depends on needs further investigation. It is likely dependent on the force transfer of other wagons to the impact interface. How these forces are transferred requires more dynamic analysis and likely a more complex model. Furthermore, R_E may also depend on the different types of buffers throughout the rake of wagons in the collision. This could indirectly mean that R_E has a minor correlation with E_{cap} at the impact interface. Furthermore, to determine the absorbed energy, as is done in equation 4.16, m_1, m_{1s} and v_{impact} were separated and R_E is the fourth parameter. By this separation it is expected that further dependency between R_E and the other three parameters is negligible.

From the above, the following dependencies are investigated:

1. Positive dependence between the masses,
2. Positive dependence between m_1 and v_{impact},
3. Positive dependence between E_{cap} and v_{impact}.
4. The dependence (negative or positive) between E_{cap} and R_E.

To investigate the sensitivity of dependency, a Spearman rank correlation (ρ_s) of 0.3, 0.5 and 0.7 are assumed; for the negative correlation, these values are assumed negative. These correlations[35] are applied separately per case, where the other variables remain independent. Since the dependencies are not investigated, the use of a Gaussian copula is arbitrary and only to investigate the sensitivity of dependence. Furthermore, the FORM results (using the design point) are used to apply importance sampling (IS) for a MC simulation. Using this technique, the COV of the MC results is around 0.04 in just 10.000 simulations.

[35] The Spearman rank correlation coefficient are transferred into a Gaussian copula, and for a Gaussian copula, OpenTURNS applies the Nataf transformation to transform the original X-space to the U-space (Baudin et al., 2015).

5.2.1 Positive dependence between the masses

The sensitivity of a positive dependency between m_1 and m_{1s} is investigated, and the results are given in the table below. The sensitivity to this dependency is negligible, with a probability increase of around $1.5\text{E-}0.5$ for a positive Spearman rank correlation of 0.7.

Table 5.5: Probability results to investigate the sensitivity of the dependence between the mass of the run-offs front wagon and the impacted wagon.

	Independent		$\rho_s = 0.3$		$\rho_s = 0.5$		$\rho_s = 0.7$	
	FORM	MC w/ IS	FORM	MC w/ IS	FORM	MC w/ IS	FORM	MC w/ IS
$P(D\|TNT)$	7.5E-05	4.0E-05	8.9E-05	4.7E-05	8.3E-05	5.2E-05	9.0E-05	5.6E-05
β	3.79	3.94	3.75	3.90	3.77	3.88	3.75	3.86
V	-	0.01	-	0.01	-	0.01	-	0.01

5.2.2 Positive dependence between the run-off's mass and the impact velocity

The dependency between m_1 and v_{impact} is investigated to gain insight into this dependency for the use of the simplified approach at other emplacements. For Kijfhoek, the distribution of the run-off's mass is conditionalized on high impact velocities, and the dependency is implicitly considered. The probabilities for different correlation coefficients are given in Table 5.6. The dependency has little effect on the results.

Table 5.6: Probability results to investigate the sensitivity of the dependence between the mass of the run-offs front wagon and the impact velocity.

	Independent		$\rho_s = 0.3$		$\rho_s = 0.5$		$\rho_s = 0.7$	
	FORM	MC w/ IS	FORM	MC w/ IS	FORM	MC w/ IS	FORM	MC w/ IS
$P(D\|TNT)$	7.5E-05	4.0E-05	9.0E-05	6.5E-05	1.0E-04	7.2E-05	9.9E-05	7.5E-05
β	3.79	3.94	3.75	3.83	3.72	3.80	3.72	3.79
V	-	0.01	-	0.01	-	0.01	-	0.01

5.2.3 Positive dependence between the buffers' capacity and the impact velocity

The sensitivity to a positive dependence between E_{cap} and v_{impact} is investigated similarly as above, and the results are given in Table 5.7. The results show a decrease in the failure probability, but it is not that significant. Furthermore, only a minor dependency may be expected and assuming independence is thus reasonable.

Table 5.7: Probability results to investigate the sensitivity of the dependence between the buffers' energy absorption capacity and the impact velocity.

	Independent		$\rho_s = 0.3$		$\rho_s = 0.5$		$\rho_s = 0.7$	
	FORM	MC w/ IS	FORM	MC w/ IS	FORM	MC w/ IS	FORM	MC w/ IS
$P(D\|TNT)$	7.5E-05	4.0E-05	5.8E-05	2.9E-05	5.3E-05	2.4E-05	4.4E-05	1.9E-05
β	3.79	3.94	3.86	4.02	3.88	4.07	3.92	4.12
V	-	0.01	-	0.01	-	0.01	-	0.01

5.2.4 Dependency between the buffers' capacity and the normalized energy factor

Lastly, the sensitivity of dependence between E_{cap} and R_E is investigated. Whether the correlation may be positive, or negative is unknown. Therefore, both are investigated, and the results are found in Table 5.8. The effect of dependency between these variables is negligible.

Table 5.8: Probability results to investigate the sensitivity of the dependence between the buffers' energy absorption capacity and the normalized energy factor.

	Independent		$\rho_s = 0.3$		$\rho_s = 0.5$		$\rho_s = 0.7$	
	FORM	MC w/ IS	FORM	MC w/ IS	FORM	MC w/ IS	FORM	MC w/ IS
$P(D\|TNT)$	7.5E-05	4.0E-05	5.7E-05	3.9E-05	6.9E-05	3.9E-05	7.7E-05	3.8E-05
β	3.79	3.94	3.86	3.95	3.81	3.95	3.78	3.96
V	-	0.01	-	0.01	-	0.01	-	0.01

	$\rho_s = -0.3$		$\rho_s = -0.5$		$\rho_s = -0.7$	
$P(D\|TNT)$	7.5E-05	4.0E-05	7.9E-05	4.2E-05	8.3E-05	4.3E-05
β	3.79	3.94	3.78	3.93	3.77	3.93
V		0.01		0.01		0.01

5.3 Suggestions and Discussion

This chapter further evaluated the simplified approach first introduced in section 4.5.4. It uses the relative difference between the failure probabilities of a tank-tank collision and a tank-no tank collision, to reduce the investigation to only tank-no tank collisions. It further showed the importance of the each of the parameters and the sensitivity to possible dependencies.

Suggestions

Investigation into only tank-no tank collisions and using a transformation to the total probability of damage is adequate. It is recommended for other emplacements to determine the probability of damage in rear-end collisions on a straight track. It limits investigations to only the five parameters in the LSF of equation 4.18 and determining the probability of TT and TNT collisions (this can be done with a flow diagram like is done in Figure 4.36). In fact, R_E and E_{cap} can be used from this thesis, due to the similarities at other emplacements and the limited influence of these parameters on the LSF. Subsequently, the investigation can be limited to three parameters: the impact velocity and the masses of the wagons impacting

each other. Furthermore, the assumption of independence between the five parameters is adequate because the investigation into dependency, using Gaussian copula and the Nataf transformation, had a minor influence on the failure probabilities.

In improving the reliability of an emplacement, the focus should lay in reducing the probability of high impact velocities ($> 6m/s$). The impact velocity is undoubtedly the most important parameter with a sensitivity factor of 0.93. Furthermore, an emplacement has little effect on the capacity of the buffers (governed by norms) and the normalized energy factor (the result of dynamic behaviour in a collision). Also, the masses of the wagons to be marshalled are often determined by the user of the emplacement and not necessarily the operator of the emplacement. Although the operator could induce a load capacity, this is not preferable because it will not satisfy the customer. Additionally, the masses have small sensitivity factors and the effect of such measures will be limited.

Discussion

The relative difference between the damage probabilities of a tank-tank and tank-no tank collision may differ at impact velocities higher than applied in this thesis ($> 11\ m/s$). For the use of the simplified approach at other emplacements the difference factor of 5 is likely similar due to the similar velocities, but for research into collisions with tank wagons at higher velocities, this factor needs to be verified and may need adjustment.

The assumption of a Gaussian copula and the Nataf transformation were arbitrary. Investigation into the actual dependence of the parameters or by doing sensitivity analyses using other transformations and other copulas are necessary to exclude the influence of dependence completely. However, due to the minimal influence of dependence found in this chapter, it is not expected to change significantly, but this cannot be verified with complete certainty.

Furthermore, the buffers energy capacity has been investigated in this thesis. However, further research into the uncertainty of buffers capacity may give more accurate results in the probability of damage. The effect of the many different types of buffers on the distribution may also benefit future studies.

Finally, adapting the method to a standardized load and resistance factor approach is possible but not recommended. There are too many physical differences at various emplacements and the distributions of the three parameters (v_{impact}, m_{1s} and m_1) may also be very different. Taking these differences into account in a standardized method may be challenging. Therefore, using the introduced simplified approach and applying a FORM or a MC simulation with importance sampling seems suitable and simple enough to determine damage to tank wagons at emplacement yards.

6. Conclusion & recommendations

This thesis investigated rear-end collisions at Kijfhoek, the largest rail emplacement yard in the Netherlands. A Monte Carlo simulation is performed in which rear-end collisions are simulated using a multi-body dynamic model to find the probability of Loss of Containment of Dangerous Goods. In the QRA proposed by the Dutch Government, LOC affecting External safety needs to be determined using out-dated deterministic values, and the method is not transparent. This thesis further pointed out weaknesses in the proposed method, and these thesis insights are used to improve the method. With the MBD model and the MC simulation results, Lu's (2002) relation for the energy absorption at the impact interface, later updated by Xu et al. (2019), is improved. It now incorporates different possible collision configurations. This newly found relation is used in the design of a simplified approach, which could be used at other emplacement yards to determine the reliability of LOC against rear-end collisions. Besides the use of the energy relation as an engineering application, it contributes to academic research in collision dynamics.

This chapter answers the research questions formulated in chapter 1, followed by recommendations for future studies.

6.1 Conclusion

First, the sub questions are answered, followed by the main research question.

Sub-questions

1. **What is the probability that Loss of Containment of Dangerous Goods affecting External Safety occurs due to rear-end collisions on the allocation track during the automated marshalling process at Kijfhoek?**

The answer to this question is found in section 4.6.2, specifically Table 4.6. The probability is highly dependent on the extrapolation of the Exit-velocity measurements. The failure probability lies somewhere between 0 and $3.9 * 10^{-4}$ per year, considering the 95% confidence interval of the Generalized Pareto Distribution fit. The best fit GPD leads to a failure probability of around 10^{-5} per year. This failure probability is higher than $4 * 10^{-7}$, for which the risk of affecting External Safety can be neglected. Furthermore, the calculated probability considers 'normal' operations and does not consider other failure mechanisms such as human error, brake failure or terrorism. If these are also considered, it is likely that rear-end collisions at Kijfhoek may not be neglected.

2. **What is the impact velocity that leads to Loss of Containment?**

This question does not have an exact answer, but from section 4.5.2, velocities $<$ $3.0\ m/s$ do not lead to Loss of Containment, which is in line with the regulations for crashworthy buffers (NEN, 2017). At velocities between 3 and $6\ m/s$, LOC can occur if the wagon's strength is lower than the combined strength of the buffers in the plastic region. The 'weakest link' in a series system like a train collision will absorb energy first, and in that case, the wagon is protecting buffers. So, for extremely weak tank wagons or complete malfunctioning of the buffers, LOC is possible at velocities lower than $6\ m/s$. Above $6\ m/s$, the energy absorption capacity of the buffers could entirely have been utilized, transferring the resulting energy to the tank wagons. After that, the probability of LOC increases at increasing velocities.

3. **Is there a simplified relation in which the energy absorption at an interface can be determined?**

A relation is found for the absorbed energy at the impact interface in section 4.5.4 and is given by equation 4.16:

$$E_{absorbed,impact} = R_E \frac{m_1 m_{1s}}{m_1 + m_{1s}} v_{impact}^2 \; [J]$$

This energy relation improves earlier found relations (Lu, 2002; Xu et al., 2019). The impact velocity is the most important parameter, followed by the masses of the impacted wagon (m_1) and the run-offs front wagon (m_{1s}). The normalized energy factor (R_E) is fitted elegantly with a scaled Lognormal distribution, with parameters: shape $\sigma = 0.63$, location $\theta = 0.48$ and scale $m = 0.064$. The normalized energy factor replaces the constant that Lu (2002) found and represents multiple parameters, such as the type of the buffers, the configuration and the number of wagons, but also some dynamic features not researched in this thesis.

4. **How can the study case at Kijfhoek be transferred to a standard for other automated marshalling yards?**

This question is answered in chapter 5 and uses the simplified energy relation found in section 4.5.4. It focuses on tank wagons colliding with regular wagons. The probability of tank-tank collisions is found to be a factor 5 lower. With the use of simple flow diagram, one can find the probability of occurrence for either type of collision, as is done for Kijfhoek in Figure 4.36. The damage probability in rear-end collisions can be found using the simplified approach applying a FORM or MC. To go from damage in a Tank-no tank collision to LOC affecting External Safety, some site-specific probabilities need to be determined, and this approach is explained in section 4.6.

5. **To what extent does the automated humping process affect the overall External Safety, considering the other processes at the yard?**

This question is not explicitly answered in this thesis and needs further investigation. The other processes at the emplacement are currently calculated using the Government's deterministic calculation method, and it is questionable if comparison with the reliability-based approach used in this thesis is valuable. However, from the investigations performed, it is likely that rear-end collisions are not negligible according to the Governments method, and it will affect the current QRA regarding External Safety. The magnitude of this effect is not calculated in this thesis.

Main research question

How can the present Dutch design guidelines for 'External Safety', to calculate the loss of containment in automated marshalling, be improved through a reliability-based analysis, focusing on rear-end collisions based on the study case at Kijfhoek?

The existing calculation method described in section 2.3 is a deterministic calculation based on data pre-1995. Besides the dated values, the origin of the failure frequencies is unclear, and the method lacks transparency. Furthermore, all emplacements are considered the same, and it does not allow for risk-reduction measures in the calculations. Although the method specifies that deviation from the method is permitted, due to the lack of clarity in the probabilities, it is unclear in which areas an emplacement is different from the 'average'

one used in the method. Specifically, in the scenario dedicated to the automated humping process, the failure frequency is vaguely described as an 'irregular event', while in the follow-up calculation, it uses the same leakage probability as in collision events of other scenarios.

The reliability-based approach used in this thesis shows which parameters influence rear-end collisions, how to deal with uncertainties and shows a transparent method. The most important parameters are given in the simplified energy relation, which is used in the simplified approach. This simplified approach is useable at other emplacement yards for the investigation of rear-end collisions. Furthermore, it allows for site-specific values of parameters and follow-up probabilities, such as the probability of occurrence of different types of collisions and the probability of a tank wagon containing a Dangerous Good.

The current method can thus be improved by implementing the simplified approach to determine damage to tank wagons and to allow for site-specific values in the follow-up probabilities.

6.2 Recommendations

In this section, the recommendations are listed, of which many are based on the discussions in chapters 4 and 5.

1. It is recommended that the calculation method for the emplacements External Safety becomes more transparent and allow room for site-specific situations. This thesis showed an improvement in the assessment of rear-end collisions in the automated humping process. Similarly, the other scenarios should be improved using reliability analyses. For scenarios involving collisions, it is recommended to use the methods applied in this thesis.
2. With the simplified independent approach proposed in this thesis, it is possible and recommended to investigate rear-end collisions in other areas of the humping process at Kijfhoek, e.g., between two brakes. Further investigation is necessary for the effect on the energy absorption capacity of the buffers on a curved track, but for a conservative approach, one could assume only a single buffer's absorption capacity. The probability distribution of the normalized energy factor may change for two moving objects and the use of a relative velocity. This effect should be checked and needs verification.
3. Other factors leading to high Exit-velocities besides 'normal' operations should be investigated, such as human error. In the last 10 years, two high Exit-velocity incidents have occurred at Kijfhoek due to human error. Although the adjustments in the system should prevent incidents such as the ethanol fire in 2011. There may be other scenarios like the $8.25\ m/s$ incident in 2018, caused by human error, affecting the failure probabilities. If every 10 years an incident like this happens, the probability of LOC due to rear-end collisions may be much higher than calculated in this thesis. Therefore, certainly more investigation or prevention in this area is recommended.
4. Sub-question 5, regarding the effect of rear-end collisions on the External Safety compared to other operations at Kijfhoek, still needs investigation, and the results from this thesis could form the basis of this investigation. It is recommended to perform this investigation for Kijfhoek before reducing the probability of rear-end

collisions. If the effect on Site-Specific or Group risk is negligible, improvement measures may not be necessary.

5. To improve the reliability against rear-end collisions in automated marshalling, the focus should lay in the most critical parameter, the impact velocity. On the allocation track this is governed by the Exit-velocity. More specifically, the focus should lay in the tail of its probability distribution. The probability of velocities $> 6\ m/s$ should be exceptionally low for rear-end collisions to be neglected from the QRA at Kijfhoek. With more knowledge of these extreme velocities, it is possible to determine the probability of damage more accurately.
6. Due to the limited amount of data, the extrapolations of the Exit-velocity measurements are uncertain. Investigations with combined data from other humping yards using similar systems may provide a solution to gain more certainty. However, the differences between these yards may be too significant for comparison. An alternative could be physical testing under different scenarios at Kijfhoek, giving insights into the system's response.
7. The tank wagon's strength and the leakage factor are uncertain parameters. It is recommended that these are appropriately investigated. The Type 1 damage is investigated thoroughly, and the probabilities of this type of damage are expected to be quite accurate. Therefore, focussing on investigating the leakage factors for Type 1 damage should be a good start. A more accurate leakage factor will have a large influence on the accuracy of the probability of LOC. Incorporating the fatigue problems emphasized by Boyko (2012) may be more challenging, but it could be implemented through the resistance parameter (the Energy capacity).
8. The improved relation found for the energy absorption at the impact interface could form the basis for further investigations regarding train collisions. More research in the normalized energy factor may provide further insight into the essential parameters of the energy absorption in a collision. Extracting more dependent variables in the energy absorption at the impact interface may reduce the uncertainty of the normalized energy factor.

References

4-axle Tank Wagon for Ammonia | Greenbrier. (n.d.). Retrieved May 18, 2021, from https://www.gbrx.com/manufacturing/europe-rail/tank-wagons/4-axle-tank-wagon-for-ammonia/

Baudin, M., Dutfoy, A., Looss, B., & Popelin, A. L. (2015). OpenTURNS: An industrial software for uncertainty quantification in simulation. *Handbook of Uncertainty Quantification*, 2001–2038. https://doi.org/10.1007/978-3-319-12385-1_64

Bhagya Lakshmi Nageswari, M., & Jyothi, U. S. (2020). Aerodynamic analysis of railway wagon on drag coefficient. *E3S Web of Conferences*, *184*. https://doi.org/10.1051/e3sconf/202018401058

Boyko, A. (2012). INFLUENCE OF BARREL DAMAGES ON LIFE TIME OF TANK WAGON. *8th International DAAAM Baltic Conference "INDUSTRIAL ENGINEERING,"* 21–26.

Cobyla — OpenTURNS documentation. (n.d.). Retrieved June 24, 2021, from https://openturns.github.io/openturns/1.12/user_manual/_generated/openturns.Cobyla.html

Cole, C., & Sun, Y. Q. (2006). Simulated comparisons of wagon coupler systems in heavy haul trains. *Proceedings of the Institution of Mechanical Engineers, Part F: Journal of Rail and Rapid Transit*, *220*(3), 247–256. https://doi.org/10.1243/09544097JRRT35

Coles, S. (2001). *An Introduction to Statistical Modeling of Extreme Values*. Springer London. https://doi.org/10.1007/978-1-4471-3675-0

DB Schenker Rail AG. (2011). *Our Freight Wagons*. https://nl.dbcargo.com/file/rail-nederland-nl/8380580/VO43wppuWQeIgyat3Ob5M_43YPg/5509816/data/freight_wagon_catalog_v2011.pdf

De Loor, ir. drs. D., Lendering, dr. ir. K., Kooiman, dr. ir. A., & Van de Voort, ir. M. (2019). *Onderzoek technische integriteit heuvel- systeem Kijfhoek*.

Elger, D. F., Williams, B. C., Crowe, C. T., & Roberson, J. A. (2013). *Engineering Fluid Mechanics* (10th ed.). Wiley.

Erasmus, M. (2020, February 10). *Buienradar.nl - Actuele neerslag, weerbericht, weersverwachting, sneeuwradar en satellietbeelden*. https://www.buienradar.nl/nederland/weerbericht/blog/windstoot-uitgelegd-25545c

Google. (n.d.). *Google Maps*. Retrieved February 26, 2021, from https://www.google.nl/maps/

Greenbrier Europe. (n.d.). *4-axle Tank Wagon for Liquefied Chlorine | Greenbrier*. Retrieved May 3, 2021, from https://www.gbrx.com/manufacturing/europe-rail/tank-wagons/4-axle-tank-wagon-for-liquefied-chlorine/

Helsloot, I., Scholtens, A., & Vis, J. (2019). *Toeval of structureel incidentalisme? Vijf 'incidenten' op Kijfhoek in de zomer van 2018 nader beschouwd*.

Hendrikx, T. (2019). *Rapportage onderzoek Remsloffen Kijfhoek* (Issue september).

Home | AHN. (n.d.). Retrieved May 2, 2020, from https://www.ahn.nl/

Jonkman, S. N., Vrouwenvelder, A. C. W. M., Steenbergen, R. D. J. M., Morales-Nápoles, O., & Vrijling, J. K. (2017). *Probabilistic Design: Risk and Reliability Analysis in Civil Engineering, Lecture notes CIE4130*. 271.

KNMI - Uurgegevens van het weer in Nederland. (n.d.). Retrieved April 28, 2021, from https://www.knmi.nl/nederland-nu/klimatologie/uurgegevens

Kolmogorov–Smirnov test - Wikipedia. (n.d.). Retrieved April 27, 2021, from https://en.wikipedia.org/wiki/Kolmogorov–Smirnov_test#cite_note-1

Lamé, J. P. A. (2018). *Safety Kijfhoek*. Inspectie Leefomgeving en Transport.

Lenssen, M. (2018). *Modernisering Heuvelsysteem Kijfhoek Operational Context Description (OCD)*.

Li, R., Xu, P., Peng, Y., & Xie, Y.-Q. (2016). Scaled tests and numerical simulations of rail vehicle collisions for various train sets. *Proc IMechE Part F: J Rail and Rapid Transit*, *230*(6), 1590–1600. https://doi.org/10.1177/0954409715605126

Lu, G. (1999). Collision behaviour of crashworthy vehicles in rakes. *Proceedings of the Institution of Mechanical Engineers, Part F: Journal of Rail and Rapid Transit*, *213*(3), 143–160. https://doi.org/10.1243/0954409991531100

Lu, G. (2002). Energy absorption requirement for crashworthy vehicles. *Proceedings of the Institution of Mechanical Engineers, Part F: Journal of Rail and Rapid Transit, 216(1), 31–39.*, *216*(1), 31–39. https://doi.org/10.1243/0954409021531665

MathWorks. (2020). *MATLAB* (R2019b academic use). The MathWorks Inc.

Ministerie van Justitie en Veiligheid. (2004, May 27). *wetten.nl - Regeling - Besluit externe veiligheid inrichtingen - BWBR0016767*. https://wetten.overheid.nl/BWBR0016767/2016-01-01

Moss, R. E. S. (2020). Component Reliability Analysis. In *Applied Civil Engineering Risk Analysis* (Second Edition, pp. 89–107). Springer International Publishing. https://doi.org/10.1007/978-3-030-22680-0_6

Nápoles, O. M. (2019). *Review of statistics and probability theory II*. TU Delft.

NEN. (2017). *NEN-EN 15551 Railway applications - Railway rolling stock - Buffers: Vol. EN 15551*.

NEN. (2020). *NEN-EN 15227:2020 Railway applications - Crashworthiness requirements for rail vehicles* (Vol. 15227, Issue april).

Newman, C. (2017). *Rolling Resistance | Advanced Steam Traction*. https://www.advanced-steam.org/ufaqs/rolling-resistance/

Orlin, F. (2020). *Reliability-Based Assessment for Fender Systems*. TU Delft.

OTIF. (2021). *RID Convention concerning International Carriage by Rail (COTIF) Appendix C-Regulations concerning the International Carriage of Dangerous Goods by Rail (RID)*.

Pereira, M. S. (2006). *Structural Crashworthiness of Railway Vehicles*.

ProRail. (n.d.-a). *Kijfhoek | Groot onderhoud emplacement Kijfhoek - Kijfhoek - ProRail*. Retrieved November 16, 2020, from https://www.prorail.nl/projecten/kijfhoek

ProRail. (n.d.-b). *Over ons | ProRail*. Retrieved February 26, 2021, from https://www.prorail.nl/over-ons

Razaghi, R., Sharavi, M., & Feizi, M. M. (2015). Investigating the Effect of Sloshing on the Energy Absorption of Tank Wagons Crash. *Transactions of the Canadian Society for Mechanical Engineering*, *39*(2), 187–200. https://doi.org/10.1139/tcsme-2015-0014

RID. (2019). *RID Convention concerning International Carriage by Rail (COTIF) Appendix C-Regulations concerning International Carriage of Dangerous Goods by Rail*.

Rijksoverheid. (n.d.). *Wat is externe veiligheid en hoe weet ik of er risico's zijn in mijn woonomgeving?* Retrieved February 26, 2021, from https://www.rijksoverheid.nl/onderwerpen/gevaarlijke-stoffen/vraag-en-antwoord/wat-is-externe-veiligheid-en-hoe-weet-ik-of-er-risico-s-zijn-in-mijn-woonomgeving

SAVE. (2006). *Rekenprotocol Vervoer Gevaarlijke Stoffen per Spoor* (Issue april).

SAVE. (2009). *Risicoanalyse goederenemplacement Kijfhoek* (Issue april).

Scholes, A. (1987). Railway passenger vehicle design loads and-structural crashworthiness. *IMechI Proceedings of the Institution of Mechanical Engineers*, *201*, 201–207.

Scholes, A., & Lewis, J. H. (1993). Development of Crashworthiness for Railway Vehicle Structures. *Proceedings of the Institution of Mechanical Engineers, Part F: Journal of Rail and Rapid Transit*, *207*(1), 1–16. https://doi.org/10.1243/PIME_PROC_1993_207_222_02

SCREW COUPLING 1350 kN: FMC Hidrolik Sistemleri Otomotiv Mak. San. Ve. Tic. (n.d.). Retrieved May 19, 2021, from https://www.virtualmarket.innotrans.com/en/SCREW-COUPLING-1350-kN,p1649807

Šťastniak, P., Moravčík, M., & Smetanka, L. (2019). Investigation of strength conditions of the new wagon prototype type Zans. *MATEC Web of Conferences*, *254*, 02037. https://doi.org/10.1051/matecconf/201925402037

Stephanie Glen. (n.d.). *"Kolmogorov-Smirnov Goodness of Fit Test" From StatisticsHowTo.com: Elementary Statistics for the rest of us!* Retrieved April 27, 2021, from https://www.statisticshowto.com/kolmogorov-smirnov-test/

Sun, Y. Q., Cole, C., & Dhanasekar, M. (2011). *MULTI-BODY MODELLING OF WAGON TRAINS FOR CRASHWORTHINESS ANALYSIS*. CQUniversity. /articles/conference_contribution/Multi-body_modelling_of_wagon_trains_for_crashworthiness_analysis/13457135/1

Sun, Y. Q., Cole, C., Dhanasekar, M., & Thambiratnam, D. P. (2012). Modelling and Analysis of the Crush Zone of a Typical Australian Passenger Train. *Vehicle System Dynamics*, *50*(7), 1137–1155. https://doi.org/10.1080/00423114.2012.656658

Sun, Y. Q., Cole, C., Spiryagin, M., Godber, T., Hames, S., & Rasul, M. (2014). Longitudinal heavy haul train simulations and energy analysis for typical Australian track routes. *Proceedings of the Institution of Mechanical Engineers, Part F: Journal of Rail and Rapid Transit*, *228*(4), 355–366. https://doi.org/10.1177/0954409713476225

Szanto, F. (2016). Rolling resistance revisited. *CORE 2016, Maintaining the Momentum, Conference on Railway Excellence, Melbourne, Victoria, 1*.

United Nations. (2019). *Recommendations on the TRANSPORT OF DANGEROUS GOODS: Vol. Volume 1* (Issue 21).

Van Gelder, P. H. A. J. M. (2008). The importance of statistical uncertainties in selecting appropriate methods for estimation of extremes. *International Journal of River Basin Management*, *6*(2), 99–107. https://doi.org/10.1080/15715124.2008.9635340

Via078. (n.d.). *Rangeerterrein Kijfhoek vanuit de lucht*. Retrieved February 26, 2021, from https://www.via078.nl/zwijndrecht/rangeerterrein-kijfhoek-vanuit-lucht/

Vrijling, prof. drs. ir. J. K., Keulen, mr. ir. B., Theunissen, ir. R., & Bruijn, ir. F. (2012). *Onderzoek heuvelproces Kijfhoek*.

Vrijling, prof. drs. ir. J. K., & Van Gelder, dr. ir. P. H. A. J. M. (2002). *Probabilistic Design in Hydraulic Engineering* (Issue August). Delft Academic Press.

Wieringa, J., & Rijkoort, P. J. (1983). *Windklimaat van Nederland*.

Xu, P., Lu, S., Yan, K., & Yao, S. (2019). Energy absorption design study of subway vehicles based on a scaled equivalent model test. *Proceedings of the Institution of Mechanical Engineers, Part F: Journal of Rail and Rapid Transit*, *233*(1), 3–15. https://doi.org/10.1177/0954409718777371

Y.S. Kok-Palma, & P.G.J. Timmers. (2014). *Towards a new risk-calculation method for the transport of dangerous goods by rail: Technical report on failure frequencies of Dutch freight wagons based on incident data*.

Zhu, T., Xiao, S., Lei, C., Wang, X., Zhang, J., Yang, B., Yang, G., & Li, Y. (2020). Rail vehicle crashworthiness based on collision energy management: an overview. *International Journal of Rail Transportation*, 1–31. https://doi.org/10.1080/23248378.2020.1777908

Appendixes:

Appendix A

Classification of wagons

Class	Wagon type	1st digit of type number (5th digit of UIC#)
E	Ordinary open high-sided wagon	5
F	Special open high-sided wagon	6
G	Ordinary covered wagon	1
H	Special covered wagon	2
I	Refrigerated van	8
K	Ordinary flat wagon with separate axles	3
L	Special flat wagon with separate axles	4
O	Open multi-purpose wagon (composite open high-sided flat wagon)	3
R	Ordinary flat wagon with bogies	3
S	Special flat wagon with bogies	4
T	Goods wagon with opening roof	0 *(before 1988: 5)*
U	Special wagons	9
Z	Tank wagon	7

https://en.wikipedia.org/wiki/UIC_classification_of_goods_wagons

1. Important preliminary remarks

The most important technical characteristics of a freight wagon are indicated by a series of letters on the wagon body. This freight wagon classification code is made up of an upper-case (capital) letter and several lower case letters.

The capital letter designates

- the class of wagon (open wagon, covered wagon, flat wagon, etc.) and
- the wagon construction type (ordinary or special).

The lower-case letters (also known as the index letters), identify the main features of the wagon from the point of view of its use.

In the following tables

- information given in metres refers to the useful (i.e. inside) length of the freight wagon (lu),
- information given in tonnes (tu) corresponds to the maximum permissible load shown on the load limit panel for the wagon in question, this limit being determined in accordance with the procedures laid down in UIC leaflet 700.

2. Index letters that are internationally valid for all wagon classes

q	with electrical heating line for all approved power supply systems
qq	with electrical heating line and heating equipment for all approved power supply systems
s	wagons approved for running under "s" conditions (V_{max} = 100 km/h)
ss	wagons approved for running under "ss" conditions (V_{max} = 120 km/h)

3. National index letters

t, u, v, w, x, y, z (meaning defined by relevant national body)

Z Tank wagons

Reference wagon

with a metal tank for transporting liquid or gaseous commodities
with 2 axles: 25 t ≤ tu ≤ 30 t
with 3 axles: 25 t ≤ tu ≤ 40 t
with 4 axles: 50 t ≤ tu ≤ 60 t
with 6 or more axles: 60 t ≤ tu ≤ 75 t

Index letters

a	with 4 axles
aa	with 6 or more axles
b	for transporting petroleum products (2)
c	unloaded using compressed gas (1)
d	for transporting food and chemical products (2)
e	fitted with heating equipment
f	suitable for traffic travelling to/from Great Britain (train-ferry and Channel Tunnel)
ff	suitable only for traffic travelling to/from Great Britain via Channel Tunnel
fff	suitable only for traffic travelling to/from Great Britain on a train-ferry
g	for transporting compressed or liquefied gases or gases dissolved under pressure (1)
i	tank of non-metallic material
j	with shock-absorbing device
k	with 2 or 3 axles : tu < 20 t with 4 axles: tu < 40 t with 6 or more axles: tu < 50 t
kk	with 2 or 3 axles : 20 t ≤ tu < 25 t with 4 axles: 40 t ≤ tu < 50 t with 6 or more axles: 50 t ≤ tu < 60 t
n	with 2 axles: tu > 30 t with 3 axles: tu > 40 t with 4 axles: tu > 60 t with 6 or more axles: tu > 75 t
p	with station for brakeman (2)

(1) The index letter "c" shall not be marked on wagons bearing index letter "g".
(2) Only applicable to wagons with a gauge of 1520 mm.

Appendix B

Information graphic of the process at Kijfhoek.

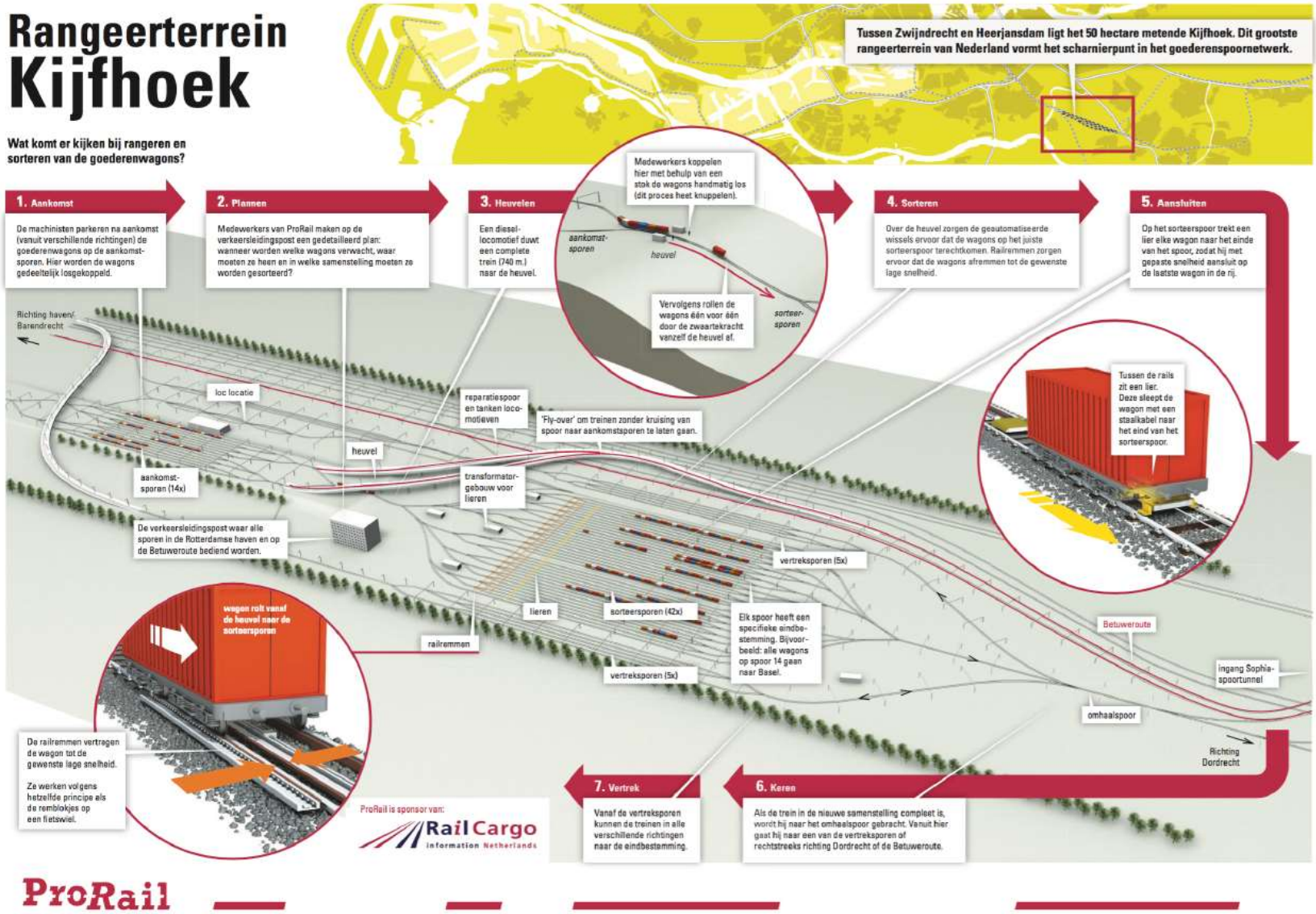

Appendix C

Failure frequency calculation per scenario of the government provided calculation method

Scenario		Formule voor bepaling van de frequentie F van scenario's op emplacementen
1A	tr/tr interactie met ATB-EG	$F_{(a/v\ trein)} = 5{,}5 \cdot 10^{-7} \times P_{vervolg} \times P_{uitstroming}\ (\times P_{ontsteking}) \times T_T$
1B	tr/tr interactie zonder ATB-EG	$F_{(a/v\ trein)} = 5 \cdot 10^{-6} \times P_{vervolg} \times P_{uitstroming}\ (\times P_{ontsteking}) \times T_T$
2	interactie tr/rangeerdeel	$F_{(a/v\ rangeer)} = 2{,}12 \cdot 10^{-5} \times P_{vervolg} \times P_{uitstroming}\ (\times P_{ontsteking}) \times T_T$
3	eenzijdig ongeval	$F_{(eenzijdig)} = 2{,}75 \cdot 10^{-5} \times P_{vervolg} \times P_{uitstroming}\ (\times P_{ontsteking}) \times T_T$
4	locwissel	$F_{(locwissel)} = 1 \cdot 10^{-6} \times P_{vervolg} \times P_{uitstroming}\ (\times P_{ontsteking}) \times$ aantal keren locwisselen $\times T_T$
5	samenstellen/omhalen	$F_{(samenstel)} = 2{,}12 \cdot 10^{-5} \times P_{vervolg} \times P_{uitstroming}\ (\times P_{ontsteking}) \times T_T$
6	heuvelen/stoten/plaatsen (h/s/p)	$F_{(h/s/p)} = 1{,}76 \cdot 10^{-5} \times P_{vervolg} \times P_{uitstroming}\ (\times P_{ontsteking}) \times N$
7	intrinsiek falen (IF)	$F_{(IF)} = 5 \cdot 10^{-7} \times (t/t_0) \times N$
8	BLEVE door brand	$F_{(BLEVE)} = 3{,}1 \cdot 10^{-7} \times N_{BVL} \times n \times T \times (t_{BGS}/8760) \times (A_p/A_{tot}) \times R$

$P_{vervolg}$ zie tabel 6.1
$p_{uitstroming}$ zie tabel 6.2
$P_{ontsteking}$ zie tabel 6.2
T_T aantal treinen per jaar waarbij voor:
- bonte treinen geldt T_T = aantal bonte treinen per jaar maal de fractie gevaarlijke stof in de bonte treinen (per stofcategorie A t/m D).
- Voor bloktreinen geldt T_T = het aantal treinen per jaar.

t gemiddelde verblijftijd (uur) van een ketelwagen op een emplacement
t_0 aantal uren in een jaar (8760 uur/jaar)
N totaal aantal wagens met gevaarlijke stoffen A t/m D per jaar
N_{BVL} aantal wagens met zeer brandbare vloeistof per jaar
n gemiddeld aantal gasketelwagens in een trein
T aantal treinen met gasketelwagens per jaar, waarbij onderscheid gemaakt wordt in T_{blok} en T_{bont}
t_{BGS} gemiddelde verblijfsduur van gasketelwagens in uur op het goederenemplacement
A_p plasoppervlak van een brand (600 m^2)
A_{tot} emplacementsoppervlak waar BLEVE door brand kan optreden
R repressiefactor (0,1), afkomstig uit [10]

Tabel 6.3: Formules voor berekening van faalfrequenties per scenario op een goederenemplacement

Scenario		F_{basis}	$P_{vervolg}$ [9)]	
			Gas	Vloeistof
1A	tr/tr interactie met ATB-EG	$5{,}5 \cdot 10^{-7}$ per trein	0,001	0,01
1B	tr/tr interactie zonder ATB-EG	$5 \cdot 10^{-6}$ per trein	0,001	0,01
2	interactie tr/rangeerdeel	$2{,}12 \cdot 10^{-5}$ per trein	0,001	0,01
3	eenzijdig ongeval	$2{,}75 \cdot 10^{-5}$ per trein	-	0,01
4	locwissel	$1 \cdot 10^{-6}$ per locwissel	0,0005	0,005
5	samenstellen/omhalen	$2{,}12 \cdot 10^{-5}$ per trein	0,001	0,01
6	heuvelen	$1{,}76 \cdot 10^{-5}$ per wagen	0,001	0,01
7	intrinsiek falen	$5 \cdot 10^{-7}$ per wagen per jaar	1	1
8	BLEVE door brand	zie formule in tabel 6.3[10)]	1	0

Tabel 6.1: Overzicht scenario's, basiskansen en vervolgkansen

$P_{uitstroom}$		$P_{ontsteking}$			
Instantaan	Continu	Instantaan direct	Instantaan vertraagd	Continu direct	Continu vertraagd
0,4	0,6	0,8 (g) 0,25 (bvl)	0,2 (g) 0 (bvl)	0,5 (g) 0,25 (bvl)	0,5 (g) 0 (bvl)

Tabel 6.2: Overzicht kansen op uitstroming en ontsteking brandbaar gas (g) en brandbare vloeistof (bvl)

Appendix D

Advantages and disadvantages of different collision energy models according to Zhu et al.

Table 2. Research approaches of crashworthiness of rail vehicles.

No.	Class	Research contents	Research methods	Research results	Features
1	Kinetic theory	EA components (coupler, anti-climber, etc.)	Simplified numerical analysis.	Basic design parameters of EA components.	Fast calculation; Simplified model;
		One-dimensional collision dynamics of train	MBD program.	Regular of longitudinal collision of train; Design of longitudinal stiffness of car body.	Conceptual design; Energy configuration; Motion observable only;
		Three-dimensional collision dynamics of train	MBD program.	Design principle of coupler; Level analysis of load and energy in EA areas of vehicle; Analysis of average deceleration.	Low accuracy.
2	FEA	Design analysis and test verification of EA components (coupler, anti-climber, etc.)	Nonlinear FEA; Quasi-static test; Dynamic test.	Design conditions and basic parameters of EA components; Load-deformation characteristic curve; Verification of simulation model.	Deformation observable; High accuracy; Data detail; Material parameters required;
		Design and analysis of collision EA zone	Quasi-static FEA; Dynamic FEA.	Load-deformation characteristic curve.	Considering elastic-plastic theory; Time consuming.
		Analysis of train collision characteristics	Collision FEA software.	Characteristics of deformation; Deformation; Evaluation of collision safety of train.	
3	MBD analysis	MBD analysis of train collision	MBD software (characteristics of the EA components and the deformation zone at end of car body)	Design principle of the coupler; Characteristics of train collision process; Force, speed and acceleration.	Faster than FEA; Rapid design & analysis; Motion observable only; Motion attitude without considering deformation.
4	Test analysis	Collision test of end structure (coupler, anti-climber, front-end EA area, etc.)	Quasi-static test; Dynamic test.	Energy configuration at all levels in deformation zone; Characteristics of deformation; Force, velocity and acceleration; Verification of simulation results.	Strong persuasion; Large space occupied; Low repeatability; High test cost; Difficulty to control the boundary conditions.
		Collision test of vehicle	Quasi-static test; Dynamic test.	Dynamic response of train collision; Characteristics of deformation; Force, velocity and acceleration; Verification of simulation results.	

(Zhu et al., 2020)

Appendix E

Modelling of the force-stroke diagram for verification of Lu's (Lu, 1999) *model.*

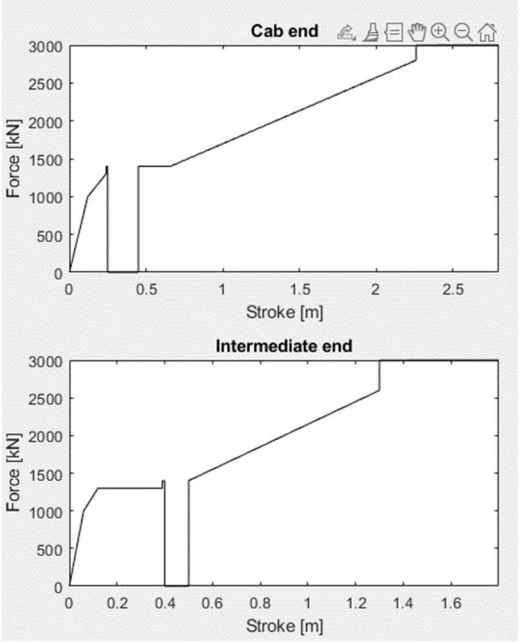

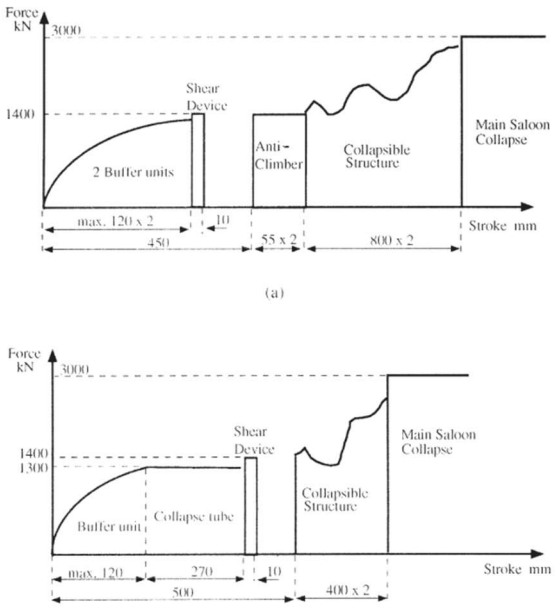

My model verification model Lu's model

Top is cab ends, bottom is intermediate ends.

Appendix F

Kolmogorov-Smirnof test

In a two-sample KS-test, simply stated the maximum difference D between the two empirical distributions is calculated (Stephanie Glen, n.d.; Vrijling & Van Gelder, 2002).

$$D_{n,m} = \sup |F_{1,n}(x) - F_{2,m}(x)| \quad 0.1$$

In which 'sup' is the supremum of the set of distances, F the empirical distributions of respectively size n and m.

If the maximum difference is larger than a specific value, depending on the number of samples and the alpha level of choice, the null hypothesis (that the samples are from the same distribution) is rejected.

$$D_{n,m} > c(\alpha)\sqrt{\frac{n+m}{n \cdot m}} \quad 0.2$$

Where α represents the alpha value and $c(\alpha)$ the corresponding value of the KS-test (*Kolmogorov–Smirnov Test - Wikipedia*, n.d.; Stephanie Glen, n.d.).

The Exit-velocity data was divided into the values in which both measurements show the same values and not.

The exact same measurements were compared to the measurements that were not the same from both measurement locations.

The KS-test rejected that the same measurements are from the same distribution as the radar measurements above the threshold 2.0 m/s with a $p_{value} = 3.03e-05$. Whereas the $p_{value} = 0.3$ for the measurements at the axle detector, and thus not rejected at an $alpha = 0.05$

Appendix G

Velocity measurements separated in categories and their GPD fits

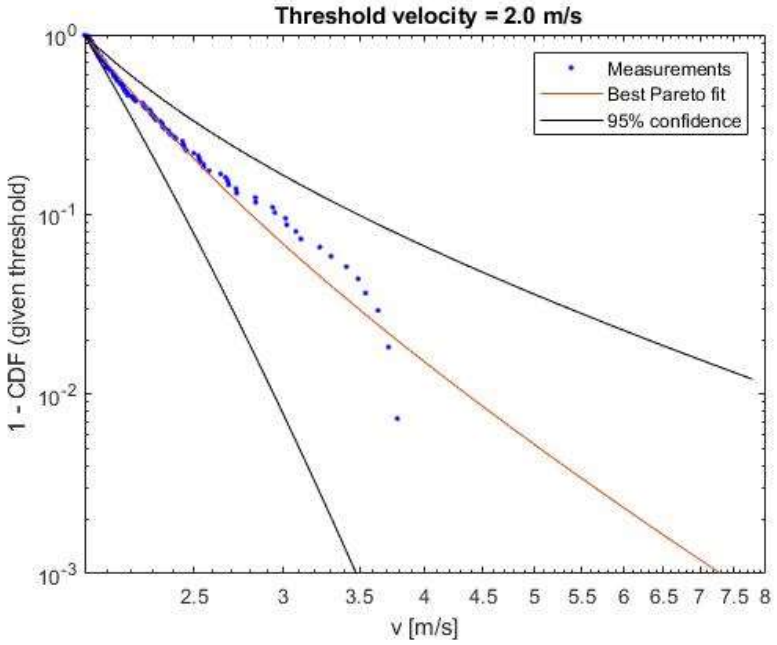

The best GPD fit for single 'full' tank wagons

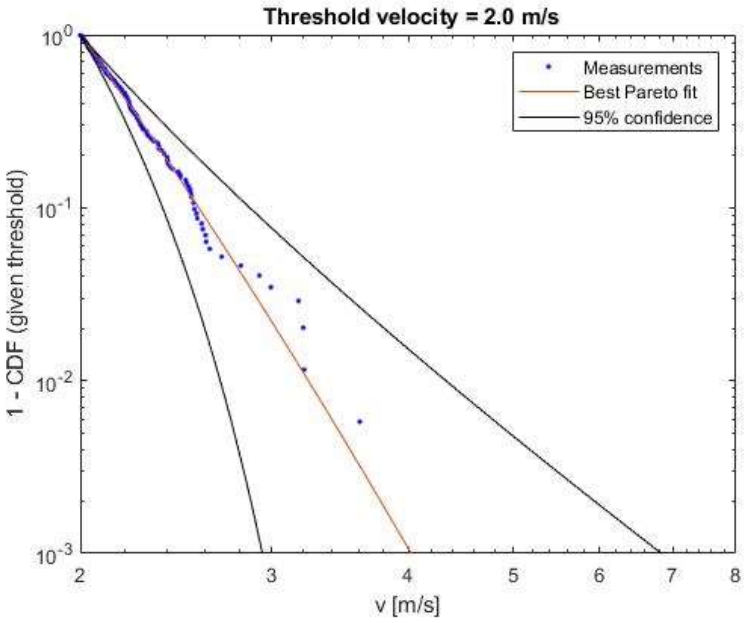

The best fit GPD for all wagons that are not 'full' and single tank wagons.

Appendix H

Part of the list of Dangerous goods, full list in (United Nations, 2019)

UN-number	GEVI	Name (Dutch)	V>2.0
Unknown			0.02%
1005	268	AMMONIAK, WATERVRIJ	0.07%
1010	239	BUTADIENEN, GESTABILISEERD of MENGSEL VAN BUTADIENEN EN KOOLWATERSTOF, GESTABILISEERD, dat bij 70 °C een dampdruk bezit van ten hoogste 1,1 MPa (11 bar) en bij 50 °C een dichtheid van ten minste 0,525 kg/l	0.06%
1040	263	ETHYLEENOXIDE MET STIKSTOF tot een maximale totale druk van 1 MPa (10 bar) bij 50 °C	0.11%
1055	23	ISOBUTEEN	0.03%
1173	225	ZUURSTOF, STERK GEKOELD, VLOEIBAAR	0.25%
1230	336	METHANOL	0.05%
1280	33	PROPYLEENOXIDE	0.03%
1710	60	TRICHLOORETHYLEEN	0.22%
1719	80	BIJTENDE ALKALISCHE VLOEISTOF, N.E.G.	0.98%
1824	80	NATRIUMHYDROXIDE, OPLOSSING (natronloog)	0.43%
1888	60	CHLOROFORM	0.48%
1965	23	MENGSEL VAN KOOLWATERSTOFGASSEN, VLOEIBAAR GEMAAKT, N.E.G. (mengsel A, A 01, A 02, A 0, A 1, B 1, B 2, B of C)	0.09%
1969	23	ISOBUTAAN	0.30%
2014	58	WATERSTOFPEROXIDE, OPLOSSING IN WATER met ten minste 20% doch ten hoogste 60% waterstofperoxide (zo nodig gestabiliseerd)	0.02%
2015	559	WATERSTOFPEROXIDE, OPLOSSING IN WATER, GESTABILISEERD, met meer dan 70% waterstofperoxide	0.04%
2023	63	EPICHLOORHYDRINE	0.22%
2055	39	STYREEN MONOMEER, GESTABILISEERD (vinylbenzeen, monomeer, gestabiliseerd)	0.06%
2218	839	ACRYLZUUR, GESTABILISEERD	0.24%
2447	446	FOSFOR, WIT, GESMOLTEN	0.64%
2810	60	GIFTIGE ORGANISCHE VLOEISTOF, N.E.G.	0.60%
2903	63	PESTICIDE, VLOEIBAAR, GIFTIG, BRANDBAAR, N.E.G., met een vlampunt gelijk aan of hoger dan 23 °C	0.15%
3082	90	MILIEUGEVAARLIJKE VLOEISTOF, N.E.G.	0.04%
3256	30	VERWARMDE VLOEISTOF, BRANDBAAR, N.E.G., met een vlampunt hoger dan 60 °C, bij een temperatuur gelijk aan of hoger dan haar vlampunt en gelijk aan of hoger dan 100 °C	0.79%

Appendix I

Further research regarding the high Exit-velocity measurements and brake number.

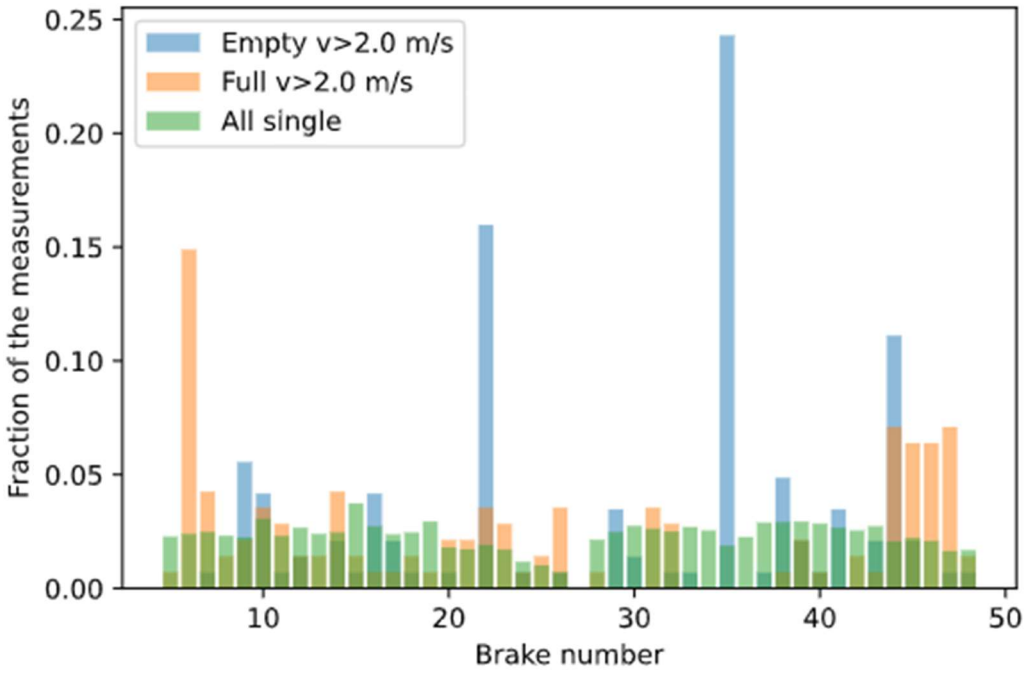

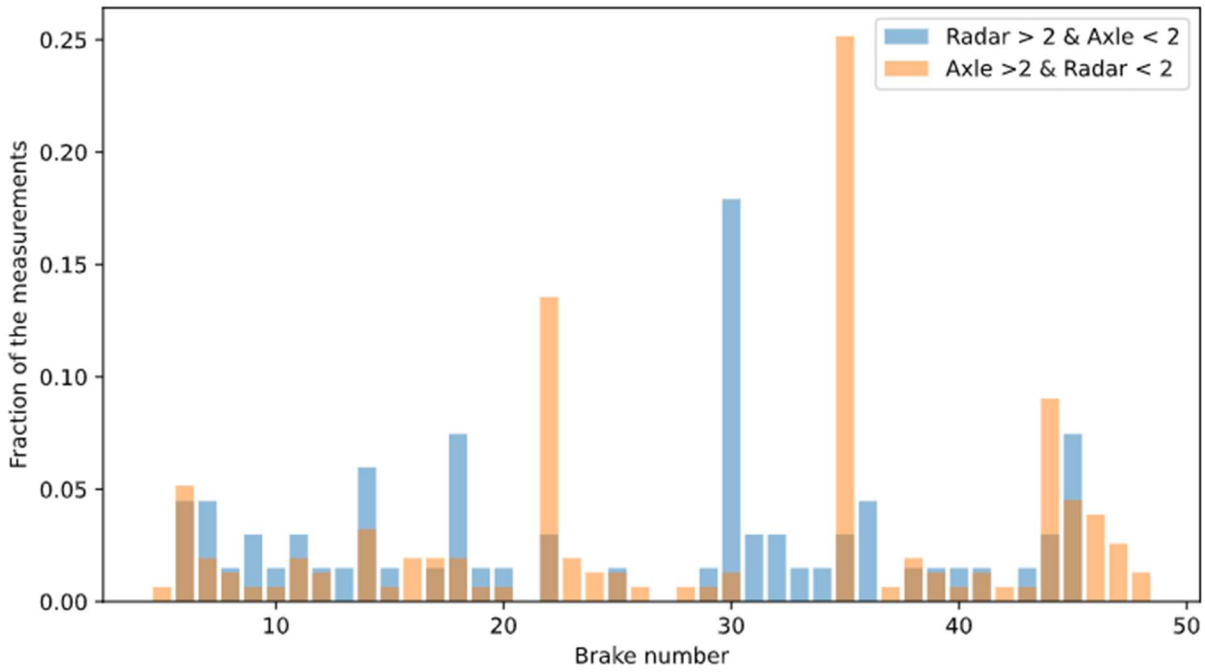

Appendix J

Comparison of the hourly and the 4-hour wind velocities in W-N direction.

The 4 hour average wind velocity is assumed independent, this data and the Weibull, Gumbel and average fits is given in the figure below. The hourly average fit is also given with the black dashed lines. The difference is relatively small, obviously the 4 hour average gives lower velocity values, but this is not representative for the effect on a run-off at any given time. Therefore, although the hourly data may be dependent, these fits are used.

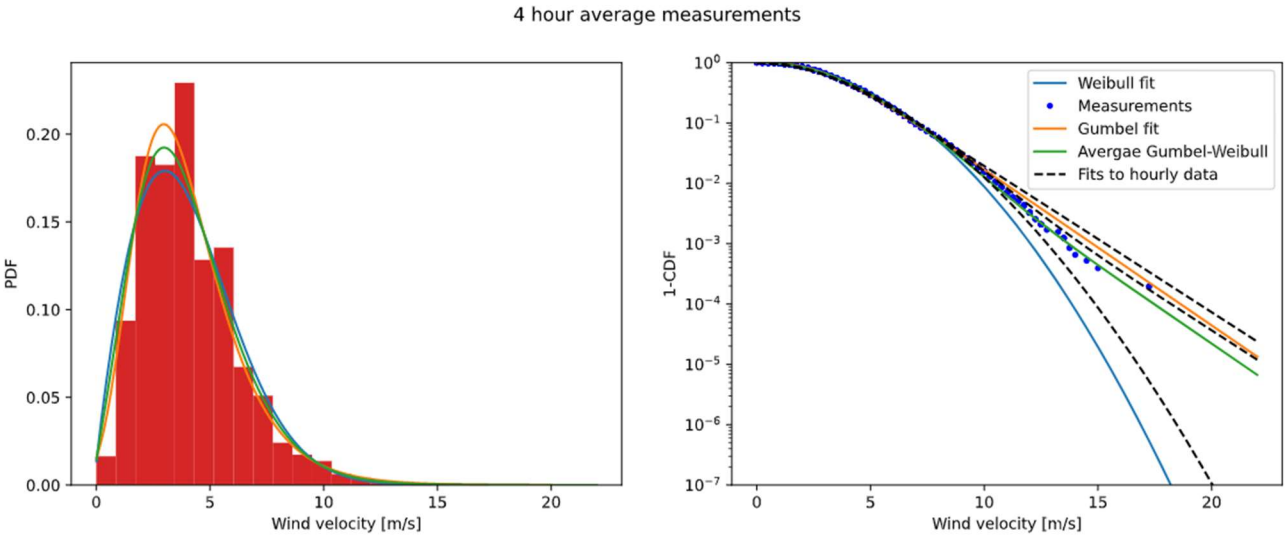

Appendix K

Product information of several crashworthy buffer manufacturers

105MM CRASH BUFFER
MIN. 400KJ

Innova
systems & technologies

REFERENCES
EN 15551
UIC 526-1; UIC 573

APPLICATIONS
Freight wagons
Locomotives

CONCEPT

- elastic deformation at impact speeds <12 km/h and forces <1.5 MN

- elastic and plastic deformation at impact speeds >12 km/h and forces >1.5 MN

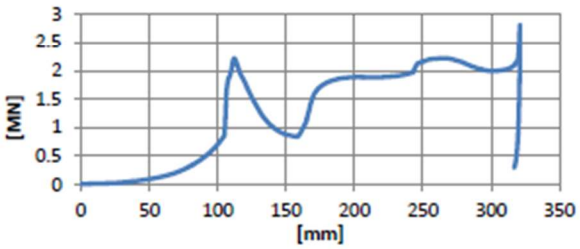

MAIN CHARACTERISTICS

Travel
Elastic Travel: 105 mm
Plastic Travel: min. 215 mm

Stored Energy
- **elastic deformation**: min. 30 kJ
- **elastic + plastic deformation**: min. 400 kJ

Mass: 99.5kg

BUFFER HEAD

Material
- type I: S355
- type II: S355 + wearing plate

Dimensions
- standard: 340mm x 450mm
- optional: 340mm x 550mm

SHOCK ABSORBER

A category thermoplastic elastomer

ENQUIRIES

INNOVA Systems & Technologies

Str. Abrud 97 bl. 168 ap. 2, 310279 Arad, Romania

Phone: +1 (646)4800335 | Phone/Fax:+40 (257)219943

www.INNOVA-SysTech.com | info@innova-systech.com

CERTIFICATIONS

2013/321/EC/Commission Decision - Technical specification for interoperability relating to the subsystem rolling stock-freight wagons of the trans-European conventional rail System amended by 2013/1236/EU Commission Regulation.

2010/713/EC/ Commission Decision on modules for the procedures for assessment of conformity, suitability for use and EC verification to be in the technical specifications for interoperability adopted under Directive 2008/57/EC of the Parliament and of the Council.

CE

BUREAU VERITAS

https://innovasystech.wpengine.com/wp-content/uploads/2014/09/105mm-Crash-Buffer-400kJ-INNOVASystemsTechnologies.pdf

VOITH

Safety for Freight Rail and Hazardous Goods Transport.

The crash buffer VSSM-105-400 is the result of the cooperation of Voith Turbo Scharfenberg GmbH Co. KG and SMW Spezialmaschinen und Werkzeugbau (special machines and tool manufacture) GmbH & Co. KG. It features a reversible stroke of 105 mm and an energy absorption of at least 400 kJ. The buffer for freightcars, tank waggons, locomotives and speciality vehicles is TSI compliant and meets the demands of the standards DIN EN 15551 and UIC 526 (Cat. A) and the crash requirements of UIC 573. The buffer plate can be variably and flexibly dimensioned. In the event of a crash, it does not enter the vehicle underframe.

Technical Data

Reversible stroke	105 mm
Energy absorption	≥ 30 kJ
Release load level	1 800 kN
Irreversible stroke	200 mm
Energy absorption	min. 400 kJ
Average force level maximum	max. 2 200 kN
Weight approx.	approx. 140 kg

Dimensions

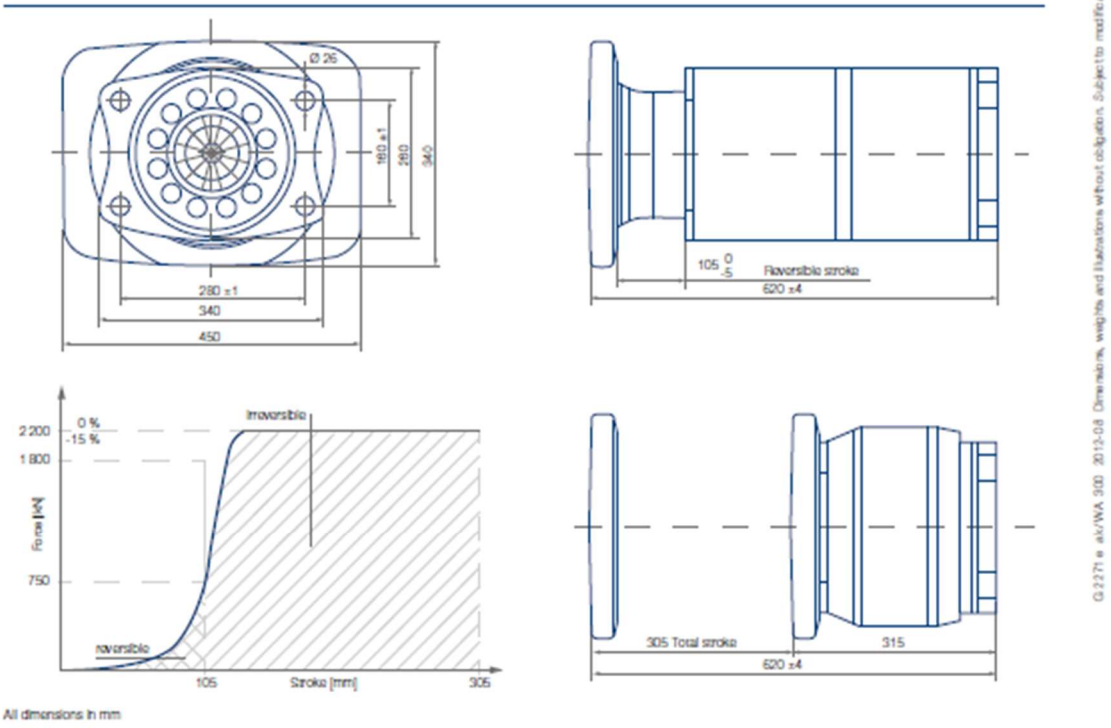

All dimensions in mm

SMW Spezialmaschinen
und Werkzeugbau GmbH & Co. KG
Kruseshofer Str. 21
17036 Neubrandenburg, Germany
Tel. +49 395 36709-0
Fax +49 395 36709-14
smw@smw-nb.de
smw-spezialmaschinen.de

Voith Turbo Scharfenberg GmbH & Co. KG
Gottfried-Linke-Str. 205
38239 Salzgitter, Germany
Tel. +49 5341 21-02
Fax +49 5341 21-4202
scharfenberg-systems@voith.com
voith.com

SMW

VOITH
Engineered Reliability

file:///C:/Users/timsl/Documents/TU%20Delft/Master/Afstuderen/Data_handling/Tim_data/Buffer_manufacturers_guides/px_6_1_1.pdf

CONFORMING TO DYNAMIC CAPACITY WITHIN EN 15551 AND UIC 526 CAT C 70KJ MIN @ 1000KN FORCE 105MM INSTALLED STROKE.

The 105mm stroke buffer was designed to meet the requirements of UIC 526 Cat C dynamic characteristics. The units operate mainly as side buffers on freight vehicles with 105mm stroke.

Capsule type: **Type 5-105**
Dynamic capacity: **80kJ @1000kN force**
Ultimate capacity: **200kJ**

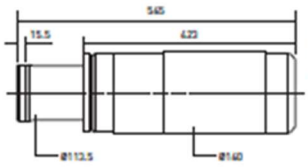

DYNAMIC DIAGRAM

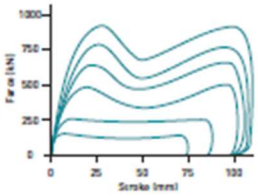

STATIC DIAGRAM

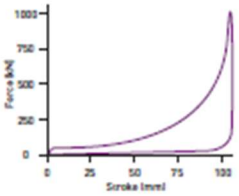

Buffer type: **Uni plus 105**
Dynamic capacity: **80kJ @1000kN force**
Ultimate capacity: **160kJ**

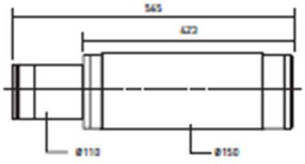

DYNAMIC DIAGRAM

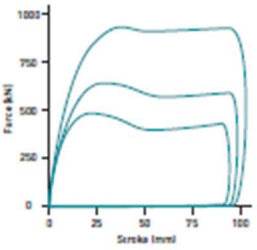

STATIC DIAGRAM

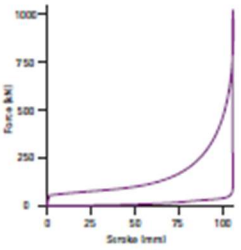

Buffer type: **Type 3RCC (combination)**
Dynamic capacity: **70kJ @1000kN force**
Ultimate capacity: **117kJ**

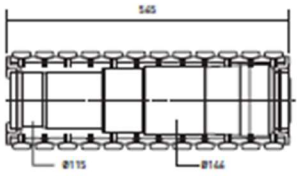

DYNAMIC DIAGRAM

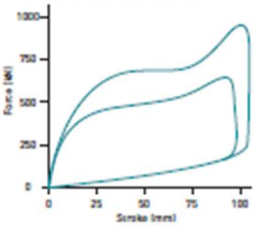

STATIC DIAGRAM

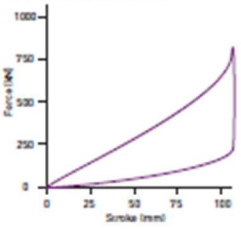

These buffers fit forged steel casings and European cast steel casings.

BUFFERS

HYBRID MULTI STAGE BUFFERS

In some applications, in order to meet crash worthiness standards, very long stroke buffers are required to meet high levels of impact energy absorption and dissipation.

This can be achieved by combining the attractive features of gas hydraulic units with deformation devices. The gas hydraulic element offers fully reversible energy absorption for slower impacts while the deformation device enables the hybrid buffer to fully stroke and maximise its potential for impact energy absorption.

Oleo has developed patented technology for such two stage devices.

TWO STAGE BUFFER IN ACCORDANCE WITH UIC 573

Projection:	620mm
Buffer head:	300mm x 450mm
Reversible	
Stroke:	105-5mm
Capacity:	greater than 120kJ
Max. buffer force:	less than 1550kN
Non reversible	
Total stroke:	greater than 550mm
Capacity:	greater than 900kJ
Buffer force:	less than 1700kN

FORCE STROKE DIAGRAM

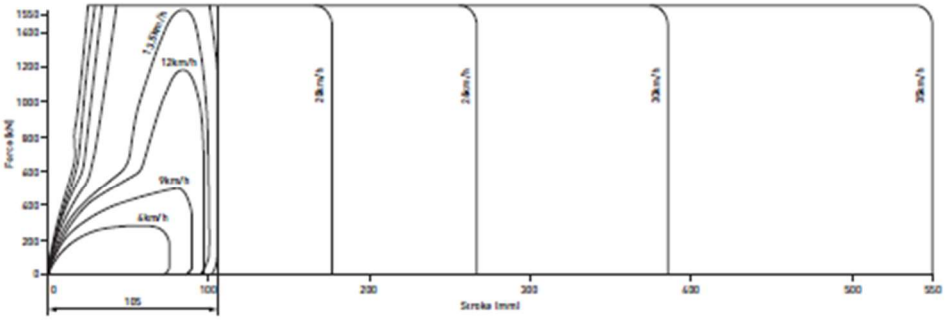

https://www.oleoinc.com/media/media_uploads/Rail-series-brochure-EN.pdf

Appendix L

Visual representation of two combined sets of buffers on 2 wagons.

The spring stiffnesses of each section, of each wagon, are combined into equivelant spring stiffnesses and twice as many sections.

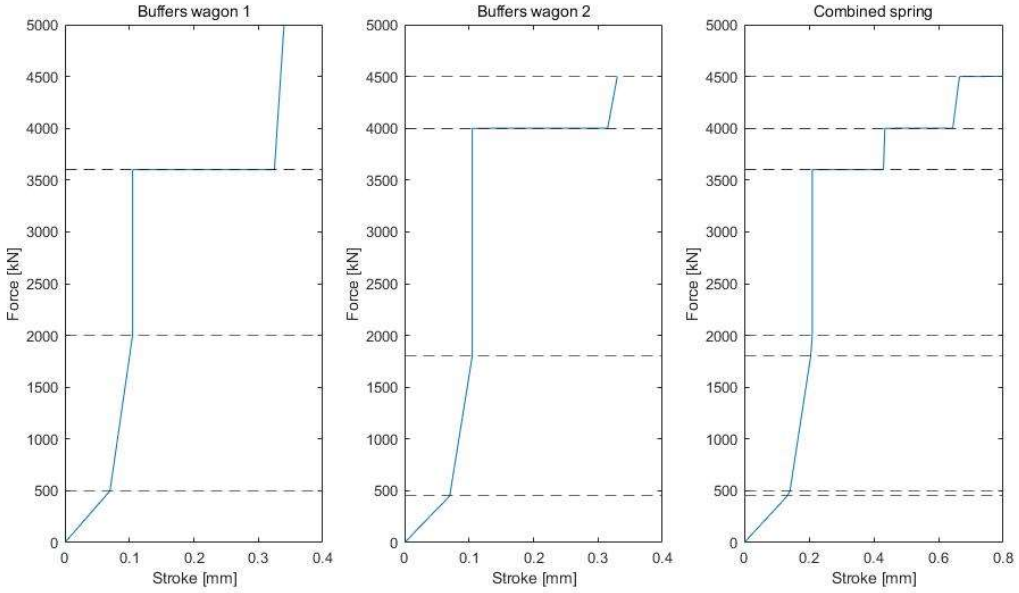

Appendix M

Damage percentages in case of a collission (not seperating tank wagons)

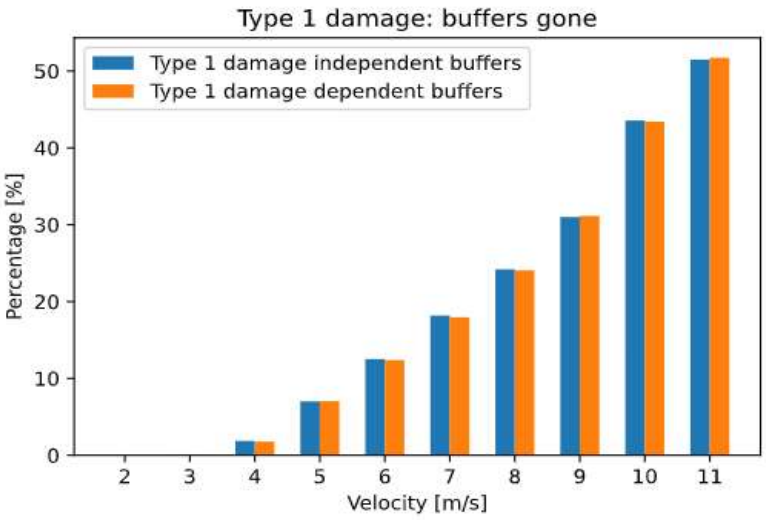

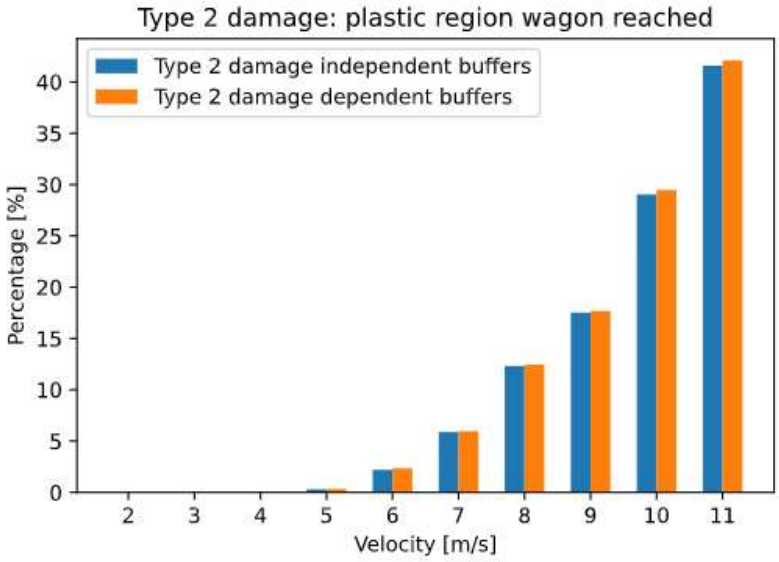

The buffers could lose capacity (type 1 damage) at 3 m/s. This only happens if 2 non-tankwagens collide, in which both tank wagons have buffers with no plastic absorption capacity, and the elastic region is minimal.

There are no cases in which this also lead to a reach of the wagons plastic capacity, type 2. This only happened at 4 m/s or higher.

Appendix N

Type 1 failure using the MC with the Dynamic model. And sensitivity to sloshing amplitude.

Number of failures are shown in one million runs given a Exit-velocity exceeding 2 m/s.

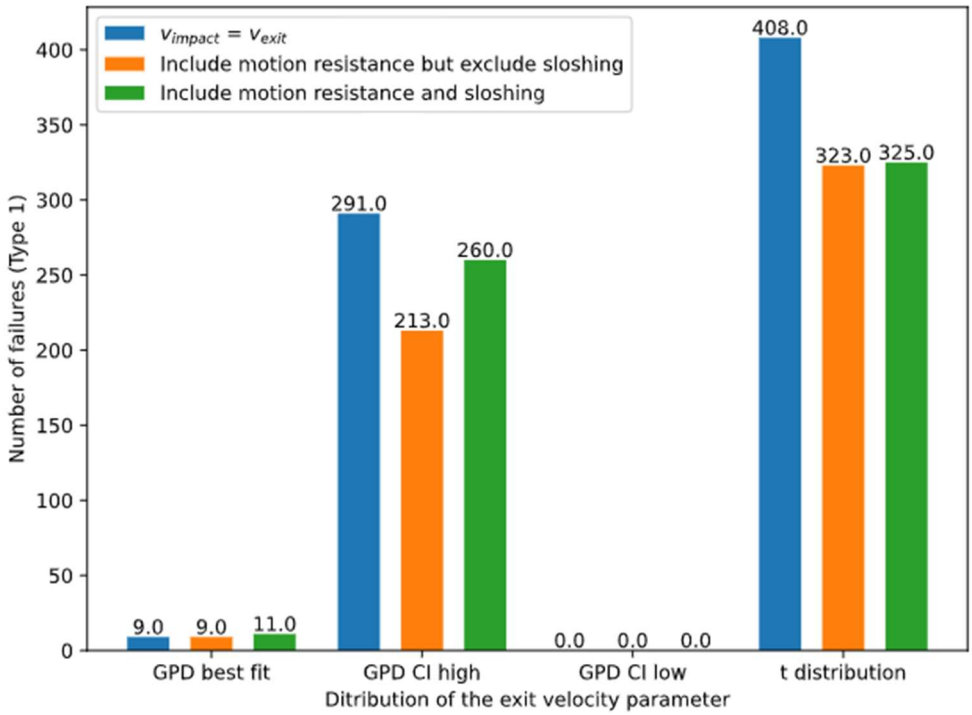

Influence of the sloshing amplitude calculated for the GPD upper bound CI.